Title
A Study of d-Density Wave States in Strongly Correlated Electron Systems

Author
Hsu, Chen-Hsuan

Publication Date
2014

Peer reviewed|Thesis/dissertation

UNIVERSITY OF CALIFORNIA
Los Angeles

A Study of d-Density Wave States in Strongly Correlated Electron Systems

A dissertation submitted in partial satisfaction
of the requirements for the degree
Doctor of Philosophy in Physics

by

Chen-Hsuan Hsu

2014

ABSTRACT OF THE DISSERTATION

A Study of d-Density Wave States in Strongly Correlated Electron Systems

by

Chen-Hsuan Hsu

Doctor of Philosophy in Physics

University of California, Los Angeles, 2014

Professor Sudip Chakravarty, Chair

Particle-hole condensates in the angular momentum $\ell = 2$ channel, known as d-density wave orders, have been suggested to be realized in strongly correlated electron systems. In this dissertation, we study singlet and triplet d-density wave orders with a form factor of $d_{x^2-y^2}$ as well as a novel topological mixed singlet-triplet d-density wave with a form factor of $(i\sigma d_{x^2-y^2} + d_{xy})$, and discuss the connections of these states to high-temperature superconductors and heavy-fermion materials.

In Chapter 2, we discuss the spin susceptibility of the singlet d-density wave, triplet d-density wave, and spin density wave orders with hopping anisotropies. From the numerical calculation, we find nearly vertical dispersion relations for spin excitations with anisotropic incommensurability at low energies in agreement with the inelastic neutron scattering experiments in the pseudogap state of the high-temperature superconductor $\mathrm{YBa_2Cu_3O_{6.6}}$. The vertical dispersion is a distinct feature of all three density wave states in contrast to the superconducting state, which shows an hourglass shape dispersion experimentally.

In Chapter 3, we explore a mixed singlet-triplet d-density wave state in a two-dimensional square lattice, which is topologically nontrivial and exhibits quantum spin Hall effect. We also study the bulk-edge correspondence and Lifshitz transition in the system. In Chapter 4, we show that the skyrmions in the system carry charge $2e$ and can condense into a superconducting state. The phase transition between the density wave and superconductivity likely leads to deconfined

quantum critical points. We suggest connections of this exotic state to the hidden-order state in the heavy-fermion compound $\mathrm{URu_2Si_2}$.

The st-DDW model is generalized to three dimensions in Chapter 5, where we propose a novel pairing mechanism in $\mathrm{URu_2Si_2}$. We assume the charge $2e$ skyrmionic spin texture in the mixed singlet-triplet d-density wave state fractionalizes into merons and antimerons at the deconfined quantum critical point. The interaction between these fractional particles results in a spin-singlet chiral d-wave superconducting state consistent with experiments. The unconventional superconductivity breaks time reversal symmetry, so we expect a polar Kerr effect at the onset of the superconductivity, but not in the time-reversal-invariant hidden-order state except perhaps for magnetic impurities.

The dissertation of Chen-Hsuan Hsu is approved.

Lincoln Chayes

Yaroslav Tserkovnyak

Sudip Chakravarty, Committee Chair

University of California, Los Angeles

2014

To my family...

TABLE OF CONTENTS

LIST OF FIGURES

ACKNOWLEDGMENTS

There are numerous people who have given me support during last six years. Without their help this dissertation would never be made possible. In this acknowledgments section I would like to express my deepest appreciation to all of them.

First, I would like to acknowledge my academic advisor, Dr. Sudip Chakravarty. He has been supporting me in all respects. He is not only a great research supervisor but also an excellent teacher in class. I was fortunate to have freedom to pursue the projects that I found interesting, and I also benefited tremendously from his willingness to share his keen insight into physics problems. In addition, he has been extremely helpful in the development of my career as a physicist. I am thankful to the graduate student researcher positions he offered, which helped me concentrate on my research after advancing to candidacy, and the opportunities to present my work at several professional conferences.

I was fortunate to have opportunities to work and discuss with faculty members in the Department of Physics and Astronomy and Department of Mathematics. I gratefully acknowledge the members of my Ph.D. committee for their time. I am grateful to Dr. Elihu Abrahams, Dr. Robijn Bruinsma, Dr. Lincoln Chayes, Dr. Alex Levine, Dr. Rahul Roy, Dr. Joseph Rudnick, and Dr. Yaroslav Tserkovnyak for their helpful discussion and excellent lectures on topics related to my research. I also thank Dr. Eric D'Hoker, Dr. James Rosenzweig, and Dr. Giovanni Zocchi for their lectures on the core graduate courses.

In addition to my advisor and the faculty members, many of my colleagues have helped me with my research and this dissertation. I would like to acknowledge Dr. Jonghyoun Eun, Dr. David Garcia-Aldea, Dr. Ipsita Mandal, Arash Bellafard, Antonio Russo, and Johnson Wang in our research group as well as Dr. Suk Bum Chung, Dr. Andrew Forrester, Dr. Silas Hoffman, Dr. Jonathan Landy, Dr. Emin Menachekanian, Dr. Koji Sato, and Scott Bender from other groups. This dissertation is based on my research papers: Chapter 2 is a modified version of Phys. Rev. B **86**, 214510 (2012); Chapter 3 is a modified version of Phys. Rev. B **84**, 155111 (2011); Chapter 4 is a modified version of Phys. Rev. B **87**, 085114 (2013); Chapter 5 is a modified version of a

manuscript which was recently submitted. I would also like to thank the co-authors, Dr. Srinivas Raghu at Stanford University and Zhiqiang Wang, for their permissions to reuse the papers in this dissertation.

Many of my friends have helped me in my life during the past six years. I cannot list all of their names due to the limitation of space. Among them, Dr. Albert Kao and Dr. Chiao-Yu Tseng have been of the most enormous assistance. Also, I would like to express my appreciation to all members of UCLA Taiwanese Student Association, which is my new family in Los Angeles.

I would like to express my sincerest gratitude to my family. My mother Chieh-Min Chou and sister Sz-Ning Hsu are always supportive of my dream to be a physicist. I also acknowledge my late grandfather Chin-Hsi Hsu, who always encouraged me. My wife Yi-Lin Chen has been with me all these years not only to help keep my life organized but also enrich my life. I deeply appreciate their support. This dissertation is dedicated to them.

Chen-Hsuan Hsu
May 2014
Los Angeles, California

VITA

2006	B.S. (Physics), National Tsing Hua University, Hsinchu, Taiwan.
2007-2008	Research assistant, Strongly Correlated Electron System Lab, Department of Physics, National Tsing Hua University, Hsinchu, Taiwan.
2008–present	PhD Student (advanced to candidacy in 2011), Condensed Matter Theory Group, Department of Physics and Astronomy, University of California, Los Angeles, USA.
2008–2012	Teaching Assistant, Department of Physics and Astronomy, University of California, Los Angeles, USA.
2012-present	Graduate Student Researcher, Department of Physics and Astronomy, University of California, Los Angeles, USA.

PUBLICATIONS AND PRESENTATIONS

Chen-Hsuan Hsu and Sudip Chakravarty, "Superconducting phase within the hidden-order state of the heavy-fermion material $\mathrm{URu_2Si_2}$," http://arxiv.org/1308.5357

Chen-Hsuan Hsu and Sudip Chakravarty, "Charge-2e skyrmion condensate in a hidden-order state," Phys. Rev. B 87, 085114 (2013)

Chen-Hsuan Hsu, Zhiqiang Wang, and Sudip Chakravarty, "Spin dynamics of possible density wave states in the pseudogap phase of high-temperature superconductors," Phys. Rev. B 86, 214510 (2012)

Yuezhen Niu, Suk Bum Chung, Chen-Hsuan Hsu, Ipsita Mandal, S. Raghu, and Sudip Chakravarty, "Majorana zero modes in a quantum Ising chain with longer-ranged interactions," Phys. Rev. B 85, 035110 (2012)

Chen-Hsuan Hsu, S. Raghu, and Sudip Chakravarty, "Topological density wave states of nonzero angular momentum," Phys. Rev. B, 84, 155111 (2011)

Chen-Hsuan Hsu and Sudip Chakravarty, "Superconducting phase within the hidden-order state of the heavy-fermion material URu_2Si_2," Aspen Winter Conference in Condensed Matter Physics (Unconventional Order in Strongly Correlated Systems), January 2014 (oral presentation)

Chen-Hsuan Hsu and Sudip Chakravarty, "Superconducting phase within the hidden-order state of an enigmatic heavy-fermion system," Lorentz Center Workshop (Hidden Order, Superconductivity, and Magnetism), November 2013 (poster presentation)

Chen-Hsuan Hsu and Sudip Chakravarty, "Charge-2e skyrmion condensate in a hidden-order state," APS March Meeting in Baltimore, March 2013 (oral presentation)

Chen-Hsuan Hsu and Sudip Chakravarty, "Charge-2e skyrmions in the topological d-density wave system," Gordon Research Conference (Correlated Electron Systems), June 2012 (poster presentation)

CHAPTER 1

Introduction

1.1 Symmetry-breaking states and topological states of matter

In condensed matter systems, atoms organize themselves to form ordered states of matter at low temperatures with properties which are fundamentally different from those of an individual atom. Identifying these ordered phases and understanding how they are formed have been a major goal for condensed matter physicists. While various orders are formed in numerous materials, they in general can be classified into two categories. The first is a class of phases which can be understood with the notion of broken symmetries invented by Landau [5, 57]. The phase transition and properties of a symmetry-breaking state can be studied in terms of a locally defined order parameter. Examples of such states are ferromagnetism and superconductivity, and the corresponding broken symmetries are spin-rotational symmetry and gauge symmetry, respectively. Since its discovery, Landau's theory of spontaneously broken symmetry has been a cornerstone of condensed matter physics.

On the other hand, quantum Hall states, which exhibit a quantized transverse conductance in the presence of an external magnetic field, fall into the other category beyond Landau's scenario [99, 102]. The quantum Hall states do not break any symmetries, so physicists must take a novel approach in order to understand them. This has led to a different classification based on the notion of topological orders [97, 103]. The states responsible for the quantum Hall effect are characterized by topological invariants, which are insensitive to smooth changes in the system (unless the system undergoes a quantum phase transition) and therefore gives rise to a quantized Hall conductance. The bulk of the two-dimensional system is insulating, and the electric current is carried by the

gapless edge states.

In 1982, Thouless et al. analyzed the quantum Hall effect in a periodic potential, and showed that the Hall conductance can be mapped to a topological invariant (Chern number) associated with filled bands [97]. In 1988, Haldane constructed a honeycomb lattice model with a quantized Hall conductance even in the absence of a net magnetic field [33]. In this model, time reversal symmetry is broken by magnetic flux penetrating the unit cell of the honeycomb lattice. The spatially inhomogeneous magnetic flux gives rise to a nonvanishing Chern number, and thus a quantized Hall conductance. The Chern number also determines the number of the topologically protected edge states. In 2005, Haldane's model was generalized to the time-reversal-invariant case [47, 48, 6]. Unlike the quantum Hall effect, where time reversal symmetry is broken, the time-reversal-invariant states reveal quantized *spin* Hall conductance. These states are characterized by a Z_2 topological invariant, which is related to the number of gapless edge states carrying spin currents. Since then, these works have led to extensive and intensive studies on topological insulators and topological superconductors [35, 79].

Although it appears that topological orders bear no relation to broken symmetries, this is, strictly speaking, not necessarily true. Intriguingly, one may still construct examples where a symmetry-breaking state has nontrivial topological properties and can even be protected by the broken symmetry itself [80, 95, 108]. Thus, the central purpose of this dissertation is to study a system in which topological orders and broken symmetries are intertwined and to discuss its realization in strongly correlated electron systems, such as high-temperature superconductors and heavy-fermion materials.

1.2 Exotic orders in strongly correlated electron systems

Strongly correlated electron systems are a wide class of materials in which electronic correlation plays an important role such that the behavior of electrons cannot be interpreted as non-interacting particles. These systems thus reveal remarkable physical properties, and exotic orders may arise in the phase diagrams of these systems such as high-temperature superconductors and heavy-fermion

materials.

One example is the mysterious pseudogap state in underdoped cuprates [10]. A generic phase diagram of high-T_c cuprates is plotted in Fig. 1.1. In undoped parent compounds, antiferromagnetism develops below the transition temperature, Neel temperature. Doping the cuprates by atomic substitutions or oxygen content weakens the antiferromagnetism and lowers the Neel temperature. Further doping results in unconventional superconductivity with a $d_{x^2-y^2}$ energy gap in a dome-like regime. In the underdoped region, there is a pseudogap state above the superconducting transition temperature. The pseudogap state possesses an energy gap with $d_{x^2-y^2}$-wave symmetry as the unconventional superconducting state [98]. Therefore, the pseudogap and superconducting states should be closely related, and it is important to study the pseudogap state in order to understand the whole phase diagram.

Despite the intense theoretical and experimental efforts over the last two decades, a full understanding of the origin of the unconventional superconductivity and the nature of the pseudogap state is still being developed. Moreover, an effective theory of such a strongly correlated system has a multitude of coupling constants, so we can generally expect a phase diagram with multiple broken-symmetry states. Therefore, it is intriguing to explore exotic orders in the angular momentum $\ell = 2$ channel, which have d-wave characters and may be relevant to the pseudogap and superconducting states.

Another example of mysterious exotic orders is the hidden-order state in the heavy-fermion compound URu_2Si_2. A schematic pressure-temperature phase diagram of URu_2Si_2 is shown in Fig. 1.2. The specific heat measurement of URu_2Si_2 indicates a second-order phase transition at $T_{\text{HO}} = 17.5$ K under the ambient pressure. However, the order parameter of the state at T_{HO} still remains unidentified despite its discovery nearly thirty years ago [69]. At lower temperatures, a superconducting phase arises below $T_c \approx 1.5$ K. Thermal conductivity and specific heat measurements indicated that the unconventional superconductivity in the system is likely a chiral d-wave pairing [50, 110]. Applying pressure leads to a large-moment antiferromagnetic state with an ordering vector $\vec{Q}_0 = (0, 0, \frac{2\pi}{c})$ as the applied pressure is higher than $P_x \sim 0.7$ GPa. Quantum oscillation measurements showed that there is no substantial Fermi surface change from the

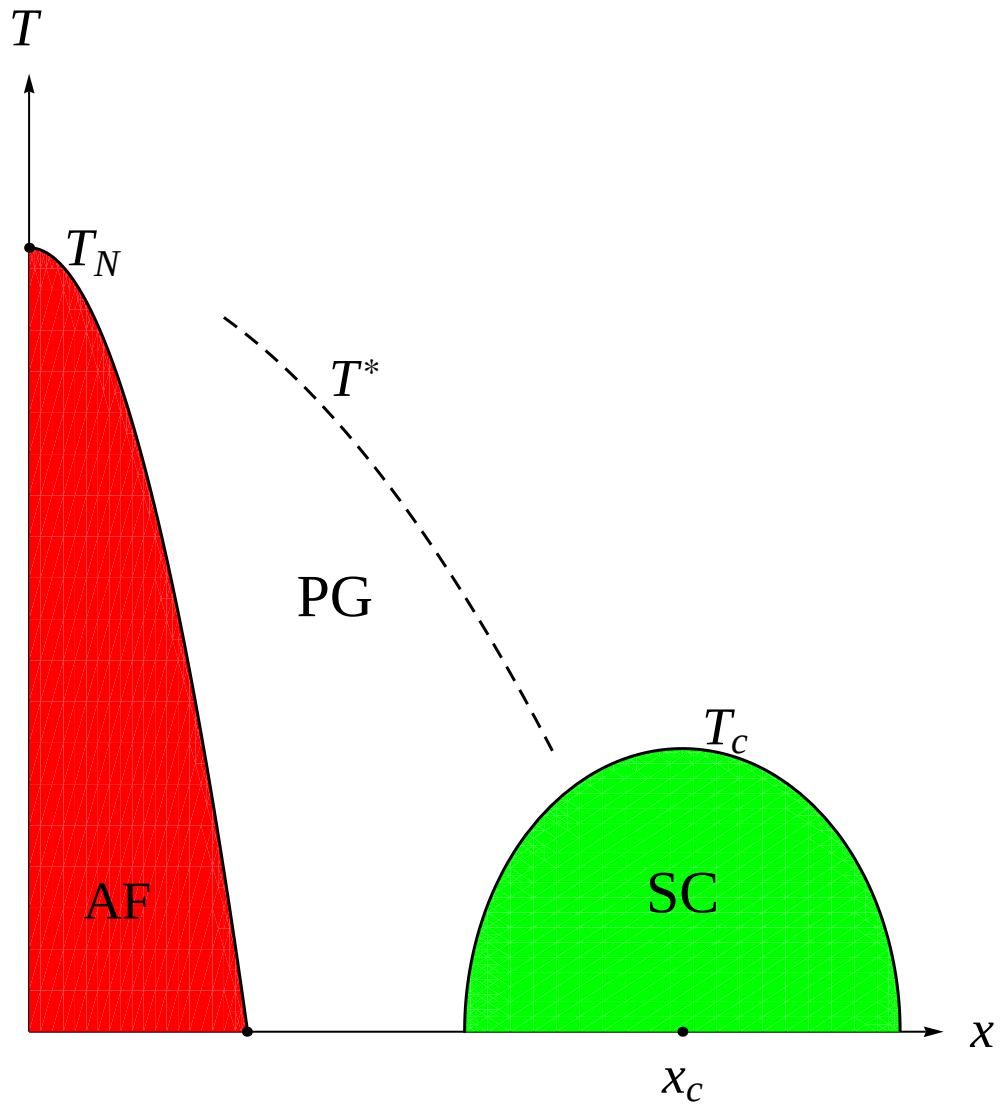

Figure 1.1: Schematic doping-temperature phase diagram of high-T_c cuprates. AF: antiferromagnetism; PG: pseudogap; SC: superconductivity. T_N denotes the transition temperature of the antiferromagnetism, Neel temperature; T_c is the superconducting transition temperature; T^* is the temperature at which the pseudogap state develops. x_c corresponds to the optimal doping, which is a putative quantum critical point.

hidden-order to the large-moment antiferromagnetic state, suggesting that the translational symmetry in the HO state is broken with the same vector $\vec{Q}_0$ [36].

From the pressure-temperature phase diagram, one can see that the superconductivity is enclosed by the hidden-order state. This implies that these two states should be closely related to each other. While numerous theoretical models have been proposed for the hidden-order state [87, 51, 37, 56, 18, 34, 42, 66, 26, 19, 24, 14, 100, 15, 84, 23, 43, 78, 85, 112], very few of them attempted to explain the mechanism of the unconventional superconducting state, which is of our central interest in Chapter 5.

1.3 d-density wave orders

Among the exotic orders which were proposed to explain the aforementioned mysterious pseudogap and hidden-order states, a class of particle-hole condensates in the angular momentum $\ell = 2$ channel [71] will be the primary topic in this dissertation. It has been suggested that the singlet counterpart of the particle-hole condensate, known as singlet d-density wave (sDDW) order, is the cause of the pseudogap [13]. (Recently it has been reported that sDDW order can be realized in cuprates using a Fermi-liquid theory with four parameters and standard Hartree-Fock methods [58, 59].) On the other hand, its triplet counterpart, triplet d-density wave (tDDW) [73], was proposed to be the hidden-order state in the heavy-fermion compound $\mathrm{URu_2Si_2}$ [42, 26]. In this dissertation, we also propose a novel mixed singlet-triplet d-density wave (st-DDW) order.

Density wave states break translational symmetry with nesting vectors, denoted by $\vec{Q}$, and the form factor of a density wave order parameter is constrained by the ordering vector $\vec{Q}$ [71]. In contrast to particle-particle condensates in a superconductor, density wave states are particle-hole condensates, where the orbital wave function does not constrain the spin wave function because there are no exchange symmetry requirements between a particle and a hole. Thus, we may assume the most general form of the density wave order parameter in the two-fold commensurate case, which has both singlet and triplet components,

$$\langle c^{\dagger}_{k+Q,\alpha} c_{k,\beta} \rangle = \Phi^s_Q f_s(\vec{k}) \delta_{\alpha\beta} + \Phi^t_Q f_t(\vec{k}) \left(\hat{N} \cdot \vec{\sigma}_{\alpha\beta} \right), \tag{1.1}$$

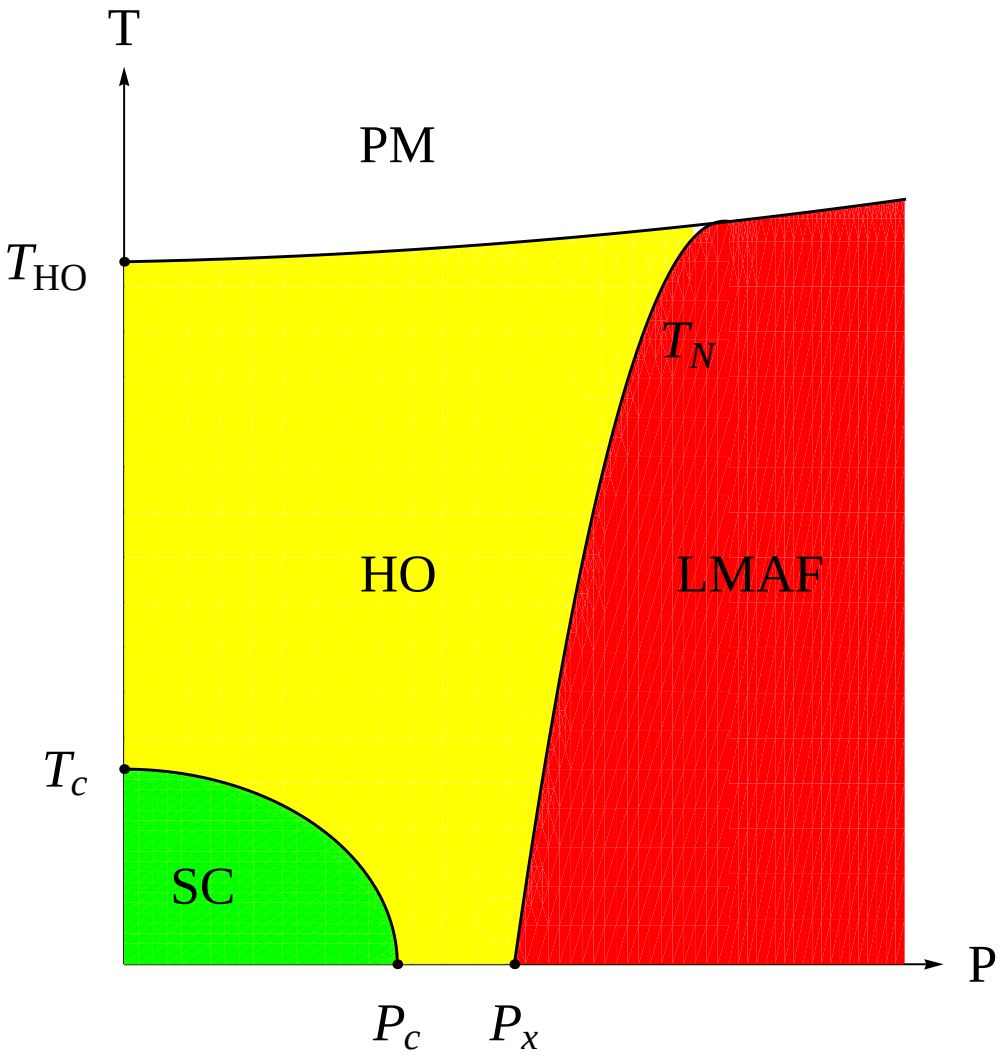

Figure 1.2: Schematic pressure-temperature phase diagram of URu_2Si_2. PM: paramagnetism; HO: hidden order; LMAF: large-moment antiferromagnetism; SC: superconductivity. T_{HO}: the transition temperature of the hidden-order state; T_c: the transition temperature of the superconducting state; T_N: the transition temperature of the large-moment antiferromagetic state; P_c: the transition pressure between the hidden-order and superconducting states; P_c: the transition pressure between the hidden-order and large-moment antiferromagnetic states. In some literatures, the critical point P_c coincides with P_x, which does not affect our main conclusion in this dissertation.

where $c_{k,\alpha}$ ($c^{\dagger}_{k,\alpha}$) is annihilation (creation) fermion operator with momentum $\vec{k}$ and spin α, $\hat{N}$ is the spin quantization axis, and $\vec{\sigma}_{\alpha\beta}$ are the Pauli matrices with spin indices α and β. Φ^s_Q and Φ^t_Q are complex numbers, and $f_s(\vec{k})$ ($f_t(\vec{k})$) is the form factor of the singlet (triplet) component. Whether Φ^s_Q (Φ^t_Q) is real or imaginary depends on the form of $f_s(\vec{k})$ ($f_t(\vec{k})$) as well as $\vec{Q}$.

Taking complex conjugate on both sides, we have

$$\begin{aligned}\langle c^{\dagger}_{k,\beta} c_{k+Q,\alpha}\rangle &= (\Phi^s_Q)^* f^*_s(\vec{k})\delta^*_{\alpha\beta} + (\Phi^t_Q)^* f^*_t(\vec{k})\left(\hat{N}\cdot\vec{\sigma}^*_{\alpha\beta}\right) \\ &= (\Phi^s_Q)^* f^*_s(\vec{k})\delta_{\beta\alpha} + (\Phi^t_Q)^* f^*_t(\vec{k})\left(\hat{N}\cdot\vec{\sigma}_{\beta\alpha}\right), \end{aligned} \tag{1.2}$$

where we have used $\delta^*_{\alpha\beta} = \delta_{\beta\alpha}$ and $\vec{\sigma}^*_{\alpha\beta} = \vec{\sigma}_{\beta\alpha}$.

Then, we may shift $\vec{k}$ to $\vec{k}+\vec{Q}$, switch α and β on both sides in the above equation, and obtain

$$\langle c^{\dagger}_{k+Q,\alpha} c_{k,\beta}\rangle = (\Phi^s_Q)^* f^*_s(\vec{k}+\vec{Q})\delta_{\alpha\beta} + (\Phi^t_Q)^* f^*_t(\vec{k}+\vec{Q})\left(\hat{N}\cdot\vec{\sigma}_{\alpha\beta}\right), \tag{1.3}$$

where we have used the fact that $\vec{k}+2\vec{Q}$ is equivalent to $\vec{k}$ in the two-fold commensurate density wave systems.

Equating the above equation and Eq.(1.1), we obtain the following relations:

$$(\Phi^s_Q)^* f^*_s(\vec{k}+\vec{Q}) = \Phi^s_Q f_s(\vec{k}), \tag{1.4}$$

$$(\Phi^t_Q)^* f^*_t(\vec{k}+\vec{Q}) = \Phi^t_Q f_t(\vec{k}). \tag{1.5}$$

In a two-dimensional square lattice, we are interested in the cases where $\vec{Q} = (\pi,\pi)$ with the lattice constants being set to unity. In Chapter 2, since we are interested in density wave orders with a form factor of $d_{x^2-y^2}$ as the pseudogap state, we may choose

$$\Phi^s_Q f_s(k) = i\frac{W_0}{2}\left(\cos k_x - \cos k_y\right), \tag{1.6}$$

$$\Phi^t_Q f_t(k) = 0 \tag{1.7}$$

for the sDDW order, or

$$\Phi^s_Q f_s(k) = 0, \tag{1.8}$$

$$\Phi^t_Q f_t(k) = i\frac{W_0}{2}\left(\cos k_x - \cos k_y\right) \tag{1.9}$$

for the tDDW order. In real space, after performing Fourier transform, we have

$$\text{For sDDW order:} \quad \langle c^{\dagger}_{j,\alpha} c_{l,\beta} \rangle = i\,(-1)^{j_x+j_y}\,\delta_{\alpha\beta} W_{jl}, \tag{1.10}$$

$$\text{For tDDW order:} \quad \langle c^{\dagger}_{j,\alpha} c_{l,\beta} \rangle = i\,(-1)^{j_x+j_y}\,\left(\hat{N}\cdot\vec{\sigma}_{\alpha\beta}\right) W_{jl}, \tag{1.11}$$

where $j \equiv (j_x, j_y)$ and $l \equiv (l_x, l_y)$, and

$$W_{jl} = \frac{W_0}{4}(\delta_{j,l\pm\hat{x}} - \delta_{j,l\pm\hat{y}}). \tag{1.12}$$

Therefore, in real space, the order parameter of the sDDW order produces staggered circulating charge currents whose directions alternate from one plaquette to the next. The order parameter of the tDDW order, on the other hand, produces staggered circulating *spin currents* but no charge currents (Fig. 1.3). This reminds us of the topological band insulators mentioned in Section 1.1, where oppositely aligned edge-spins travel in opposite directions. However, the bulk of the tDDW order is not fully gapped, but is a semimetal instead, so there is no topological protection for the edge states.

A more interesting case is the st-DDW order. In addition to the same spin current patterns as the tDDW state, the order parameter of the st-DDW state also produces modulations of hopping terms due to its real singlet component as shown in Fig. 1.3. The addition of the singlet component makes the bulk spectrum of the st-DDW order fully gapped, and the system becomes topologically nontrivial with a quantized spin Hall conductance. Notice that the st-DDW order preserves time-reversal invariance, analogous to time-reversal-invariant band insulators in Section 1.1.

In Chapters 3 and 4, we choose a form factor of $(i\sigma d_{x^2-y^2} + d_{xy})$ in order to study the interwining between broken symmetries and nontrivial topology. To be explicit, the nesting vector is $\vec{Q} = (\pi, \pi)$ and the form factor is

$$\Phi^s_Q f_s(k) = \Delta_0 \sin k_x \sin k_y, \tag{1.13}$$

$$\Phi^t_Q f_t(k) = i\frac{W_0}{2}\left(\cos k_x - \cos k_y\right), \tag{1.14}$$

which satisfies Eqs.(1.4)-(1.5). In real space, we have

$$\langle c^{\dagger}_{j,\alpha} c_{l,\beta} \rangle = i\,(-1)^{j_x+j_y}\,\left(\hat{N}\cdot\vec{\sigma}_{\alpha\beta}\right) W_{jl} + (-1)^{j_x+j_y}\delta_{\alpha\beta}\Delta_{jl}, \tag{1.15}$$

where W_{jl} is the same as Eq.(1.12), and

$$\Delta_{jl} = \frac{\Delta_0}{4}(\delta_{j,l\pm\hat{x}\pm\hat{y}} - \delta_{j,l\pm\hat{x}\mp\hat{y}}). \tag{1.16}$$

In the discussion of the hidden-order state of $\mathrm{URu_2Si_2}$ in Chapter 5, the nesting vector is chosen to be $\vec{Q} = (0, 0, \frac{2\pi}{c})$ in a three-dimensional body-centered-tetragonal (bct) lattice in order to be consistent with quantum oscillation experiments [36, 69]. Notice that in the bct lattice $2\vec{Q} = \vec{G}$ with a reciprocal lattice vector $\vec{G}$. The st-DDW order is assumed to be formed on the diagonal planes in the bct lattice to account for the anisotropic spin susceptibility observed in spin torque measurements [75, 93]. To be specific, the order parameter considered in Chapter 5 is

$$\langle c^\dagger_{k+Q,\alpha} c_{k,\beta}\rangle = \delta_{\alpha\beta}\Delta_k + i\left(\hat{N}\cdot\vec{\sigma}_{\alpha\beta}\right) W_k, \tag{1.17}$$

with the form factors

$$W_k = W_0 \sin\left(\frac{k_{x'}a'}{2}\right)\sin\left(\frac{k_{z'}c}{2}\right), \tag{1.18}$$

$$\Delta_k = \frac{\Delta_0}{2}\left[\cos\left(k_{x'}a'\right) - \cos\left(k_{z'}c\right)\right], \tag{1.19}$$

where the coordinate is rotated along z axis by 45°, i.e. $x' = (x-y)/\sqrt{2}$, $y' = (x+y)/\sqrt{2}$, and $z' = z$. Here $a' = \sqrt{2}a$ is the lattice constant after the coordinate rotation.

Therefore, the order parameter of the st-DDW order has the form of $(i\sigma d_{x'z'} + d_{x'^2-z'^2})$. Generalizing the model to three dimensions is necessary to explain the quantum oscillation experiments in $\mathrm{URu_2Si_2}$. However, the topological features of the st-DDW order which lead to a novel pairing mechanism discussed in Chapter 5 are in the fully gapped diagonal planes. Therefore, we may treat the system as a collection of quasi-two-dimensional diagonal planes, and each of them is topologically nontrivial with a quantized spin Hall conductance. The spin current pattern and modulation of the hopping terms are on the diagonal planes as shown in Chapter 5. Notice that the st-DDW order preserves time reversal symmetry, and does not produce net charges, magnetic moments or charge currents to be detected by common s-wave probes, so it is a good candidate for a hidden-order state.

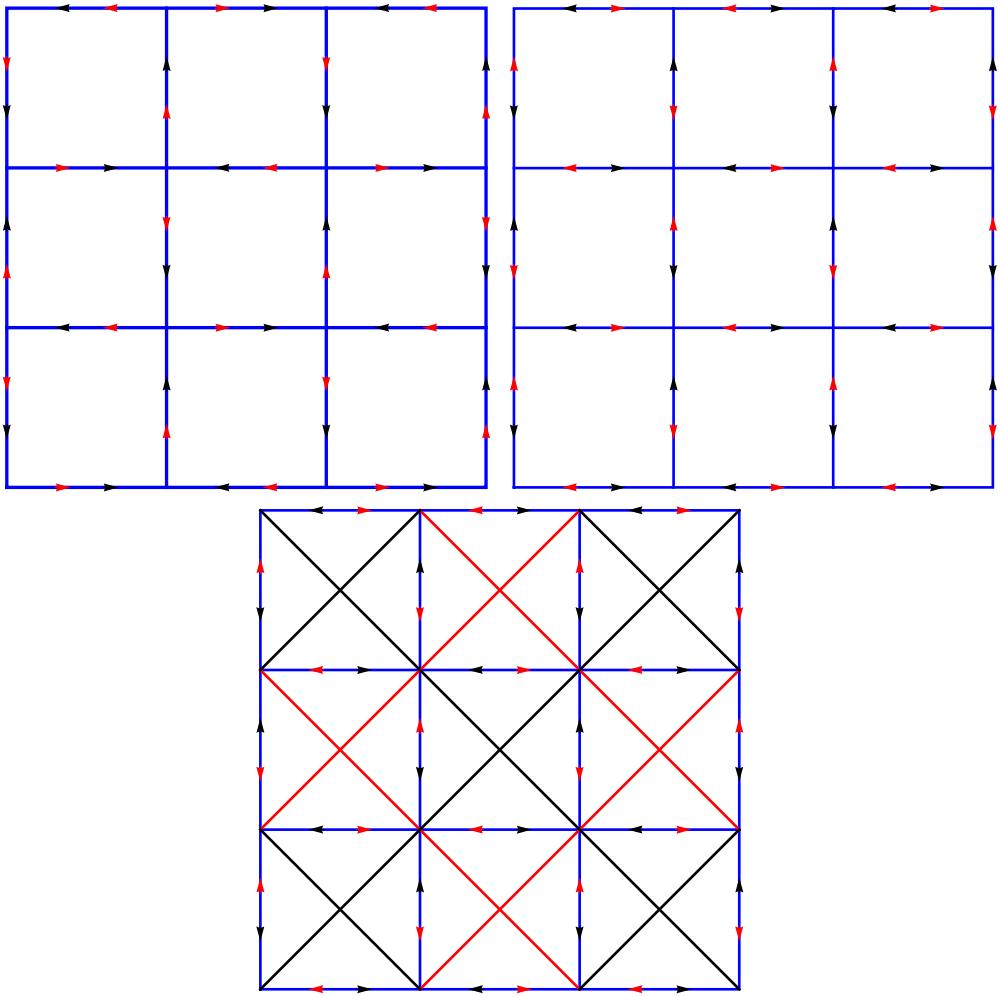

Figure 1.3: The sDDW, tDDW and st-DDW orders on a square lattice. The black (red) arrowheads indicate the directions of up- (down-) spins. The black and red lines indicate different signs of modulations of the hopping along diagonal directions. Upper-left: charge current pattern of the sDDW order. Upper-right: spin current pattern of the tDDW order. Bottom: spin current pattern and modulation of the hopping terms of the st-DDW order.

1.4 Contents of this dissertation

In this section, we will layout the structure of this dissertation and briefly discuss our motivations within each chapter. Notice that the notations and abbreviations for each chapter are defined independently.

In a recent inelastic neutron scattering experiment in the pseudogap state of the high-temperature superconductor $\mathrm{YBa_2Cu_3O_{6.6}}$, an unusual "vertical" dispersion of the spin excitations with a large in-plane anisotropy was observed [39]. Since high-T_c superconductors have a rich phase diagram, which hosts many possible competing orders, it is both important and interesting to examine the properties of various density wave order parameters, which may be relevant to the pseudogap state. In Chapter 2, we discuss in detail the spin susceptibility of the sDDW, tDDW, as well as the more common spin density wave orders with hopping anisotropies. From numerical calculations within the framework of random phase approximation, we find nearly vertical dispersion relations for spin excitations with anisotropic incommensurability at low energies $\omega \leq 90$ meV, which are reminiscent of the experiments. At very high energies $\omega \geq 165$ meV, we also find energy-dependent incommensurability. Although there are some important differences between the three cases, unpolarized neutron measurements cannot discriminate between these alternate possibilities; the vertical dispersion, however, is a distinct feature of all three density wave states in contrast to the superconducting state, which shows an hourglass shape dispersion.

The pseudogap state of high-temperature superconductors is a profound mystery. It has tantalizing evidence of a number of broken symmetry states, not necessarily conventional charge- and spin-density waves. In Chapter 3, we explore a class of more exotic st-DDW order on a two-dimensional square lattice, which is characterized by topological properties observed in recently discovered topological insulators [35, 79]. We compute the topological invariant, spin Chern number, in momentum space, where periodic boundary conditions are imposed. We also study bulk-edge correspondence by numerically diagonalizing the Hamiltonian with cylindrical geometry, and find gapless states carrying spin currents on the edges. The evolution of successive Lifshitz transitions in the system is tracked as the mean-field parameters are changed. Finally, we suggest that

these rich topological density wave states deserve closer attention not only in high-temperature superconductors but in other correlated electron states as well.

The mixed st-DDW state admits skyrmionic textures. In Chapter 4, we show that the skyrmions in the system carry charge $2e$ by following Grover and Senthil's adiabatic argument [31]. The skyrmions have zero spin and are bosons, so they may undergo Bose-Einstein condensate and condense into a spin-singlet s-wave superconducting state. In addition, a charge current can be induced by a time-dependent inhomogeneous spin texture, leading to quantized charge pumping. The quantum phase transition between this st-DDW and skyrmionic superconducting condensate likely leads to deconfined quantum critical points. We suggest connections of this exotic state to electronic materials that are strongly correlated, such as the heavy-fermion material $\mathrm{URu_2Si_2}$. At the very least, we provide a concrete example in which the topological order and broken symmetry are intertwined, which can give rise to non-BCS superconductivity.

In Chapter 5, we propose a novel pairing mechanism in the heavy-fermion material $\mathrm{URu_2Si_2}$ (other than the Bose-Einstein condensate of skyrmions discussed in Chapter 4). In this chapter, the st-DDW model is generalized to three dimensions and the st-DDW order is assumed to be formed on the diagonal planes in the body-centered-tetragonal lattice. The exotic order is topologically nontrivial and supports a charge $2e$ skyrmionic spin texture as shown in Chapter 4. We then assume the skyrmions fractionalize into merons and antimerons at the deconfined quantum critical point. The interaction between these fractional particles results in a spin-singlet chiral d-wave superconducting state, which breaks time reversal symmetry. We expect nonzero signals of the polar Kerr effect at the onset of the superconductivity, but not in the time-reversal-invariant hidden-order state, except perhaps for magnetic impurities.

To make the dissertation succinct and more accessible, the details of derivations of equations in Chapters 4 and 5 are included in Appendices A and B.

CHAPTER 2

Spin dynamics of various density wave states

2.1 Introduction

The pseudogap state of high-temperature superconductors has been studied with numerous experimental tools, yet its origin is not resolved [74]. One view proposes that the pseudogap state is a particle-hole condensate, a density wave. Of all such states that break translational symmetry and have strong momentum dependence of the type $d_{x^2-y^2}$, two candidate density wave orders that can couple to inelastic neutron scattering have been proposed: the singlet $d_{x^2-y^2}$-density wave (sDDW) [13], corresponding to angular momentum $\ell = 2$ but a spin singlet, and the spin density wave order (SDW); in the general classification of density wave orders [71], the latter corresponds to $\ell = 0$ but a spin triplet. In addition to the sDDW order, its triplet counterpart [73] ($i\sigma d_{x^2-y^2}$, or tDDW, where $\sigma = \pm 1$ corresponds to up- and down-spins with the $\hat{z}$ axis as the axis of spin quantization) also has interesting properties and deserves more attention [73]. Recently, Fujimoto proposed that a triplet d-wave particle-hole condensate may be realized in the hidden-order state of the URu_2Si_2 system [26], which will be the main focus in Chapters 4 and 5. Since high-T_c superconductors have a rich phase diagram, which hosts many possible competing orders, it is both important and interesting to examine the properties of various density wave order parameters of higher angular momentum. In this chapter we discuss the three order parameters mentioned above.

Inelastic neutron scattering can directly probe magnetic excitations. The scattering cross-section is proportional to the magnetic structure factor, which is proportional to the imaginary part of the dynamic spin susceptibility via the fluctuation-dissipation theorem [2]. Thus, a calculation of the spin susceptibility will provide a link between theoretical models and neutron scattering

experiments.

In particular, we want to address a recent experiment in underdoped $YBa_2Cu_3O_{6.6}$. The most striking aspect of this experiment is a vertical dispersion relation of the spin excitations with a large in-plane anisotropy in the pseudogap state in contrast to the "hourglass" dispersion observed in the superconducting state [39]. The qualitatively different behavior between the superconducting and the pseudogap states suggests different mechanisms. Motivated by the experimental observations, we study the spin susceptibility of the three density wave orders mentioned above with hopping anisotropy, which breaks C_4 rotational symmetry and mimics an "electron nematic" state, which is a collective phenomenon not described by the density functional theory [52, 32, 107]. Here we consider a phenomenological model [111], where we set the hopping terms to be anisotropic along a and b axes, and study the energy-momentum dispersion relations of the dynamical spin susceptibility. The explicit calculation involves random phase approximation (RPA) that has been widely discussed in the literature; for some representative papers, see Refs. [90, 25, 89, 44].

The structure of this chapter is as follows: in Sec. 2.2, we sketch the calculation of the spin susceptibility and discuss the numerical results of the sDDW order. In Sec. 2.3, we discuss the numerical results of the tDDW order. In Sec. 2.4, we also discuss the numerical results of the SDW order.

2.2 Spin susceptibility: singlet d-density wave order

In this section we set up the calculation of the spin susceptibility using sDDW as an example. In the following sections, we will give the results of the other order parameters. To capture the in-plane anisotropic feature of the pseudogap state in the neutron scattering experiment, we consider the sDDW order with anisotropic hopping terms. In the momentum space, the order parameter can be written in terms of the fermion operators as

$$\langle c^\dagger_{k+Q,\alpha} c_{k,\beta} \rangle \propto i\delta_{\alpha\beta} W_k \tag{2.1}$$

with $W_k \equiv \frac{W_0}{2}[\cos(k_x a) - \cos(k_y b)]$, where a and b are lattice constants. For orthorhombic $YBa_2Cu_3O_{6.6}$, a and b are unequal, but the difference is very small. ($a = 3.82$ Å, $b = 3.87$ Å.)

The two-dimensional mean-field Hamiltonian will be

$$\mathcal{H}_{\rm sDDW} = \sum_{\sigma}\sum_{k}\left(\epsilon_k c^{\dagger}_{k,\sigma}c_{k,\sigma} + \epsilon_{k+Q}c^{\dagger}_{k+Q,\sigma}c_{k+Q,\sigma} + iW_k c^{\dagger}_{k,\sigma}c_{k+Q,\sigma} + h.c.\right), \quad (2.2)$$

where the summation is over the reduced Brillouin zone (RBZ) bounded by $(k_y b) \pm (k_x a) = \pm\pi$, $Q = (\pi/a, \pi/b)$ is the nesting vector, and $\epsilon_k \equiv \epsilon_{1k} + \epsilon_{2k}$ with [77]

$$\epsilon_{1k} \equiv -2t\left[(1+r)\cos(k_x a) + (1-r)\cos(k_y b)\right], \quad (2.3)$$

$$\epsilon_{2k} \equiv 4t'\cos(k_x a)\cos(k_y b) - 2t''\left[(1+r)\cos(2k_x a) + (1-r)\cos(2k_y b)\right] - \mu. \quad (2.4)$$

For $r \neq 0$, we have anisotropic hopping terms which breaks fourfold rotational symmetry. Note that although the anisotropy also modifies the next-nearest-neighbor hopping, it is simply a parameter and is lumped into the definition of t' in our model. The eigenvalues of the Hamiltonian are $\lambda_{k,\pm} = \epsilon_{2k} \pm E_k$ with $E_k \equiv \sqrt{\epsilon_{1k}^2 + W_k^2}$.

The one-loop spin susceptibility in the momentum and Matsubara frequency space is defined as, N being the number of lattice sites,

$$\chi_0^{ij}(q, q', i\omega_n) = -\frac{1}{N}\int_0^{\beta} d\tau e^{i\omega_n \tau}\langle \mathrm{T}_\tau S_q^i(\tau) S_{-q'}^j\rangle, \quad (2.5)$$

where $i, j = x, y, z$, $\beta = 1/k_B T$, τ is the imaginary time, T_τ is the time-ordering symbol, and the spin operators are

$$S_q^i \equiv \sum_{k,\sigma,\sigma'} c^{\dagger}_{k+q,\sigma}\hat{\sigma}^i_{\sigma\sigma'}c_{k,\sigma'}. \quad (2.6)$$

Here $\hat{\sigma}_{\sigma\sigma'}$ are the Pauli matrices with spin indices σ and σ'. We can define the longitudinal and the transverse susceptibilities as $\chi_0^{zz}(q, q', \omega)$ and $\chi_0^{+-}(q, q', \omega)$, respectively, with $S_q^{\pm} \equiv S_q^x \pm iS_q^y$ and analytic continuation, $i\omega_n \to \omega + i\delta$.

In the density wave systems, the Green's functions form matrices

$$\hat{G}_\sigma(k, i\omega_m) \equiv \begin{pmatrix} g_\sigma(k, k, i\omega_m) & g_\sigma(k, k+Q, i\omega_m) \\ g_\sigma(k+Q, k, i\omega_m) & g_\sigma(k+Q, k+Q, i\omega_m) \end{pmatrix}, \quad (2.7)$$

where

$$g_\sigma(k,k',i\omega_m) = -\int_0^\beta d\tau e^{i\omega_m\tau}\langle \mathrm{T}_\tau c_{k,\sigma}(\tau)c^\dagger_{k',\sigma}\rangle. \tag{2.8}$$

The one-loop spin susceptibility also has diagonal and off-diagonal terms

$$\chi_0^{zz}(q,q',i\omega_m) = \delta_{q,q'}\chi^{zz}_{\text{diag}}(q,i\omega_m) + \delta_{q,q'+Q}\chi^{zz}_{\text{off}}(q,i\omega_m), \tag{2.9}$$

$$\chi_0^{+-}(q,q',i\omega_m) = \delta_{q,q'}\chi^{+-}_{\text{diag}}(q,i\omega_m) + \delta_{q,q'+Q}\chi^{+-}_{\text{off}}(q,i\omega_m), \tag{2.10}$$

where the subscripts "diag" and "off" refer to the diagonal and off-diagonal terms of the one-loop spin susceptibility, respectively.

With a quadratic Hamiltonian, these terms can be written in terms of the Green's function matrices by applying Wick's theorem [9] , and we have

$$\chi^{zz}_{\text{diag}}(q,i\omega_m) = \frac{1}{\beta N}\sum_{k,n,\sigma}\mathrm{Tr}[\hat{G}_\sigma(k+q,i\epsilon_n+i\omega_m)\hat{G}_\sigma(k,i\epsilon_n)], \tag{2.11}$$

$$\chi^{zz}_{\text{off}}(q,i\omega_m) = \frac{1}{\beta N}\sum_{k,n,\sigma}\sum_{j\neq l}[\hat{G}_\sigma(k+q,i\epsilon_n+i\omega_m)\hat{G}_\sigma(k,i\epsilon_n)]_{jl}, \tag{2.12}$$

$$\chi^{+-}_{\text{diag}}(q,i\omega_m) = \frac{1}{\beta N}\sum_{k,n}\mathrm{Tr}[\hat{G}_\uparrow(k+q,i\epsilon_n+i\omega_m)\hat{G}_\downarrow(k,i\epsilon_n)], \tag{2.13}$$

$$\chi^{+-}_{\text{off}}(q,i\omega_m) = \frac{1}{\beta N}\sum_{k,n}\sum_{j\neq l}[\hat{G}_\uparrow(k+q,i\epsilon_n+i\omega_m)\hat{G}_\downarrow(k,i\epsilon_n)]_{jl}, \tag{2.14}$$

where Tr is the trace, and $\hat{G}_\sigma(k,i\epsilon_n)$ can be obtained from the Hamiltonian.

For the sDDW order, the up-spin and down-spin components are identical. For $\sigma =\uparrow$ or $\downarrow$, we have

$$\hat{G}_\sigma(k,i\epsilon) = \frac{1}{(i\epsilon-\epsilon_{2k})^2 - E_k^2}\begin{pmatrix} i\epsilon+\epsilon_{1k}-\epsilon_{2k} & iW_k \\ -iW_k & i\epsilon-\epsilon_{1k}-\epsilon_{2k}\end{pmatrix}. \tag{2.15}$$

Therefore, we have

$$\chi_0^{zz}(q,q',\omega) = \delta_{q,q'}\chi_{\text{diag}}(q,\omega) + \delta_{q,q'+Q}\chi_{\text{off}}(q,\omega), \tag{2.16}$$

$$\chi_0^{+-}(q,q',\omega) = \frac{1}{2}\chi_0^{zz}(q,q',\omega), \tag{2.17}$$

where

$$
\begin{aligned}
&\chi_{\text{diag}}(q,\omega) \\
= \;& \frac{1}{N}\sum_k \left(1-\frac{\epsilon_{1k}\epsilon_{1k+q}+W_kW_{k+q}}{E_kE_{k+q}}\right) \\
&\quad\times\left[\frac{n_F(\epsilon_{2k}+E_k)-n_F(\epsilon_{2k+q}-E_{k+q})}{\omega-\epsilon_{2k}-E_k+\epsilon_{2k+q}-E_{k+q}+i\delta}+\frac{n_F(\epsilon_{2k}-E_k)-n_F(\epsilon_{2k+q}+E_{k+q})}{\omega-\epsilon_{2k}+E_k+\epsilon_{2k+q}+E_{k+q}+i\delta}\right] \\
&+\frac{1}{N}\sum_k \left(1+\frac{\epsilon_{1k}\epsilon_{1k+q}+W_kW_{k+q}}{E_kE_{k+q}}\right) \\
&\quad\times\left[\frac{n_F(\epsilon_{2k}+E_k)-n_F(\epsilon_{2k+q}+E_{k+q})}{\omega-\epsilon_{2k}-E_k+\epsilon_{2k+q}+E_{k+q}+i\delta}+\frac{n_F(\epsilon_{2k}-E_k)-n_F(\epsilon_{2k+q}-E_{k+q})}{\omega-\epsilon_{2k}+E_k+\epsilon_{2k+q}-E_{k+q}+i\delta}\right],
\end{aligned}
\tag{2.18}
$$

$$
\begin{aligned}
&\chi_{\text{off}}(q,\omega) \\
= \;& \frac{i}{N}\sum_k \left(\frac{-\epsilon_{1k}W_{k+q}+\epsilon_{1k+q}W_k}{E_kE_{k+q}}\right) \\
&\quad\times\left[-\frac{n_F(\epsilon_{2k}+E_k)-n_F(\epsilon_{2k+q}-E_{k+q})}{\omega-\epsilon_{2k}-E_k+\epsilon_{2k+q}-E_{k+q}+i\delta}-\frac{n_F(\epsilon_{2k}-E_k)-n_F(\epsilon_{2k+q}+E_{k+q})}{\omega-\epsilon_{2k}+E_k+\epsilon_{2k+q}+E_{k+q}+i\delta}\right. \\
&\quad\left.+\frac{n_F(\epsilon_{2k}+E_k)-n_F(\epsilon_{2k+q}+E_{k+q})}{\omega-\epsilon_{2k}-E_k+\epsilon_{2k+q}+E_{k+q}+i\delta}+\frac{n_F(\epsilon_{2k}-E_k)-n_F(\epsilon_{2k+q}-E_{k+q})}{\omega-\epsilon_{2k}+E_k+\epsilon_{2k+q}-E_{k+q}+i\delta}\right],
\end{aligned}
\tag{2.19}
$$

where $n_F(E)$ is Fermi-Dirac distribution function, and δ is set to $0.06t$ for the numerical calculation in order to obtain smooth curves. Notice that, for the sDDW order, $\chi_0^{zz}(q,q',\omega) = 2\chi_0^{+-}(q,q',\omega)$ because up-spin and down-spin parts of the Hamiltonian are identical.

Applying random phase approximation, we obtain the RPA susceptibility [90, 17]

$$
\hat{\chi}^{zz}_{\text{RPA}}(q,q',\omega) = \sum_{q_1}\frac{\hat{\chi}_0^{zz}(q,q_1,\omega)}{\hat{I}-U\hat{\chi}_0^{zz}(q_1,q',\omega)} \tag{2.20}
$$

$$
\hat{\chi}^{+-}_{\text{RPA}}(q,q',\omega) = \sum_{q_1}\frac{\hat{\chi}_0^{+-}(q,q_1,\omega)}{\hat{I}-U\hat{\chi}_0^{+-}(q_1,q',\omega)} \tag{2.21}
$$

where $\hat{\chi}_0^{zz}(q,q',\omega)$ and $\hat{\chi}_0^{+-}(q,q',\omega)$ are the 2×2 matrices from Eqs. (2.16) and (2.17), respectively. For the numerical calculation, we compute the imaginary part of the diagonal terms of the RPA susceptibility ($q = q'$).

For unpolarized measurements, the scattering intensity I contains both the spin-flip and the non-spin-flip channels, $I \propto (\chi^{zz} + 2\chi^{+-})/3$. However, we will present the longitudinal and transverse susceptibilities separately so that it can provide more information about the polarized neutron scattering experiments, which may be achieved in the future.

For illustrative purposes, we set $t = 0.15$ eV, $t' = 0.32t$, $t'' = 0.1t'$ [3, 77, 28, 27], $W_0 = U = 0.65t$, $r = -0.1$ [111], and $k_BT = 0.05t$. The chemical potential is set to $\mu = -0.805t$ in order to obtain a hole doping level of $n_h \approx 10.07\%$, approximately the doping level in the experiment [39]. Other similar choices of the parameters will not change the conclusions.

In Fig. 2.1, the constant energy cuts of the imaginary part of the transverse spin susceptibility along a^* axis for $\omega \leq 0.6t$ are plotted. The results along b^* axis are similar and are not shown here. Away from $Q = (\pi/a, \pi/b)$, the magnetic excitations are peaked at the incommensurate positions $(q_x a, q_y b) = (\pi \pm \delta_a, \pi)$ and $(\pi, \pi \pm \delta_b)$, where we define the incommensurability δ_a and δ_b along a^* and b^* axes, respectively. From the numerical results, one finds that δ_a and δ_b are weakly energy dependent, similar to the inelastic neutron scattering experiment [39]. Furthermore, a prominent anisotropy in the incommensurability $\delta_b < \delta_a$ can be seen. With the hopping anisotropy $r = -0.1$, we obtain $\delta_a \approx (0.30 \pm 0.01)\pi$ and $\delta_b \approx (0.235 \pm 0.015)\pi$, which gives $\delta_b/\delta_a \approx 0.78$, which would be again similar to $\delta_b/\delta_a \approx 0.6$ reported in the neutron scattering experiments [39].

One may further adjust the parameters of this model to fit the experimental data, but that is not the goal of this work. We have varied the chemical potential, μ, to check how the dispersion relations vary with hole doping; results for different doping levels are qualitatively similar. In the doping range $8\% \leq n_h \leq 20\%$, there are always weakly energy-dependent incommensurate excitations, and the incommensurability δ_a and δ_b increase with increasing doping level n_h as shown in Fig. 2.2.

Note that hopping anisotropy is not necessary for the existence of the nearly vertical dispersions. To demonstrate this, the numerical results with isotropic hopping are plotted in Fig. 2.3. Here r is set to 0, $\mu = -0.806t$, and the hole doping level is $n_h = 10.03\%$. All the other parameters are the same as in Fig. 2.1. One can still find nearly vertical dispersions with incommensurability $\delta_a \approx (0.255 \pm 0.015)\pi$ even without the hopping anisotropy [45].

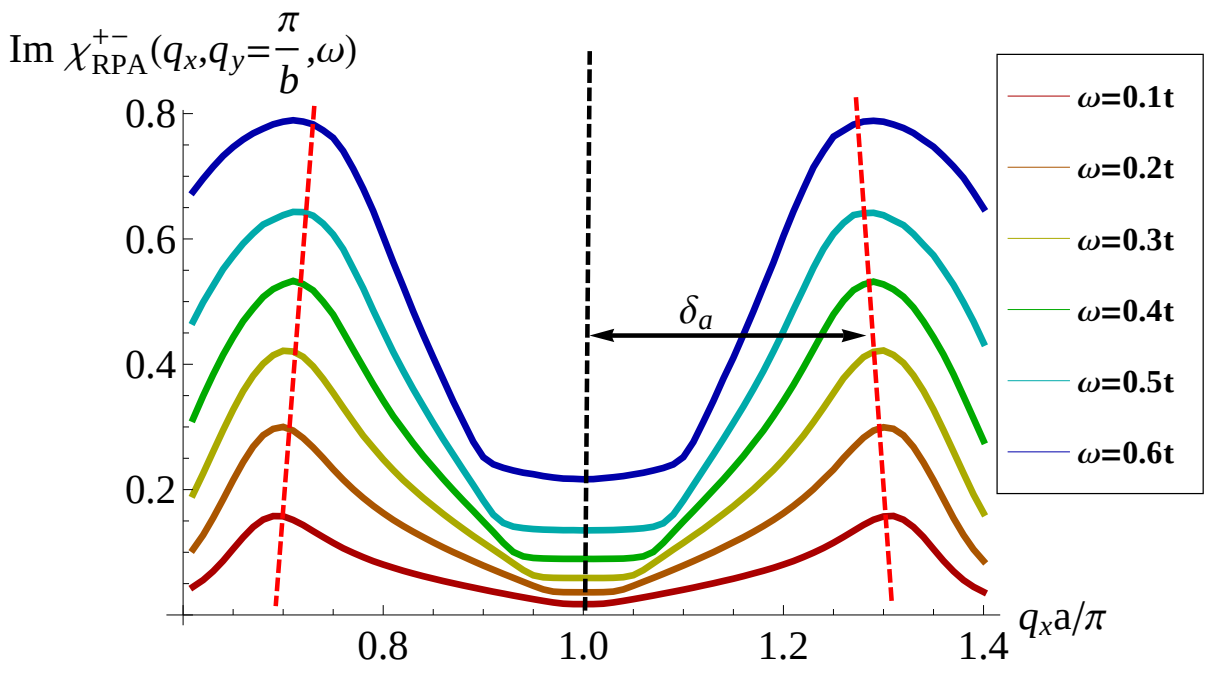

Figure 2.1: Constant energy cuts of $\mathrm{Im}\chi^{+-}_{\mathrm{RPA}}(q,\omega)$ along a^* axis when $q_y = \pi/b$ and $0.1t \leq \omega \leq 0.6t$ for the sDDW order. The weakly energy-dependent incommensurate peak positions are marked with red dashed lines. The results of $\mathrm{Im}\chi^{zz}_{\mathrm{RPA}}(q,\omega)$ are similar and omitted.

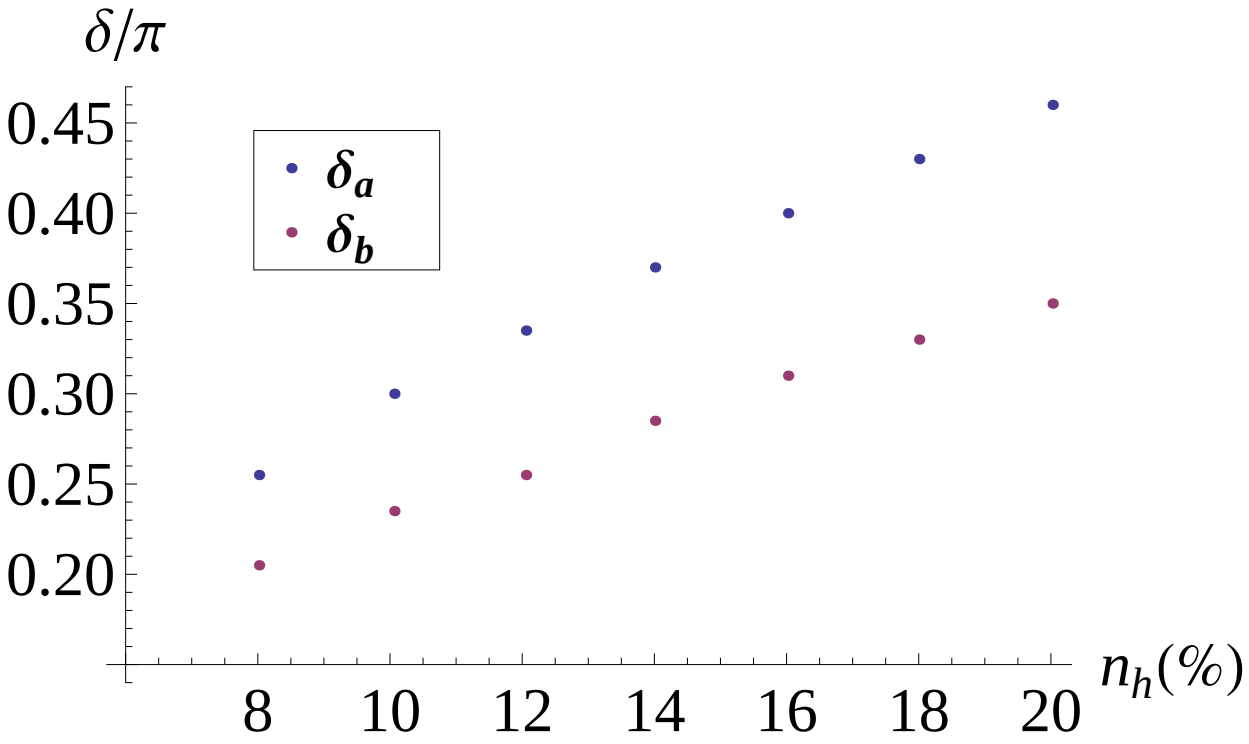

Figure 2.2: Doping-dependence of incommensurability δ_a and δ_b. Here μ is adjusted to obtain different doping levels, and all the other parameters are the same as in Fig. 2.1.

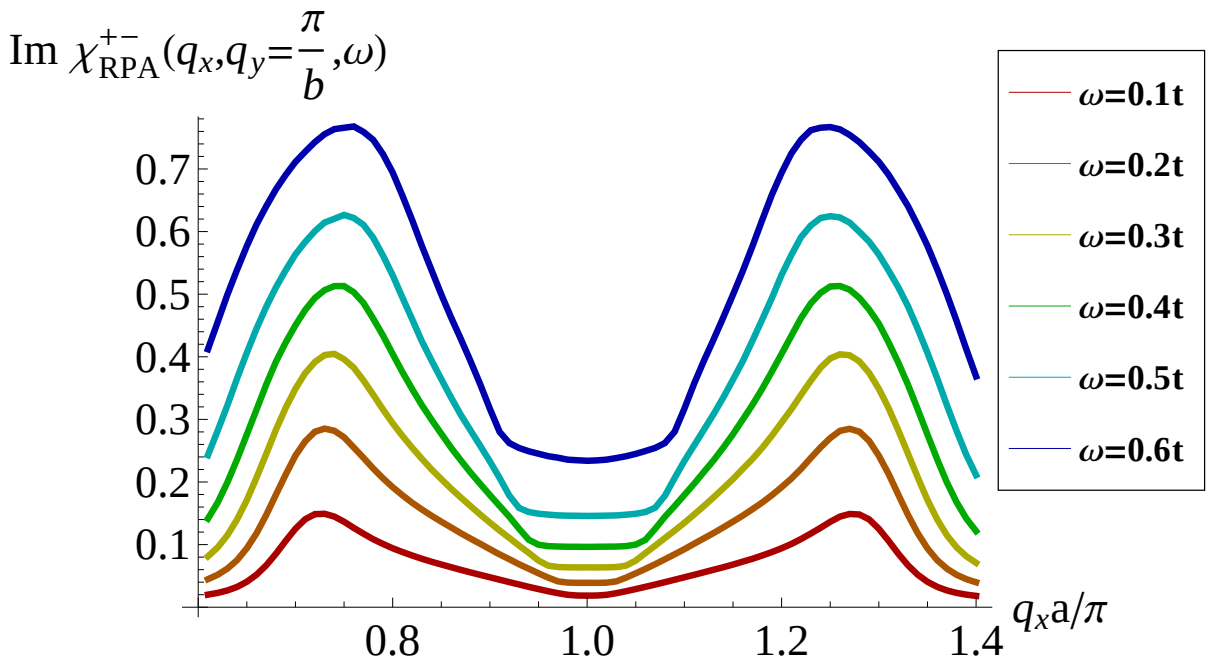

Figure 2.3: Constant energy cuts of $\mathrm{Im}\chi^{+-}_{\mathrm{RPA}}(q,\omega)$ along a^* axis when $q_y = \pi/b$ for the sDDW order without anisotropies. Here $r = 0$, $\mu = -0.806t$, and all the other parameters are the same as in Fig. 2.1.

The neutron scattering experiments show vertical dispersions in the energy range 30 meV $\leq \omega \leq 60$ meV [39], and the numerical results exhibit a nearly vertical dispersions up to $\omega \leq 0.6t = 90$ meV with the chosen parameters, which are similar to experiments. It is interesting to see how the excitation peaks evolve at higher energies, so in Fig. 2.4 we present the numerical results along the a^* axis for $0.7t \leq \omega \leq 1.4t$, where all the parameters are the same as in Fig. 2.1 except for the energy ω. The results along b^* axis are again so similar that they are not shown here. In Fig. 2.4, one finds that the high energy spin excitations are strongly energy dependent. The incommensurate peaks move toward $q = Q$ in the range $0.7t \leq \omega \leq 0.9t$, and eventually disappear at $\omega \approx 1.0t$, where the intensity around $q = Q$ is enhanced. When $\omega \approx 1.1t$, a central peak emerges at the commensurate position $q = Q$. As the energies are further increased, the central peak splits into two peaks deviating from Q with incommensurability δ'_a and δ'_b, which are marked by dashed lines. Unlike the low-energy incommensurability δ_a and δ_b, δ'_a and δ'_b are energy dependent and increase with increasing energies. Note that to observe δ'_a and δ'_b, the neutron scattering experiment needs to be performed with very high energies ($\omega \geq 1.1t = 165$ meV), or perhaps high-energy resonant inelastic x-ray scattering can be of use [60].

The reason for the unusual vertical dispersions at low energies and a different behavior at high energies can be understood by examining the imaginary part of Eq. (2.18). In this equation, the first two terms are interband contribution arising from the scattering from the upper band ($\epsilon_{2k} + E_k$) to the lower band ($\epsilon_{2k+q} - E_{k+q}$), and the scattering from the lower band ($\epsilon_{2k} - E_k$) to the upper band ($\epsilon_{2k+q} + E_{k+q}$). The last two terms, on the other hand, are intraband scattering. For the purpose of illustration, an example of the band structure and the scattering process is plotted in Fig. 2.5, where the interband and intraband scattering are shown with arrows.

The interband and intraband terms of Eq. (2.18) for $0.1t \leq \omega \leq 0.6t$ are plotted in Fig. 2.6 and Fig. 2.7, respectively. The results for higher energies $0.7t \leq \omega \leq 1.4t$ are not shown because they are very similar. From Fig. 2.6 and Fig. 2.7, one finds that the intensity near $q = Q$ is mainly from the contribution of the interband terms, whereas the contribution of the intraband terms arise when q is away from Q. From Eq. (2.18), we can see that at $q = Q$, the intraband terms vanish and only the interband terms contribute, leading to magnetic excitations peaked around $\omega \approx 1.1t$.

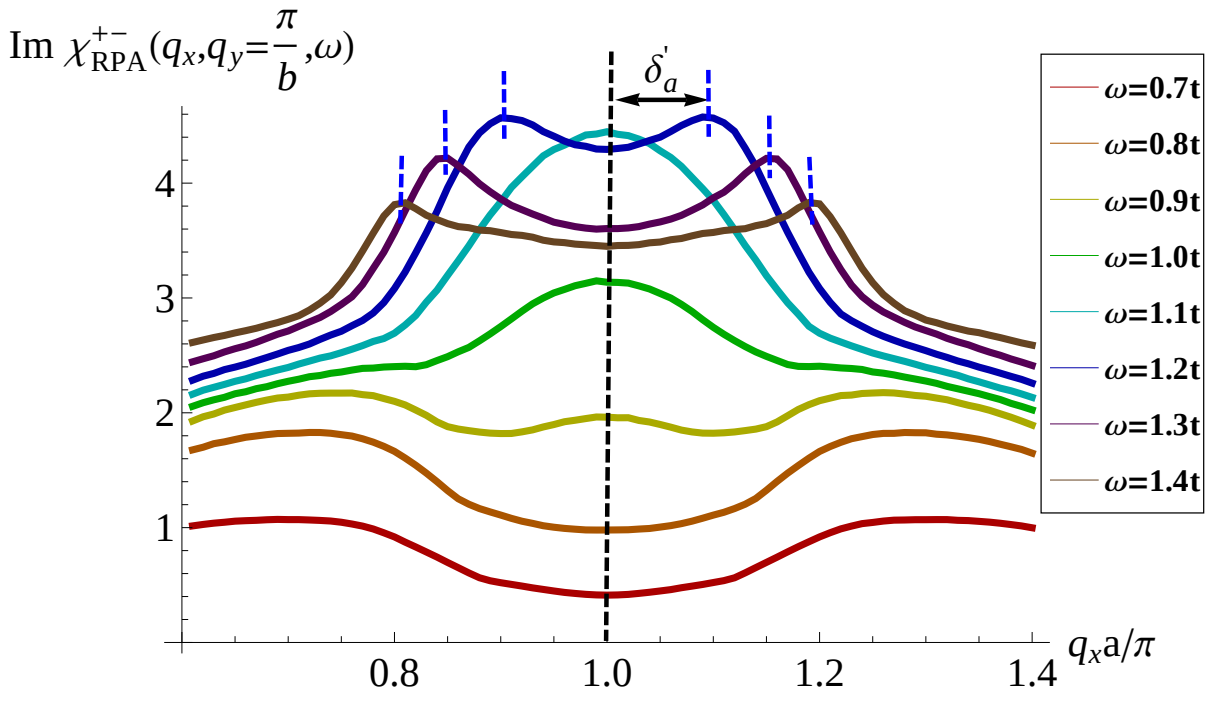

Figure 2.4: Constant energy cuts of $\mathrm{Im}\chi^{+-}_{\mathrm{RPA}}(q,\omega)$ along a^* axis when $q_y = \pi/b$ and $0.7t \leq \omega \leq 1.4t$ for the sDDW order. The energy-dependent incommensurate peak positions are marked with blue dashed lines.

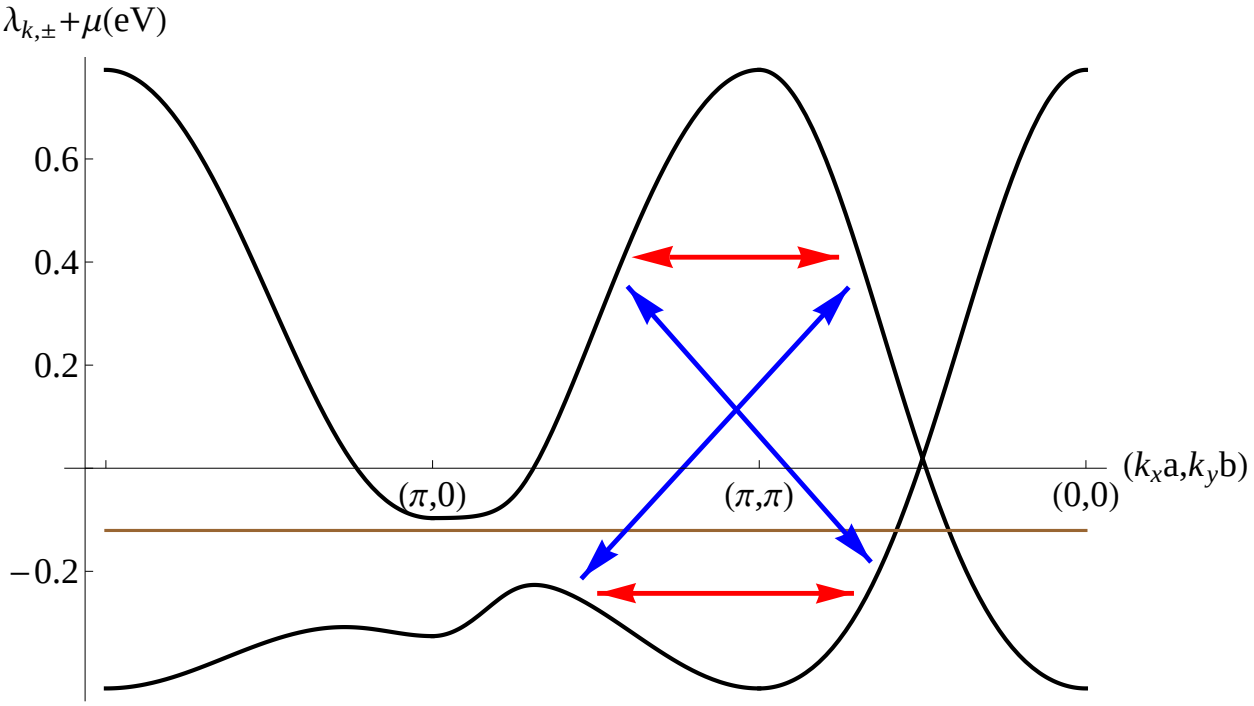

Figure 2.5: Energy spectrum $(\lambda_{k,\pm} + \mu)$ of the sDDW system as $(k_x a, k_y b)$ goes along the route: $(0,0) \rightarrow (\pi,0) \rightarrow (\pi,\pi) \rightarrow (0,0)$. The blue (red) arrows indicate the interband (intraband) scattering, and the brown line is the chemical potential μ. The parameters are the same as in Fig. 2.1.

In the vicinity of $q = Q$, interband terms still dominate, and we may expand them to first order in $\delta q \equiv |q - Q|$ and obtain

$$\begin{aligned} & \frac{-\pi}{N} \sum_k \left[n_F(\epsilon_{2k} \pm E_k) - n_F(\epsilon_{2k+q} \mp E_{k+q}) \right] \delta(\omega - \epsilon_{2k} \mp E_k + \epsilon_{2k+q} \mp E_{k+q}) \\ \simeq \; & \frac{\pi}{N} \sum_k \left[n_F(\epsilon_{2k} \mp E_k) - n_F(\epsilon_{2k} \pm E_k) + \vec{\nabla}_k(\epsilon_{2k} \mp E_k) \cdot \delta q \left. \frac{\partial n_F(E)}{\partial E} \right|_{E=\epsilon_{2k} \mp E_k} \right] \\ & \times \delta(\omega \mp 2E_k + \vec{\nabla}_k(\epsilon_{2k} \mp E_k) \cdot \delta q), \end{aligned} \tag{2.22}$$

which will be peaked at $\delta q = (\pm 2E_k - \omega) / \left[\vec{\nabla}_k(\epsilon_{2k} \mp E_k) \right]$. However, for low energies, the energy conservation condition cannot be satisfied unless E_k is very small, which diminishes the difference between the Fermi functions and thus suppresses the intensity. Therefore, there is no enhanced peak in the vicinity of $q = Q$ for low energies. For higher energies, the energy conservation factor will be satisfied, and the intensity at the incommensurate positions (δ'_a and δ'_b) will be enhanced and the excitation peaks can be seen as $\omega \gtrsim 1.1t$ in Fig. 2.4.

In contrast, away from $q = Q$, the intraband terms dominate. The peak positions of the energy conservation factor, $\delta(\omega - \epsilon_{2k} \mp E_k + \epsilon_{2k+q} \pm E_{k+q})$, move away from Q with increasing ω. On the other hand, the coherence factor $[1 + (\epsilon_{1k}\epsilon_{1k+q} + W_k W_{k+q})/(E_k E_{k+q})]$ vanishes at $q = Q$ and develops with increasing $|q - Q|$. For the chosen parameters, the energy dependence of these two opposite effects almost cancels out in the energy range $0 \leq \omega \leq 0.6t$, leading to the weakly energy-dependent positions of local maxima (δ_a and δ_b) as in Fig. 2.7. Such a dispersionless feature is sensitive to the parameters because it depends on whether the contribution of the intraband terms overcomes that of the interband terms away from Q. The nature of the excitation peaks due to the interband terms is distinct from the intraband terms. The dominant contribution of the interband terms are determined by the energy conservation factor and the Fermi functions, leading to sharper excitation peaks at $(\pi \pm \delta'_a, \pi)$ and $(\pi, \pi \pm \delta'_b)$, whereas the intraband terms also depend on the coherence factor, resulting in relatively broadened local maxima instead of sharp peaks at $(\pi \pm \delta_a, \pi)$ and $(\pi, \pi \pm \delta_b)$.

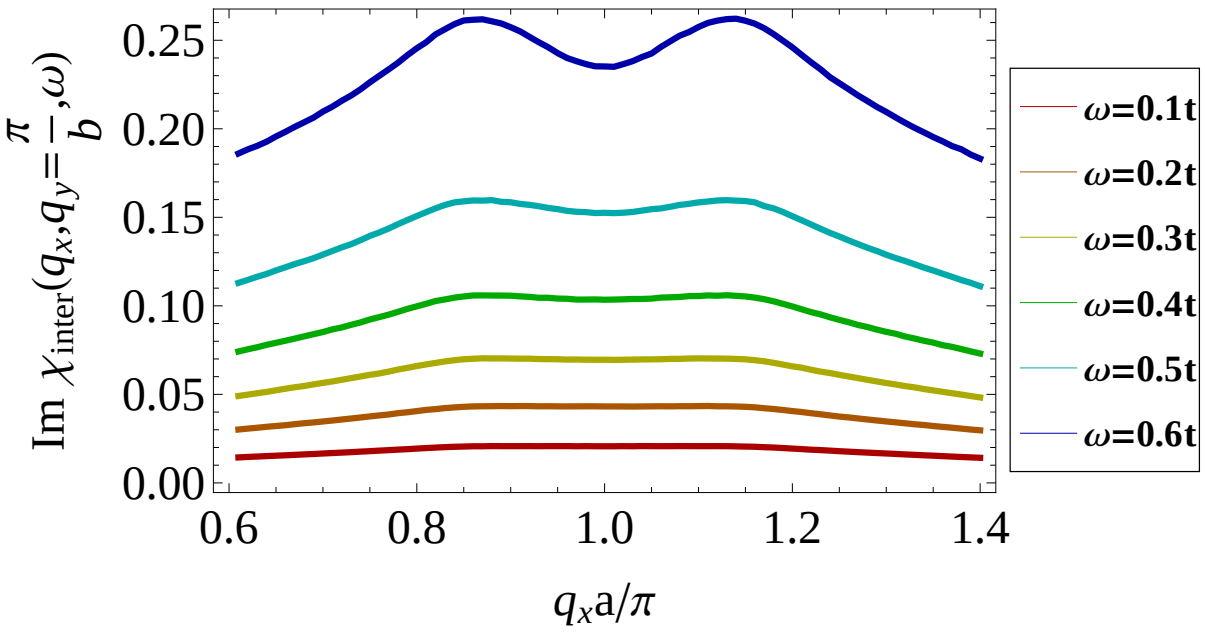

Figure 2.6: Constant energy cuts of the interband terms of $\text{Im}\chi_{\text{diag}}(q,\omega)$ in Eq. (2.18) along a^* axis when $q_y = \pi/b$ for $0.1t \leq \omega \leq 0.6t$.

2.3 Triplet d-density wave order

We now consider the tDDW order, and choose the spin quantization axis to be the z axis without any loss of generality, that is,

$$\langle c^\dagger_{k+Q,\alpha} c_{k,\beta} \rangle \propto i(\hat{d}\cdot\vec{\sigma}_{\alpha\beta})W_k = i(\hat{z}\cdot\vec{\sigma}_{\alpha\beta})W_k. \tag{2.23}$$

The tDDW mean-field Hamiltonian is therefore

$$\mathcal{H}_{\text{tDDW}} = \sum_\sigma \sum_k \left(\epsilon_k c^\dagger_{k,\sigma} c_{k,\sigma} + \epsilon_{k+Q} c^\dagger_{k+Q,\sigma} c_{k+Q,\sigma} + i\sigma W_k c^\dagger_{k,\sigma} c_{k+Q,\sigma} + h.c. \right), \tag{2.24}$$

which has the same eigenvalues as the sDDW Hamiltonian.

For the tDDW order, the Green's function matrices become

$$\hat{G}_\sigma(k, i\epsilon) = \frac{1}{(i\epsilon - \epsilon_{2k})^2 - E_k^2} \begin{pmatrix} i\epsilon + \epsilon_{1k} - \epsilon_{2k} & i\sigma W_k \\ -i\sigma W_k & i\epsilon - \epsilon_{1k} - \epsilon_{2k} \end{pmatrix}, \tag{2.25}$$

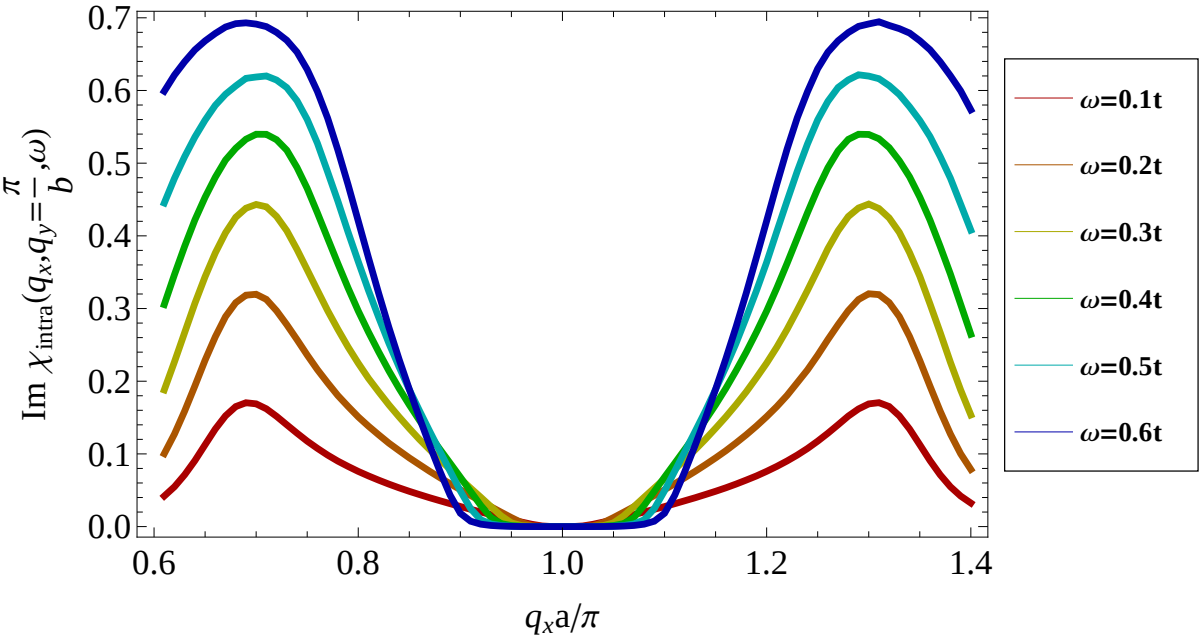

Figure 2.7: Constant energy cuts of the intraband terms of $\mathrm{Im}\chi_{\mathrm{diag}}(q,\omega)$ in Eq. (2.18) along a^* axis when $q_y = \pi/b$ for $0.1t \leq \omega \leq 0.6t$.

where $\sigma = +1$ for up-spin and $\sigma = -1$ for down-spin, and the spin susceptibility will become

$$\chi_0^{zz}(q,q',\omega) = \delta_{q,q'}\chi_{\rm diag}^{zz}(q,\omega), \tag{2.26}$$

$$\chi_0^{+-}(q,q',\omega) = \delta_{q,q'}\chi_{\rm diag}^{+-}(q,\omega) + \delta_{q,q'+Q}\chi_{\rm off}^{+-}(q,\omega), \tag{2.27}$$

where $\chi_{\rm diag}^{zz}(q,\omega)$ is the same as $\chi_{\rm diag}(q,\omega)$ in Eq. (2.18),

$$\begin{aligned}
&\chi_{\rm diag}^{+-}(q,\omega) \\
=\ & \frac{1}{2N}\sum_k \left(1 - \frac{\epsilon_{1k}\epsilon_{1k+q} - W_k W_{k+q}}{E_k E_{k+q}}\right) \\
&\quad \times \left[\frac{n_F(\epsilon_{2k}+E_k) - n_F(\epsilon_{2k+q}-E_{k+q})}{\omega - \epsilon_{2k} - E_k + \epsilon_{2k+q} - E_{k+q} + i\delta} + \frac{n_F(\epsilon_{2k}-E_k) - n_F(\epsilon_{2k+q}+E_{k+q})}{\omega - \epsilon_{2k} + E_k + \epsilon_{2k+q} + E_{k+q} + i\delta}\right] \\
&+\frac{1}{2N}\sum_k \left(1 + \frac{\epsilon_{1k}\epsilon_{1k+q} - W_k W_{k+q}}{E_k E_{k+q}}\right) \\
&\quad \times \left[\frac{n_F(\epsilon_{2k}+E_k) - n_F(\epsilon_{2k+q}+E_{k+q})}{\omega - \epsilon_{2k} - E_k + \epsilon_{2k+q} + E_{k+q} + i\delta} + \frac{n_F(\epsilon_{2k}-E_k) - n_F(\epsilon_{2k+q}-E_{k+q})}{\omega - \epsilon_{2k} + E_k + \epsilon_{2k+q} - E_{k+q} + i\delta}\right],
\end{aligned} \tag{2.28}$$

and

$$\begin{aligned}
&\chi_{\rm off}^{+-}(q,\omega) \\
=\ & \frac{-i}{2N}\sum_k \left(\frac{\epsilon_{1k}W_{k+q} + \epsilon_{1k+q}W_k}{E_k E_{k+q}}\right) \\
&\quad \times \left[-\frac{n_F(\epsilon_{2k}+E_k) - n_F(\epsilon_{2k+q}-E_{k+q})}{\omega - \epsilon_{2k} - E_k + \epsilon_{2k+q} - E_{k+q} + i\delta} - \frac{n_F(\epsilon_{2k}-E_k) - n_F(\epsilon_{2k+q}+E_{k+q})}{\omega - \epsilon_{2k} + E_k + \epsilon_{2k+q} + E_{k+q} + i\delta}\right. \\
&\quad \left. +\frac{n_F(\epsilon_{2k}+E_k) - n_F(\epsilon_{2k+q}+E_{k+q})}{\omega - \epsilon_{2k} - E_k + \epsilon_{2k+q} + E_{k+q} + i\delta} + \frac{n_F(\epsilon_{2k}-E_k) - n_F(\epsilon_{2k+q}-E_{k+q})}{\omega - \epsilon_{2k} + E_k + \epsilon_{2k+q} - E_{k+q} + i\delta}\right].
\end{aligned} \tag{2.29}$$

The RPA susceptibility of the tDDW order will be

$$\chi_{\rm RPA}^{zz}(q,q',\omega) = \frac{\chi_0^{zz}(q,q',\omega)}{1 - U\chi_0^{zz}(q,q',\omega)} \tag{2.30}$$

$$\hat{\chi}_{\rm RPA}^{+-}(q,q',\omega) = \sum_{q_1} \frac{\hat{\chi}_0^{+-}(q,q_1,\omega)}{\hat{I} - U\hat{\chi}_0^{+-}(q_1,q',\omega)}, \tag{2.31}$$

where $\chi_0^{zz}(q,q',\omega)$ is from Eq. (2.26) and $\hat{\chi}_0^{+-}(q,q',\omega)$ is a 2×2 matrix from Eq. (2.27).

The constant energy cuts of the imaginary part of the spin susceptibility of the tDDW order along a^* axis are shown in Fig. 2.8. The hopping anisotropy r is set to 0 for simplicity and the parameters are the same as in Fig. 2.3. The longitudinal susceptibility behaves similar to the sDDW order, whereas the transverse susceptibility is significantly different in the vicinity of $q = Q$. In comparison with the sDDW order, the intensity of $\mathrm{Im}\chi^{+-}_{\mathrm{RPA}}(q,\omega)$ of the tDDW order is suppressed in the vicinity of $q = Q$. The intensity exhibits a V-shaped curve around $q = Q$ at $\omega = 0.1t$, which evolves gradually to a U-shaped curve at $\omega = 0.6t$. Here we can also see the nearly vertical dispersion of the incommensurate spin excitations $\delta_a \approx (0.255 \pm 0.015)\pi$. Notice that for unpolarized measurements, with $I \propto (\chi^{zz} + 2\chi^{+-})/3$, there will still be the vertical dispersion away from $q = Q$.

The difference between the sDDW and tDDW order is that in $\chi^{+-}_{\mathrm{diag}}(q,\omega)$ of the tDDW order, Eq. (2.28), the $W_k W_{k+q}$ term of the coherence factor changes sign and reduces the interband contribution. As a result, the intensity in the vicinity of $q = Q$ is suppressed. The significant difference between the transverse and the longitudinal susceptibilities should permit one to distinguish the singlet and the triplet orders in spin-polarized measurements. On the other hand, the sign change of $W_k W_{k+q}$ does not affect the intraband terms as much as the interband terms, so the nearly vertical dispersions due to the intraband contribution can still be seen away from $q = Q$.

2.4 Spin density wave order

Finally, we also consider the SDW order, which has the order parameter

$$\langle c^\dagger_{k+Q,\alpha} c_{k,\beta} \rangle \propto (\hat{z} \cdot \vec{\sigma}_{\alpha\beta})\Delta_s. \tag{2.32}$$

The SDW mean-field Hamiltonian will be

$$\mathcal{H}_{\mathrm{SDW}} = \sum_\sigma \sum_k \left(\epsilon_k c^\dagger_{k,\sigma} c_{k,\sigma} + \epsilon_{k+Q} c^\dagger_{k+Q,\sigma} c_{k+Q,\sigma} + \sigma \Delta_s c^\dagger_{k,\sigma} c_{k+Q,\sigma} + h.c. \right), \tag{2.33}$$

where the eigenvalues now become $\lambda^S_{k,\pm} = \epsilon_{2k} \pm E^S_k$ with $E^S_k \equiv \sqrt{\epsilon^2_{1k} + \Delta^2_s}$.

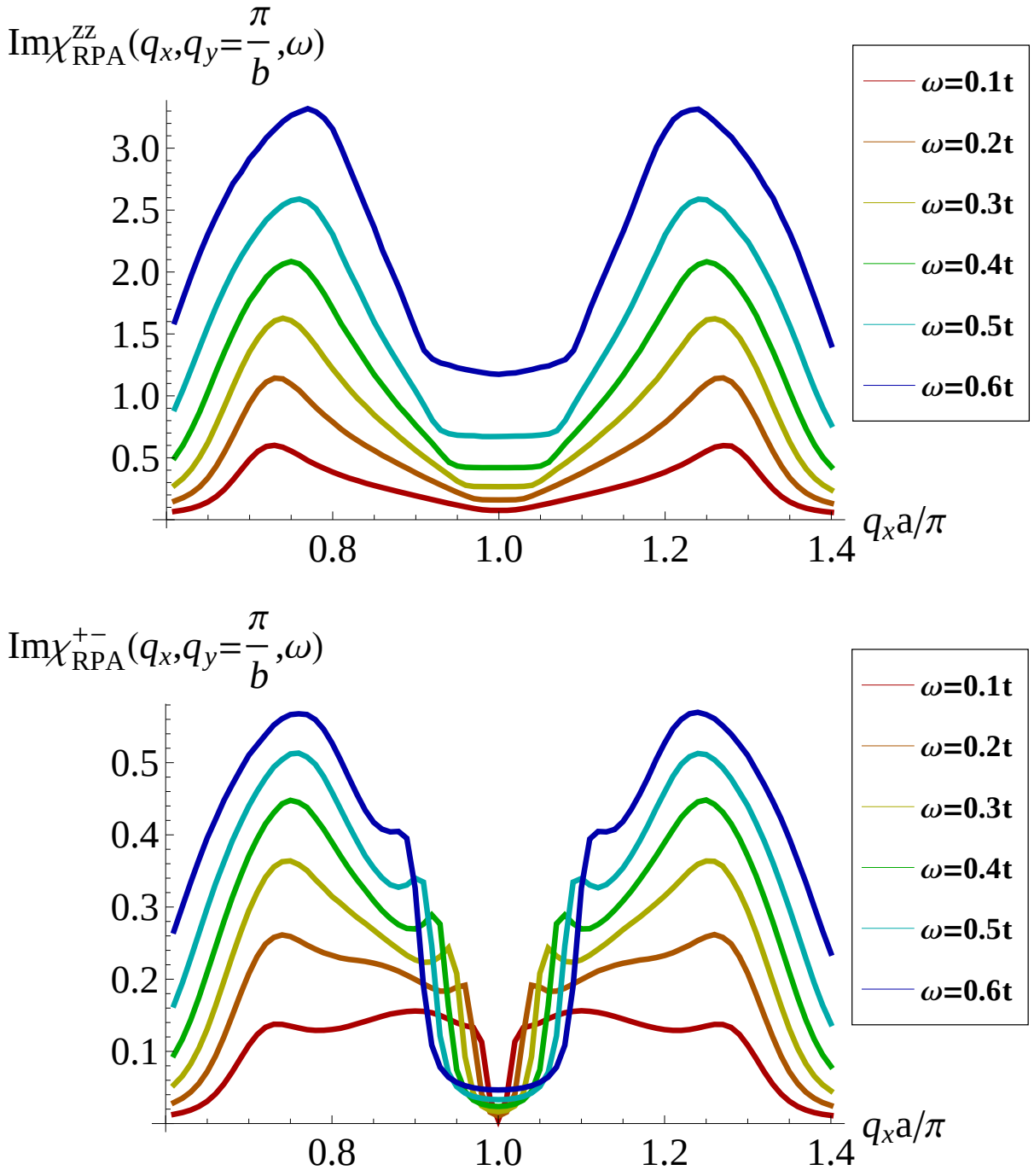

Figure 2.8: Constant energy cuts of $\mathrm{Im}\chi^{zz}_{\mathrm{RPA}}(q,\omega)$ (upper) and $\mathrm{Im}\chi^{+-}_{\mathrm{RPA}}(q,\omega)$ (lower) for the tDDW order along a^* axis when $q_y = \pi/b$. The parameters are the same as in Fig. 2.3.

For the SDW order, the Green's function matrices become

$$\hat{G}_\sigma(k,i\epsilon) = \frac{1}{(i\epsilon-\epsilon_{2k})^2-(E_k^S)^2}\begin{pmatrix} i\epsilon+\epsilon_{1k}-\epsilon_{2k} & \sigma\Delta_s \\ \sigma\Delta_s & i\epsilon-\epsilon_{1k}-\epsilon_{2k}\end{pmatrix}. \tag{2.34}$$

The longitudinal and transverse spin susceptibility are

$$\chi_0^{zz}(q,q',\omega) = \delta_{q,q'}\chi_{\rm diag}^{zz}(q,\omega), \tag{2.35}$$

$$\chi_0^{+-}(q,q',\omega) = \delta_{q,q'}\chi_{\rm diag}^{+-}(q,\omega)+\delta_{q,q'+Q}\chi_{\rm off}^{+-}(q,\omega), \tag{2.36}$$

where $\chi_{\rm diag}^{zz}(q,\omega)$, $\chi_{\rm diag}^{+-}(q,\omega)$, and $\chi_{\rm off}^{+-}(q,\omega)$ now become

$$\begin{aligned}
&\chi_{\rm diag}^{zz}(q,\omega) \\
=\;& \frac{1}{N}\sum_k\left(1-\frac{\epsilon_{1k}\epsilon_{1k+q}+\Delta_s^2}{E_k^S E_{k+q}^S}\right) \\
&\quad\times\left[\frac{n_F(\epsilon_{2k}+E_k^S)-n_F(\epsilon_{2k+q}-E_{k+q}^S)}{\omega-\epsilon_{2k}-E_k^S+\epsilon_{2k+q}-E_{k+q}^S+i\delta}+\frac{n_F(\epsilon_{2k}-E_k^S)-n_F(\epsilon_{2k+q}+E_{k+q}^S)}{\omega-\epsilon_{2k}+E_k^S+\epsilon_{2k+q}+E_{k+q}^S+i\delta}\right] \\
&+\frac{1}{N}\sum_k\left(1+\frac{\epsilon_{1k}\epsilon_{1k+q}+\Delta_s^2}{E_k^S E_{k+q}^S}\right) \\
&\quad\times\left[\frac{n_F(\epsilon_{2k}+E_k^S)-n_F(\epsilon_{2k+q}+E_{k+q}^S)}{\omega-\epsilon_{2k}-E_k^S+\epsilon_{2k+q}+E_{k+q}^S+i\delta}+\frac{n_F(\epsilon_{2k}-E_k^S)-n_F(\epsilon_{2k+q}-E_{k+q}^S)}{\omega-\epsilon_{2k}+E_k^S+\epsilon_{2k+q}-E_{k+q}^S+i\delta}\right],
\end{aligned} \tag{2.37}$$

$$\begin{aligned}
&\chi_{\rm diag}^{+-}(q,\omega) \\
=\;& \frac{1}{2N}\sum_k\left(1-\frac{\epsilon_{1k}\epsilon_{1k+q}-\Delta_s^2}{E_k^S E_{k+q}^S}\right) \\
&\quad\times\left[\frac{n_F(\epsilon_{2k}+E_k^S)-n_F(\epsilon_{2k+q}-E_{k+q}^S)}{\omega-\epsilon_{2k}-E_k^S+\epsilon_{2k+q}-E_{k+q}^S+i\delta}+\frac{n_F(\epsilon_{2k}-E_k^S)-n_F(\epsilon_{2k+q}+E_{k+q}^S)}{\omega-\epsilon_{2k}+E_k^S+\epsilon_{2k+q}+E_{k+q}^S+i\delta}\right] \\
&+\frac{1}{2N}\sum_k\left(1+\frac{\epsilon_{1k}\epsilon_{1k+q}-\Delta_s^2}{E_k^S E_{k+q}^S}\right) \\
&\quad\times\left[\frac{n_F(\epsilon_{2k}+E_k^S)-n_F(\epsilon_{2k+q}+E_{k+q}^S)}{\omega-\epsilon_{2k}-E_k^S+\epsilon_{2k+q}+E_{k+q}^S+i\delta}+\frac{n_F(\epsilon_{2k}-E_k^S)-n_F(\epsilon_{2k+q}-E_{k+q}^S)}{\omega-\epsilon_{2k}+E_k^S+\epsilon_{2k+q}-E_{k+q}^S+i\delta}\right],
\end{aligned} \tag{2.38}$$

and

$$
\begin{aligned}
&\chi^{+-}_{\rm off}(q,\omega) \\
= \;& \frac{\Delta_s}{2N}\sum_k \Bigg[\left(\frac{-E^S_k + E^S_{k+q}}{E^S_k E^S_{k+q}}\right) \frac{n_F(\epsilon_{2k}+E^S_k) - n_F(\epsilon_{2k+q}+E^S_{k+q})}{\omega+\epsilon_{2k}+E^S_k-\epsilon_{2k+q}-E^S_{k+q}+i\delta} \\
&+ \left(\frac{E^S_k - E^S_{k+q}}{E^S_k E^S_{k+q}}\right) \frac{n_F(\epsilon_{2k}-E^S_k) - n_F(\epsilon_{2k+q}-E^S_{k+q})}{\omega+\epsilon_{2k}-E^S_k-\epsilon_{2k+q}+E^S_{k+q}+i\delta} \\
&+ \left(\frac{E^S_k + E^S_{k+q}}{E^S_k E^S_{k+q}}\right) \frac{n_F(\epsilon_{2k}+E^S_k) - n_F(\epsilon_{2k+q}-E^S_{k+q})}{\omega+\epsilon_{2k}+E^S_k-\epsilon_{2k+q}+E^S_{k+q}+i\delta} \\
&- \left(\frac{E^S_k + E^S_{k+q}}{E^S_k E^S_{k+q}}\right) \frac{n_F(\epsilon_{2k}-E^S_k) - n_F(\epsilon_{2k+q}+E^S_{k+q})}{\omega+\epsilon_{2k}-E^S_k-\epsilon_{2k+q}-E^S_{k+q}+i\delta} \Bigg] .
\end{aligned} \tag{2.39}
$$

The RPA susceptibility of the SDW order is in the same form as the tDDW order in Eqs. (2.30) and (2.31).

The constant energy cuts of $\mathrm{Im}\chi^{zz}_{\rm RPA}(q,\omega)$ and $\mathrm{Im}\chi^{+-}_{\rm RPA}(q,\omega)$ for the SDW order along a^* axis are plotted in Fig. 2.9. Here we set the SDW gap to be $\Delta_s = 0.65t$ and $\mu = -1.026t$. The hole doping level is $n_h = 10.02\%$. The results are interesting: $\mathrm{Im}\chi^{zz}_{\rm RPA}(q,\omega)$ and $\mathrm{Im}\chi^{+-}_{\rm RPA}(q,\omega)$ for SDW order seem to be 'interchanged' in comparison with those for the tDDW order in Fig. 2.8. In addition to this interchange, there is also a difference in the intensity around $q = Q$ between tDDW and SDW, which could be observed if spin-polarized experiments with high resolution could be achieved, although one cannot be sure because of the non-universal nature of this difference. Away from $q = Q$, we can also see the vertical dispersions of the incommensurate spin excitations with $\delta_a \approx 0.28\pi$. Again, for unpolarized measurements, there will still be the vertical dispersion away from $q = Q$.

To understand the swap of the susceptibilities between tDDW and SDW, we should compare Eq. (2.18) and Eq. (2.28) for the tDDW with Eq. (2.37) and Eq. (2.38) for the SDW; we can see that at $q = Q$, $W_k W_{k+q} = -W_k^2$ in tDDW, and this leads to a minus sign, while Δ_s^2 in SDW does not. Therefore, the form of the coherence factors of SDW is opposite to tDDW in the vicinity of $q = Q$. As a result, the intensity of $\mathrm{Im}\chi^{+-}_{\rm RPA}(q,\omega)$ for SDW in the vicinity of $q = Q$ is enhanced due to the dominant interband contribution, whereas the intensity of $\mathrm{Im}\chi^{zz}_{\rm RPA}(q,\omega)$ is suppressed in the vicinity of $q = Q$. Thus, the difference in coherence factors leads to the "interchanging" behavior

between tDDW and SDW; the different momentum dependence of the order parameters also leads to distinct momentum dependence around $q = Q$. Away from $q = Q$, on the other hand, both $\mathrm{Im}\chi^{+-}_{\mathrm{RPA}}(q,\omega)$ and $\mathrm{Im}\chi^{zz}_{\mathrm{RPA}}(q,\omega)$ show vertical dispersion relations due to intraband contributions.

2.5 Conclusion

In conclusion, we have attempted to provide an explanation of a recent neutron scattering measurement in an underdoped high-temperature superconductor, which points to the fact that the pseudogap state is not a continuation of the superconducting state below T_c. The salient feature is a vertical dispersion seen above T_c in the spin excitations, as opposed to an hourglass shape dispersion seen below T_c. We have also explicitly checked that the consistency with experiments does not require any fine tuning of the parameter. In fact, as demonstrated, the vertical dispersion observed in our calculation does not require a-b anisotropy (see Fig. 2.3); of course, on phenomenological grounds, anisotropy should be included, as it has been included here. Note that our peaks appear to be sharper than those observed in experiments.

Although couched in the language of Hartree-Fock theory augmented by RPA, a thorough analysis of the properties of various alternate order parameters should be a useful guide. We also checked a band structure to contain electron pockets as well, but the robust aspects of the conclusions were unchanged. The vertical dispersion feature appears to persist in the doping range $8\% \leq n_h \leq 20\%$. At higher energies, we find energy-dependent incommensurability due to the interband contributions. We also contrast the spin dynamics of the tDDW and SDW orders, which exhibit different features around $q = Q$, which could, in principle, allow one to identify the spin nature of the underlying phase in a spin-polarized neutron scattering experiment with high resolution. The transverse and the longitudinal spin dynamics are interchanged between SDW and tDDW. In principle, a whole class of higher angular momentum particle-hole condensates are possible. Experimental evidence of these order parameters should be a major step forward. The tDDW is such an unconventional hidden order that its discovery would be of great importance. Note that tDDW is even invariant under time reversal.

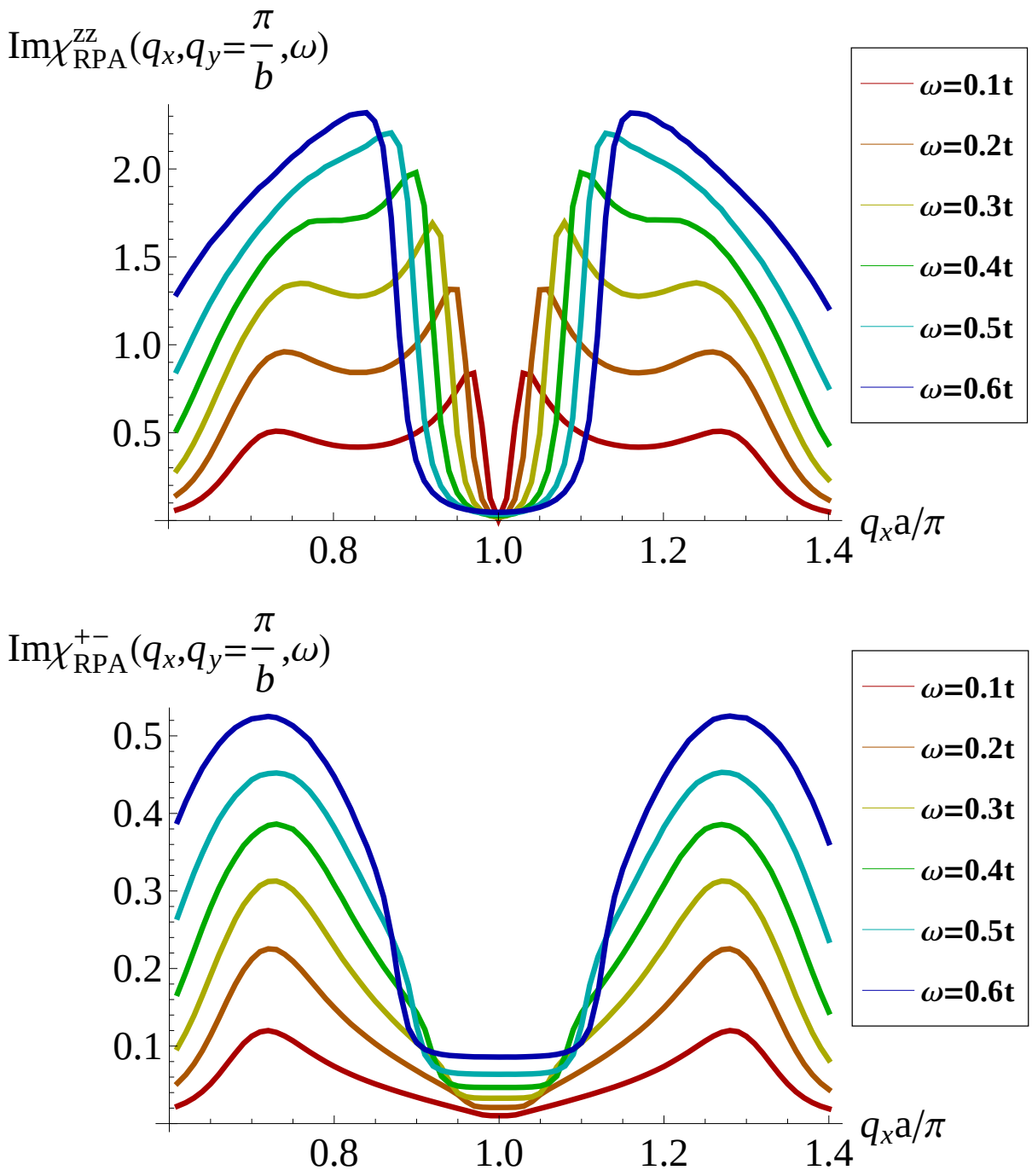

Figure 2.9: Constant energy cuts of $\mathrm{Im}\chi^{zz}_{\mathrm{RPA}}(q,\omega)$ (upper) and $\mathrm{Im}\chi^{+-}_{\mathrm{RPA}}(q,\omega)$ (lower) for the SDW order along a^* axis when $q_y = \pi/b$. Here $\Delta_s = 0.65t$, $\mu = -1.026t$, and the other parameters are the same as in Fig. 2.8.

CHAPTER 3

Topology of the mixed singlet-triplet d-density wave state

3.1 Introduction

In a recent paper, Nayak [71] provided an elegant classification of density wave states of nonzero angular momentum. The surprise is that given the roster of the multitude of such states, so few are experimentally observed. Of these, the angular momentum $\ell = 2$, spin singlet has taken on a special significance in the context of pseudogaps in cuprate high-temperature superconductors [13]. It breaks translational symmetry and gives rise to a momentum-dependent $d_{x^2-y^2}$ gap. The so called singlet d-density wave (sDDW) order does not modulate charge or spin, but produces staggered circulating charge currents from plaquette to plaquette much like an antiferromagnet. In its pristine form, in the half-filled limit, that is, for one electron per site, the Fermi surface of sDDW consists of four Dirac points and is therefore a semimetal. This broken symmetry state has inspired much effort in characterizing the pseudogap as a phase with an order parameter distinct from a fluctuating superconducting order parameter.

Presently, it appears from many experiments that the pseudogap may be susceptible to a host of possible competing orders [105, 62, 1, 16, 29, 8]. Thus it is important and interesting to explore an order parameter closely related to the sDDW, which retains many of its primary signatures, such as the broken translational symmetry or a particle-hole condensate of higher angular momentum. In particular we consider a density wave of nonzero angular momentum of mixed singlet and triplet varieties such that in the half-filled limit, it is a gapped insulator. Unlike the semimetallic sDDW, it has a nonvanishing quantized spin Hall effect for a range of values of the chemical potential. This is in fact a topological Mott insulator [80] because it is the electron-electron interaction that

is necessary for it to be realized. Further addition of charge carriers, doping, leads to Lifshitz transitions destroying the quantization but not the very existence of the spin Hall effect.

It is remarkable that such an unconventional broken symmetry, possibly relevant to high-temperature superconductors, belongs to the same class of recently discussed novel state of matter known as topological insulators; in fact, our work is to some extent motivated by these recent developments [35, 79]. We wish to emphasize that the undoped parent compounds of high-temperature superconductors are proven to be antiferromagnets with sizeable moments and the spin density wave transforms according to $\ell = 0$ [11]. The proposed topological density wave should therefore be relevant at larger doping that perhaps originates from a nearby insulating state. In no way is this different from the original suggestion of the sDDW order.

It has been known that triplet $i\sigma d_{x^2-y^2}$ order parameter corresponds to staggered circulating spin currents around a square plaquette [73], wherein the oppositely aligned spins circulate in opposite directions, as shown in Fig. 3.1. This reminds us of topological band insulators where oppositely aligned edge-spins travel in opposite directions. However, there is no topological protection because the bulk is not gapped, but is a semimetal instead. A more interesting case is the order parameter $(i\sigma d_{x^2-y^2} + d_{xy})$, where $\sigma = \pm 1$ for up and down spins, with the quantization axis along $\hat{z}$. Such a mixed singlet-triplet d-density wave (st-DDW) state not only satisfies time-reversal invariance but is also fully gapped, analogous to time-reversal-invariant band insulators discovered recently [47, 48]. A singlet chiral $(id_{x^2-y^2} + d_{xy})$ density wave that breaks macroscopic time-reversal symmetry was employed to deduce a possible polar Kerr effect and an anomalous Nernst effect [96, 113, 53, 54] in the pseudogap phase of the cuprates. Another topological state with a different symmetry of the order parameter was discussed in Ref. [83].

As to topological properties of superfluids, we refer to the book by Volovik [101]. Superconductors are particle-particle condensates, and, as such, the orbital wave function constrains the spin wave function because of the exchange symmetry. What we are discussing here are particle-hole condensates, and there is no exchange requirement between a particle and a hole. Thus, the orbital wave function *cannot* constrain the spin wave function. Thus an orbital wave function with even parity can come in both spin-singlet and -triplet varieties.

The plan of this chapter is as follows. Section 3.2 is divided into three parts. Section 3.2.1 discusses the topological aspects in the absence of magnetic field, while Sec. 3.2.2 contains results for a perpendicular magnetic field. Section 3.2.3 consists of a thorough discussion of the bulk-edge correspondence that follows from topological considerations. In Sec. 3.3, we discuss Fermi surface reconstruction via a Lifshitz transition as the system is doped. In Sec. 3.4, possible experimental detection schemes are suggested. The symmetry of the order parameter that we have introduced is such that the necessary experimental techniques are more subtle than the detection of more common broken symmetries, such as spin- or charge-density waves.

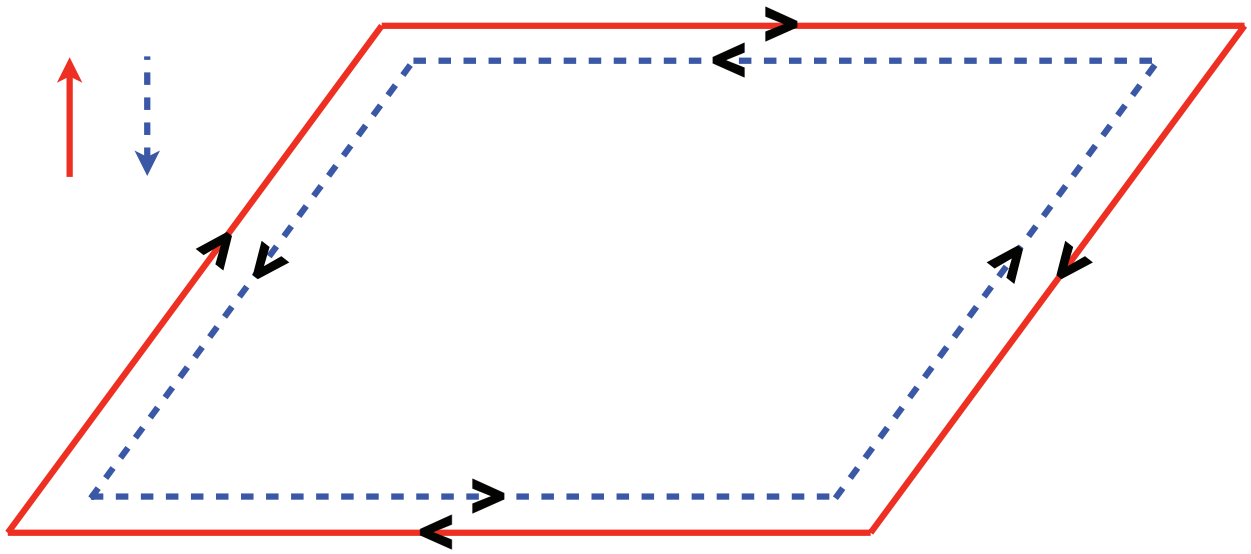

Figure 3.1: Triplet $i\sigma d_{x^2-y^2}$ density wave in the absence of an external magnetic field. The current pattern of each spin species on an elementary plaquette is shown. The state is a semimetal. On the other hand, $i\sigma d_{x^2-y^2} + d_{xy}$ can be fully gapped for a range of chemical potential. An example is shown in Fig. 3.2.

3.2 Order parameter topology

3.2.1 Zero external magnetic field

The order parameter that we consider is

$$\langle c^{\dagger}_{k+Q,\sigma} c_{k,\sigma'} \rangle = [\Phi^{\mu}(k)\tau^{\mu}]_{\sigma\sigma'}, \tag{3.1}$$

where $c^{\dagger}_{k,\sigma}(c_{k,\sigma})$ is the Fermion creation (annihilation) operator with momentum k and spin component σ; $\mu = 0, \cdots 3$; τ_1, τ_2, and τ_3 are the standard Pauli matrices and $\tau_0 = \mathbb{I}$ is the identity matrix. The nesting vector $\vec{Q} = (\pi/a, \pi/a)$. We choose the components of the order parameter to be

$$\Phi^3(k) \propto i\frac{W_0}{2}(\cos k_x - \cos k_y) \equiv iW_k \tag{3.2}$$

$$\Phi^0(k) \propto \Delta_0 \sin k_x \sin k_y \equiv \Delta_k. \tag{3.3}$$

and the remaining components are set to zero. The right-hand side is written in terms of the gap parameters and the conversion involves suitable coupling constants, which we do not need to specify in a non-self-consistent Hartree-Fock theory. The lattice spacing a is set to unity.

In the absence of an external magnetic field, the st-DDW Hamiltonian is

$$\mathcal{H}_{\text{st-DDW}} - \mu N = \sum_k \Psi^{\dagger}_k A_k \Psi_k, \tag{3.4}$$

where the summation is over the reduced Brillouin zone (RBZ) bounded by $k_y \pm k_x = \pm\pi$, and the spinor, $\Psi^{\dagger}_k$, is defined as $(c^{\dagger}_{k,\uparrow}, c^{\dagger}_{k+Q,\uparrow}, c^{\dagger}_{k,\downarrow}, c^{\dagger}_{k+Q,\downarrow})$. The chemical potential is subtracted for convenience, N being the number of particles. The matrix A_k is

$$A_k = \begin{pmatrix} \epsilon_k - \mu & \Delta_k + iW_k & 0 & 0 \\ \Delta_k - iW_k & \epsilon_{k+Q} - \mu & 0 & 0 \\ 0 & 0 & \epsilon_k - \mu & \Delta_k - iW_k \\ 0 & 0 & \Delta_k + iW_k & \epsilon_{k+Q} - \mu \end{pmatrix}, \tag{3.5}$$

with a generic set of band parameters,

$$\epsilon_k = \epsilon_{1k} + \epsilon_{2k} \tag{3.6}$$

$$\epsilon_{1k} = -2t(\cos k_x + \cos k_y),\ \epsilon_{2k} = 4t' \cos k_x \cos k_y. \tag{3.7}$$

We may choose $t = 0.15$ eV, renormalized by about a factor of 2 from band calculations [3, 77, 28, 27], $t' = 0.3t$, and $W_0 \sim -\Delta_0 \sim t \sim J$, where J is the antiferromagnetic exchange constant in high-temperature superconductors, for the purpose of illustration. Each of the two 2×2 blocks can be written in terms of two-component spinors, $\psi_{k,\sigma} = (c_{k,\sigma}, c_{k+Q,\sigma})^T$, $\sigma = \pm 1 \equiv (\uparrow, \downarrow)$; for example, for the up spin block we have

$$\mathcal{H}_\uparrow = \sum_k \psi^\dagger_{k,\uparrow} \left[(\epsilon_{2k} - \mu)\tau^0 + \epsilon_{1k}\tau^3 + \Delta_k \tau^1 - W_k \tau^2 \right] \psi_{k,\uparrow}. \tag{3.8}$$

The eigenvalues ($\pm$ refers to the upper and the lower bands, respectively)

$$\lambda_{k,\pm} = \epsilon_{2k} - \mu \pm E_k, \;\; E_k = \sqrt{\epsilon_{1k}^2 + W_k^2 + \Delta_k^2}. \tag{3.9}$$

are plotted in Fig. 3.2.

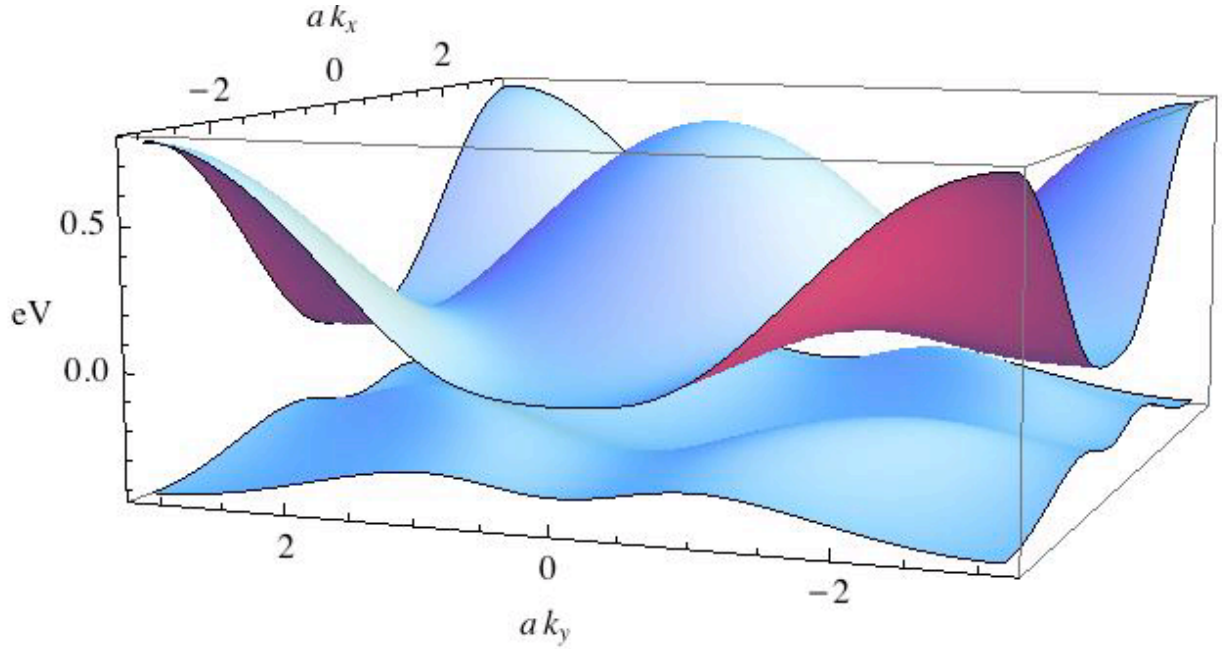

Figure 3.2: Energy spectra $\lambda_{k,\pm} + \mu$ of the st-DDW state. Here, for illustration, we have chosen $W_0 = t$, $\Delta_0 = -t$ and the band parameters, as described in the text. For the chemical potential μ anywhere within the spectral gap, the system is exactly half-filled and is a Mott insulator, unlike the semimetallic sDDW at half-filling.

Since up- and down-spin components are decoupled, the Chern number for each component

can be computed separately. Note that while the $(\epsilon_{2k}-\mu)$ term is present in the eigenvalues, it does not enter the eigenvectors, because the identity matrix commutes with the Pauli matrices. After diagonalizing the Hamiltonian, we can obtain the eigenvectors

$$|\Phi_{\sigma,\pm}(\mathbf{k})\rangle = (u_{\pm}e^{i\sigma\theta_k/2}, v_{\pm}e^{-i\sigma\theta_k/2})^{\mathbf{T}}, \tag{3.10}$$

where

$$u_{\pm}^2 = \frac{1}{2}\left(1 \pm \frac{\epsilon_{1k}}{E_k}\right), \tag{3.11}$$

$$v_{\pm}^2 = \frac{1}{2}\left(1 \mp \frac{\epsilon_{1k}}{E_k}\right), \tag{3.12}$$

$$\theta_k = \arctan\left(\frac{W_k}{\Delta_k}\right) + \pi\Theta(-\Delta_k), \tag{3.13}$$

where $\Theta(x)$ is Heaviside step function.

To compute the Berry phase of the eigenstates, we define the Berry curvature, $\vec{\Omega}_{\sigma,\pm}$ as

$$\vec{\Omega}_{\sigma,\pm} \equiv i\vec{\bigtriangledown}_k \times \langle\Phi_{\sigma,\pm}(\mathbf{k})|\vec{\bigtriangledown}_k|\Phi_{\sigma,\pm}(\mathbf{k})\rangle \tag{3.14}$$

Substituting the eigenstates into the above equation, the Berry curvature can be written as

$$\vec{\Omega}_{\sigma,\pm} = i\vec{\bigtriangledown}_k \times \left[(u_{\pm}^2 - v_{\pm}^2)\vec{\bigtriangledown}_k\left(i\sigma\frac{\theta_k}{2}\right)\right]. \tag{3.15}$$

Since $u_{\pm}$, $v_{\pm}$, and θ_k only depend on k_x and k_y, only the z component, $\Omega_{\sigma,\pm}$, is nonzero, which is given by

$$\begin{aligned}\Omega_{\sigma,\pm} &= \mp\frac{\sigma}{2}\left[\frac{\partial}{\partial k_x}\left(\frac{\epsilon_{1k}}{E_k}\right)\frac{\partial\theta_k}{\partial k_y} - \frac{\partial}{\partial k_y}\left(\frac{\epsilon_{1k}}{E_k}\right)\frac{\partial\theta_k}{\partial k_x}\right] \\ &= \pm\sigma\frac{1}{2E_k^3}\begin{vmatrix} \Delta_k & W_k & \epsilon_{1k} \\ \frac{\partial\Delta_k}{\partial k_x} & \frac{\partial W_k}{\partial k_x} & \frac{\partial\epsilon_{1k}}{\partial k_x} \\ \frac{\partial\Delta_k}{\partial k_y} & \frac{\partial W_k}{\partial k_y} & \frac{\partial\epsilon_{1k}}{\partial k_y} \end{vmatrix}.\end{aligned} \tag{3.16}$$

From the above determinant, we can see that the Berry curvature will be zero if one of Δ_k and W_k is zero, so we need a mixing of the $d_{x^2-y^2}$ and d_{xy} components to have a nontrivial topological invariant.

If we define the unit vector $\hat{n}_\sigma \equiv \vec{h}_\sigma/|\vec{h}_\sigma|$ with the pseudospin vector $\vec{h}_\sigma = (\Delta_k, -\sigma W_k, \epsilon_1)$, the Berry curvature can be written as

$$\Omega_{\sigma,\pm} = \mp\frac{1}{2}\hat{n}_\sigma \cdot \left(\frac{\partial \hat{n}_\sigma}{\partial k_x} \times \frac{\partial \hat{n}_\sigma}{\partial k_y}\right). \tag{3.17}$$

Now we will show that the Chern number for a general two by two Hamiltonian, which can be written in terms of the pseudospin vector (e.g. $\vec{h}_\sigma$ in this case), is quantized [81]. The Chern number, which is the Berry phase divided by 2π, can be written as

$$\begin{aligned} N_{\sigma,\pm} &= \int_{\text{RBZ}} \frac{d^2k}{2\pi}\, \Omega_{\sigma,\pm} \\ &= \mp \int_{\text{RBZ}} \frac{d^2k}{4\pi}\, \hat{n}_\sigma \cdot \left(\frac{\partial \hat{n}_\sigma}{\partial k_x} \times \frac{\partial \hat{n}_\sigma}{\partial k_y}\right). \end{aligned} \tag{3.18}$$

Since $\hat{n}_\sigma$ is a unit vector with three components, it can be parametrized with two variables, the polar angle and azimuthal angle; that is,

$$\hat{n}_\sigma = (\sin\theta_\sigma \cos\phi_\sigma, \sin\theta_\sigma \sin\phi_\sigma, \cos\theta_\sigma), \tag{3.19}$$

where $\theta_\sigma \in [0, \pi)$ and $\phi_\sigma \in [0, 2\pi)$. By utilizing the chain rule, we obtain

$$\begin{aligned} N_{\sigma,\pm} &= \mp\frac{1}{4\pi}\int_{\text{RBZ}} d^2k\, \hat{n}_\sigma \cdot \left[\left(\frac{\partial \hat{n}_\sigma}{\partial \theta_\sigma}\frac{\partial \theta_\sigma}{\partial k_x} + \frac{\partial \hat{n}_\sigma}{\partial \phi_\sigma}\frac{\partial \phi_\sigma}{\partial k_x}\right) \times \left(\frac{\partial \hat{n}_\sigma}{\partial \theta_\sigma}\frac{\partial \theta_\sigma}{\partial k_y} + \frac{\partial \hat{n}_\sigma}{\partial \phi_\sigma}\frac{\partial \phi_\sigma}{\partial k_y}\right)\right] \\ &= \mp\frac{1}{4\pi}\int_{\text{RBZ}} d^2k\, \hat{n}_\sigma \cdot \left(\frac{\partial \hat{n}_\sigma}{\partial \theta_\sigma} \times \frac{\partial \hat{n}_\sigma}{\partial \phi_\sigma}\right)\left(\frac{\partial \theta_\sigma}{\partial k_x}\frac{\partial \phi_\sigma}{\partial k_y} - \frac{\partial \theta_\sigma}{\partial k_y}\frac{\partial \phi_\sigma}{\partial k_x}\right) \\ &= \mp\frac{1}{4\pi}\int_{\text{int}} d\theta_\sigma d\phi_\sigma\, \hat{n}_\sigma \cdot \left(\frac{\partial \hat{n}_\sigma}{\partial \theta_\sigma} \times \frac{\partial \hat{n}_\sigma}{\partial \phi_\sigma}\right), \end{aligned} \tag{3.20}$$

where in the last step we change the integral from k-space to the internal space of $\hat{n}_\sigma$, and we also use the Jacobian of the change of variables from (k_x, k_y) to $(\theta_\sigma, \phi_\sigma)$; in other words,

$$d\theta_\sigma d\phi_\sigma = dk_x dk_y \begin{vmatrix} \frac{\partial \theta_\sigma}{\partial k_x} & \frac{\partial \theta_\sigma}{\partial k_y} \\ \frac{\partial \phi_\sigma}{\partial k_x} & \frac{\partial \phi_\sigma}{\partial k_y} \end{vmatrix}. \tag{3.21}$$

To proceed, we may use the following relations.

$$\frac{\partial \hat{n}_\sigma}{\partial \theta_\sigma} = \hat{\theta}_\sigma, \tag{3.22}$$

$$\frac{\partial \hat{n}_\sigma}{\partial \phi_\sigma} = \sin\theta_\sigma\, \hat{\phi}_\sigma. \tag{3.23}$$

Therefore,

$$\begin{aligned} N_{\sigma,\pm} &= \mp\frac{1}{4\pi}\int_{\text{int}} d\theta_\sigma d\phi_\sigma \sin\theta_\sigma \\ &= \mp\frac{1}{4\pi}\int_{\text{int}} d\Omega_\sigma^{\text{int}}, \end{aligned} \tag{3.24}$$

where $d\Omega_\sigma^{\text{int}}$ is the differential solid angle in the internal (pseudospin) space. Since the above integral is the solid angle spanned by the unit vector $\hat{n}_\sigma$, which is a multiple of 4π, $N_{\sigma,\pm}$ is therefore an integer.

For the st-DDW Hamiltonian, the Chern numbers are

$$\begin{aligned} N_{\sigma,\pm} &= \pm\sigma\int_{\text{RBZ}}\frac{d^2k}{2\pi}\frac{tW_0\Delta_0}{E_k^3}(\sin^2 k_y + \sin^2 k_x\cos^2 k_y) \\ &= \begin{cases} \pm\sigma, & \text{if } tW_0\Delta_0 \neq 0, \\ 0, & \text{if } tW_0\Delta_0 = 0. \end{cases} \end{aligned} \tag{3.25}$$

We can focus on the lower band as long as there is a gap between the upper and the lower bands. Then,

$$N_{\text{total}} = N_{\uparrow,-} + N_{\downarrow,-} = 0, \tag{3.26}$$

$$N_{\text{spin}} = N_{\uparrow,-} - N_{\downarrow,-} = (-1) - 1 = -2, \tag{3.27}$$

irrespective of the magnitudes of the dimensionful parameters. Note, however, that the Chern numbers vanish unless both Δ_0 and W_0 are nonvanishing. The quantization holds for a range of chemical potential μ, as can be seen from Fig. 3.2.

For the fully gapped case, there will be a quantized spin Hall conductance associated with the eigenstates. The ratio of the dimensions of the quantized spin Hall conductance to the quantized Hall conductance should be the same as the ratio of the spin to the charge carried by a particle, since in two dimensions for both quantities the scale dependence L^{d-2} cancels, that is,

$$\frac{[\sigma_{xy}^{\text{spin}}]}{[\sigma_{xy}]} = \frac{\frac{\hbar}{2}}{e}. \tag{3.28}$$

So, the quantized spin Hall conductance will be

$$\sigma_{xy}^{\text{spin}} = -\frac{e^2}{h}\frac{\hbar}{2e}N_{\text{spin}} = \frac{e}{2\pi} \tag{3.29}$$

The eigenstates, $|\Psi_{\sigma,\pm}(k)\rangle$, are also the eigenstates of $\mathbf{S}^2$ and $\mathbf{S}_z$ with eigenvalues $S^2 = \frac{3}{4}$ and $S_z = -\frac{\sigma}{2}$. Since the spin SU(2) is broken by the triplet component of the st-DDW order, one might wonder if the Goldstone modes not contained in the Hartree-Fock picture may not ruin the quantization. If SU(2) is broken down to U(1), then there is still a quantum number corresponding to, say S_z, which is transported by the edge currents in the system. More succinctly, as long as time-reversal symmetry is preserved, we will still have Kramers degeneracy in our Hartree-Fock state, and therefore the edge modes will remain protected.

3.2.2 Nonzero external magnetic field

In an infinitesimal external magnetic field, $\vec{H}$, there will be a spin flop transition in the absence of explicit spin-orbit coupling, as shown in Fig. 3.3. We can assume $\vec{H} = H\hat{z}$ and the spins quantized along the $\hat{x}$ direction without any loss of generality. Then the Hamiltonian now becomes

$$\mathcal{H}_{\text{st-DDW}} = \sum_k \Psi_k^\dagger A_k \Psi_k \tag{3.30}$$

As before, the summation is over the RBZ, and the spinor is the same. The matrix A_k is now

$$A_k = \begin{pmatrix} \epsilon_{k,\uparrow} & 0 & 0 & \Delta_k + iW_k \\ 0 & \epsilon_{k+Q,\uparrow} & -\Delta_k - iW_k & 0 \\ 0 & -\Delta_k + iW_k & \epsilon_{k,\downarrow} & 0 \\ \Delta_k - iW_k & 0 & 0 & \epsilon_{k+Q,\downarrow} \end{pmatrix}, \tag{3.31}$$

where $\epsilon_{k,\sigma} = \epsilon_k + \sigma\frac{g\mu_B H}{2} = \epsilon_k + \sigma\gamma$. Although the spin-up and -down components are coupled, particles with momentum k and spin up only couple to holes with momentum $k+Q$ and spin down, and vice versa. Therefore, by redefining the spinor, $\Psi_k^{'\dagger} \equiv (c_{k,\uparrow}^\dagger, c_{k+Q,\downarrow}^\dagger, c_{k,\downarrow}^\dagger, c_{k+Q,\uparrow}^\dagger)$, the Hamiltonian can still be expressed as a block diagonal matrix: $\mathcal{H}_{\text{st-DDW}} = \sum_k \Psi_k^{'\dagger} A_k' \Psi_k'$. The Chern numbers for each subblock, $i = 1, 2$, can be calculated as before. Therefore, defining η_i = + 1 or -1 for $i = 1$ or 2, we obtain $E_{k,i} = [(\epsilon_{1k} + \eta_i\gamma)^2 + W_k^2 + \Delta_k^2]^{1/2}$, and the Berry curvature

$$\Omega_{i,\pm} = \mp\frac{1}{2E_{k,i}^3}\vec{h}_i \cdot (\frac{\partial\vec{h}_i}{\partial k_x} \times \frac{\partial\vec{h}_i}{\partial k_y}), \tag{3.32}$$

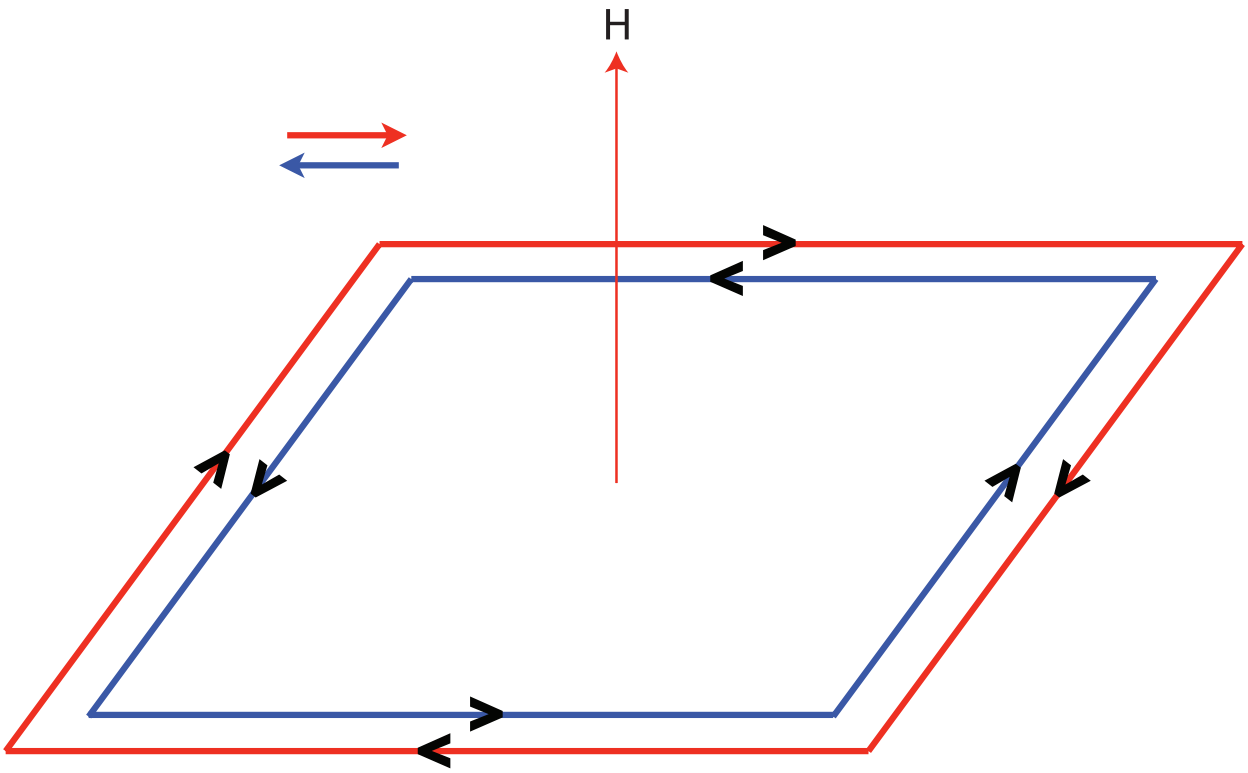

Figure 3.3: Spins are flopped perpendicular to the applied magnetic field $\vec{H} = H\hat{z}$. Contrast with Fig. 3.1.

where $\vec{h}_i = (\eta_i \Delta_k, -W_k, \epsilon_1 + \eta_i \gamma)$. Performing a surface integration of the Berry curvature we get

$$\begin{aligned} N_{i,\pm} &= \int_{\text{RBZ}} \frac{d^2k}{2\pi} \Omega_{i,\pm} \\ &= \pm \eta_i t W_0 \Delta_0 \int_{\text{RBZ}} \frac{d^2k}{2\pi E_{k,i}^3} \Big[\sin^2 k_y + \sin^2 k_x \cos^2 k_y \\ &\qquad - \frac{\eta_i \gamma}{4t} (\cos k_x \sin^2 k_y + \sin^2 k_x \cos k_y) \Big] . \end{aligned} \tag{3.33}$$

The $\pm$ refers to the upper and the lower band, respectively. The integral does not depend on the external field, nor on the magnitude of the parameters t, W_0, and Δ_0. The Chern numbers are

$$N_{i,\pm} = \pm \eta_i, \tag{3.34}$$

$$N_{\text{total}} = N_{1,-} + N_{2,-} = 0, \tag{3.35}$$

$$N_{\text{spin}} = N_{1,-} - N_{2,-} = -2, \tag{3.36}$$

Once again the spin Hall conductance is quantized, but the charge quantum Hall effect vanishes. The flopped spins carry the same current as before. The corresponding spin Hall conductance, as long as the gap survives, is

$$\sigma_{xy}^{\text{spin}} = \frac{e}{2\pi}. \tag{3.37}$$

The eigenstates, $|\Phi_{i,\pm}(k)\rangle$, are the eigenstates of $\mathbf{S}^2$ with eigenvalues $S^2 = \frac{3}{4}$, but not eigenstates of $\mathbf{S}_z$ because of the mixing of up and down spins.

3.2.3 Bulk-edge correspondence

For the st-DDW order, the bulk-edge correspondence can be studied by open boundary condition in the x direction but periodic boundary condition in the y direction, that is, by cutting open the torus. The edge modes, if they exist, will reside on the ends of the cylinder. The cut then leads to a Hamiltonian

$$\mathcal{H}_{\text{cylinder}} = \sum_{k_y,i,j} \Psi_{i,k_y}^\dagger A_{ij}(k_y) \Psi_{j,k_y}, \tag{3.38}$$

where the spinor is $\Psi_{i,k_y} = (c_{i,k_y\uparrow}c_{i,k_y+\pi\uparrow}, c_{i,k_y\downarrow}c_{i,k_y+\pi\downarrow})^T$, and $A_{ij}(k_y)$ is a $4N \times 4N$ matrix parametrized by the wave vector k_y, which is given by

$$A_{ij}(k_y) = \begin{pmatrix} T_{ij}(k_y) & S_{ij,\uparrow}(k_y) & 0 & 0 \\ S^{\dagger}_{ij,\uparrow}(k_y) & T_{ij}(k_y+\pi) & 0 & 0 \\ 0 & 0 & T_{ij}(k_y) & S_{ij,\downarrow}(k_y) \\ 0 & 0 & S^{\dagger}_{ij,\downarrow}(k_y) & T_{ij}(k_y+\pi) \end{pmatrix}, \tag{3.39}$$

where $T_{ij}(k_y)$ and $S_{ij,\sigma}(k_y)$ are $N \times N$ matrices,

$$T_{ij}(k_y) = \begin{pmatrix} -\mu - 2t\cos k_y & -t + 2t'\cos k_y & 0 & \cdots & \cdots \\ -t + 2t'\cos k_y & -\mu - 2t\cos k_y & -t + 2t'\cos k_y & \cdots & \cdots \\ 0 & -t + 2t'\cos k_y & -\mu - 2t\cos k_y & -t + 2t'\cos k_y & \cdots \\ \vdots & \vdots & \vdots & \ddots & -t + 2t'\cos k_y \\ & & & -t + 2t'\cos k_y & -\mu - 2t\cos k_y \end{pmatrix} \tag{3.40}$$

and

$$S_{ij,\sigma}(k_y) = i\sigma\frac{W_0}{4}\begin{pmatrix} -2\cos k_y & -1 & 0 & \cdots & \\ 1 & 2\cos k_y & 1 & \cdots & \\ 0 & -1 & -2\cos k_y & -1 & \cdots \\ \vdots & \vdots & \vdots & \ddots & (-1)^{N-1} \\ & & & (-1)^N & (-1)^N 2\cos k_y \end{pmatrix}$$
$$+ i\frac{\Delta_0}{2}\sin k_y \begin{pmatrix} 0 & 1 & 0 & \cdots & \\ 1 & 0 & -1 & \cdots & \\ 0 & -1 & 0 & 1 & \cdots \\ \vdots & \vdots & \vdots & \ddots & (-1)^N \\ & & & (-1)^N & 0 \end{pmatrix}. \tag{3.41}$$

The corresponding one-dimensional system with N sites depends on the band structure and the order parameters defined above.

The eigenvalue spectra are shown in Fig 3.4. The spectra, degenerate for up and down spins, are plotted in the range $0 \leq k_y \leq \pi$ ($k_y < 0$ can be obtained by reflection). To find the edge states,

we choose the chemical potential in the gap. In Fig. 3.4, we put $\mu = -0.075$ eV for the purpose of illustration. There are two edge states with positive group velocity, one with up spin and the other with down spin. Let them be $\psi_{>,\uparrow}$ and $\psi_{>,\downarrow}$, respectively. There are also two edge modes with negative group velocity denoted as $\psi_{<,\uparrow}$ and $\psi_{<,\downarrow}$ for up spin and down spin, respectively. By explicitly computing the support of each of these wave functions, we have verified that electrons in states $\psi_{>,\downarrow}$ and $\psi_{<,\uparrow}$ are localized near the left edge of the system whereas those in states $\psi_{<,\downarrow}$ and $\psi_{>,\uparrow}$ are localized near the right edge. The localization length of these states is essentially a lattice spacing; an example is shown in Fig 3.4.

It is interesting to see how this spectra compare with the one where periodic boundary conditions are applied in both x and y directions. After diagonalizing the Hamiltonian, we plot the spectra for a fixed value of k_y for all values of the energies. The results are shown in Fig. 3.5, which are essentially identical to Fig. 3.4, except that the edge states are missing.

3.3 Fermi surface and Lifshitz transition

It is interesting to track the evolution of successive Lifshitz transitions as we change the parameters. At first, when we lower the chemical potential, four hole pockets will open up in the full Brillouin zone, as shown in Fig. 3.6, and the corresponding spin Hall effect will lose its quantization but not the effect itself. However, in mean-field theory this cannot continue indefinitely with the nodal or the antinodal gaps fixed, so the parameters W_0 and Δ_0 will also decrease and will lead to a further opening of two electron pockets in the full Brillouin zone, as shown in Fig. 3.6. Ultimately, when the doping is increased further, the large Fermi surface will emerge as a further Lifshitz transition. There is good evidence that such Lifshitz transitions indeed occur in high-temperature superconductors [61, 22, 21].

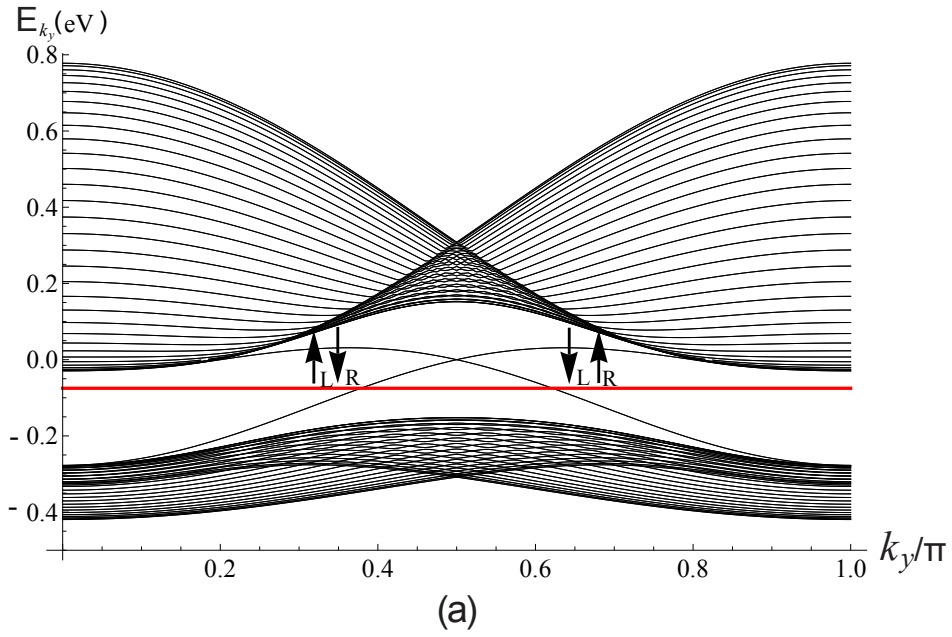

(a)

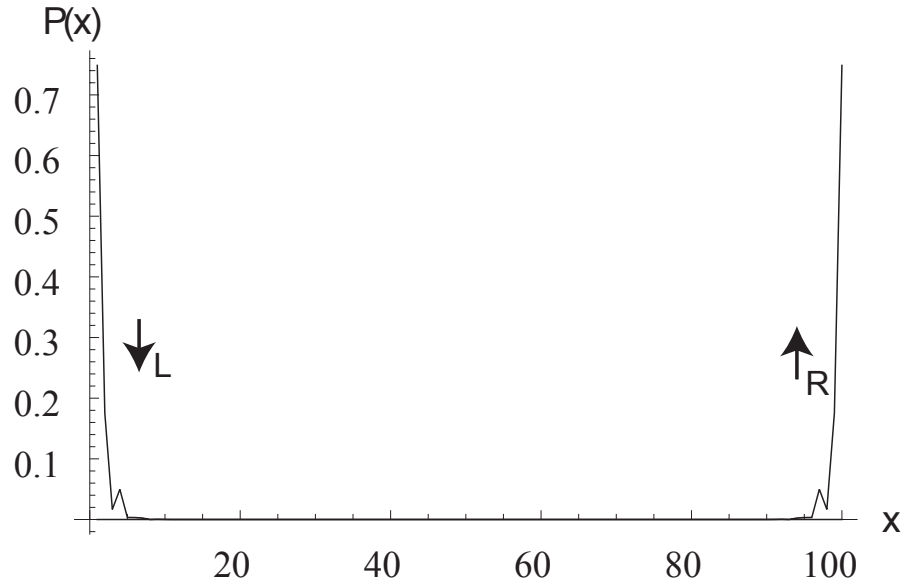

(b)

Figure 3.4: (a) Spectrum of the st-DDW state on a cylinder. Parameters are $t = 0.15$ eV, $t' = 0.3t, \mu = -0.075$ eV, $W_0 = t$, and $\Delta_0 = -t$. The subscripts L and R to the spins correspond to left and right modes. (b) The probability density for positive group velocity for L and R spins for a lattice of $N = 100$ sites.

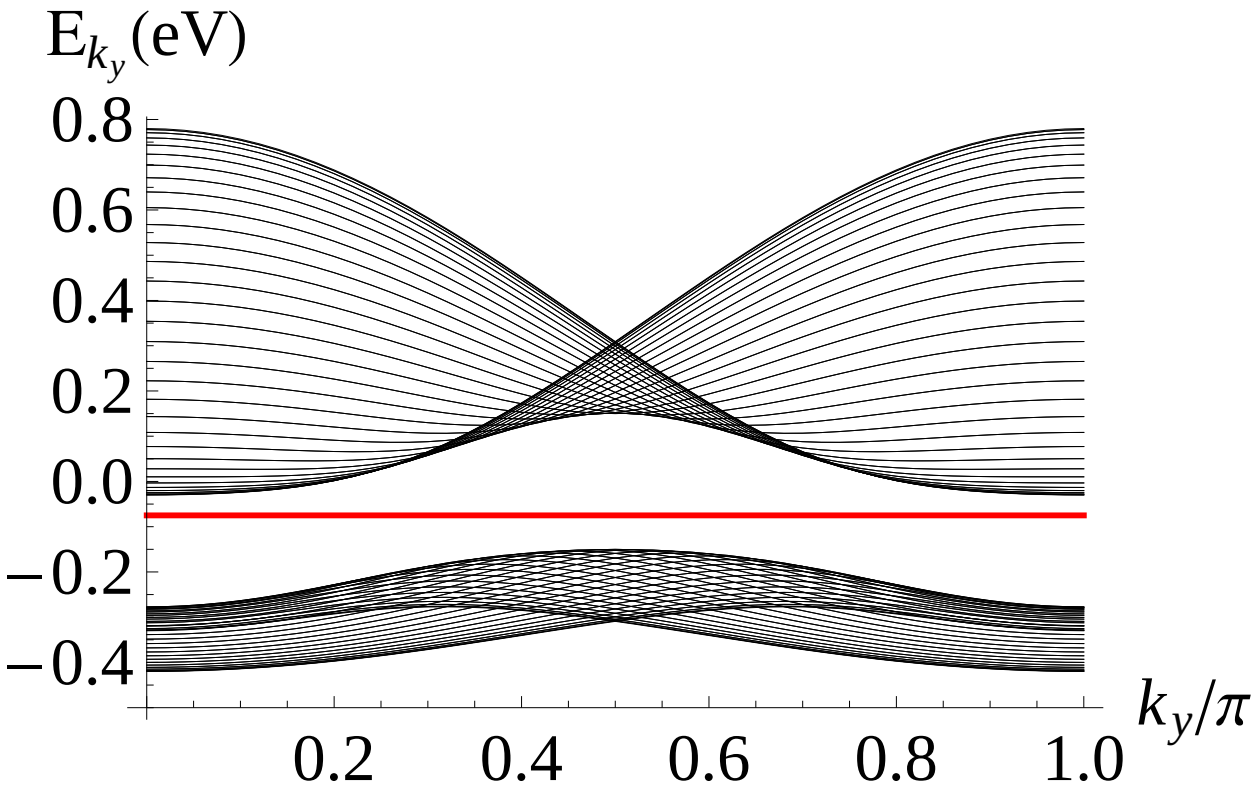

Figure 3.5: The bulk spectra for fixed values of k_y with the same parameters, as in Fig. 3.4.

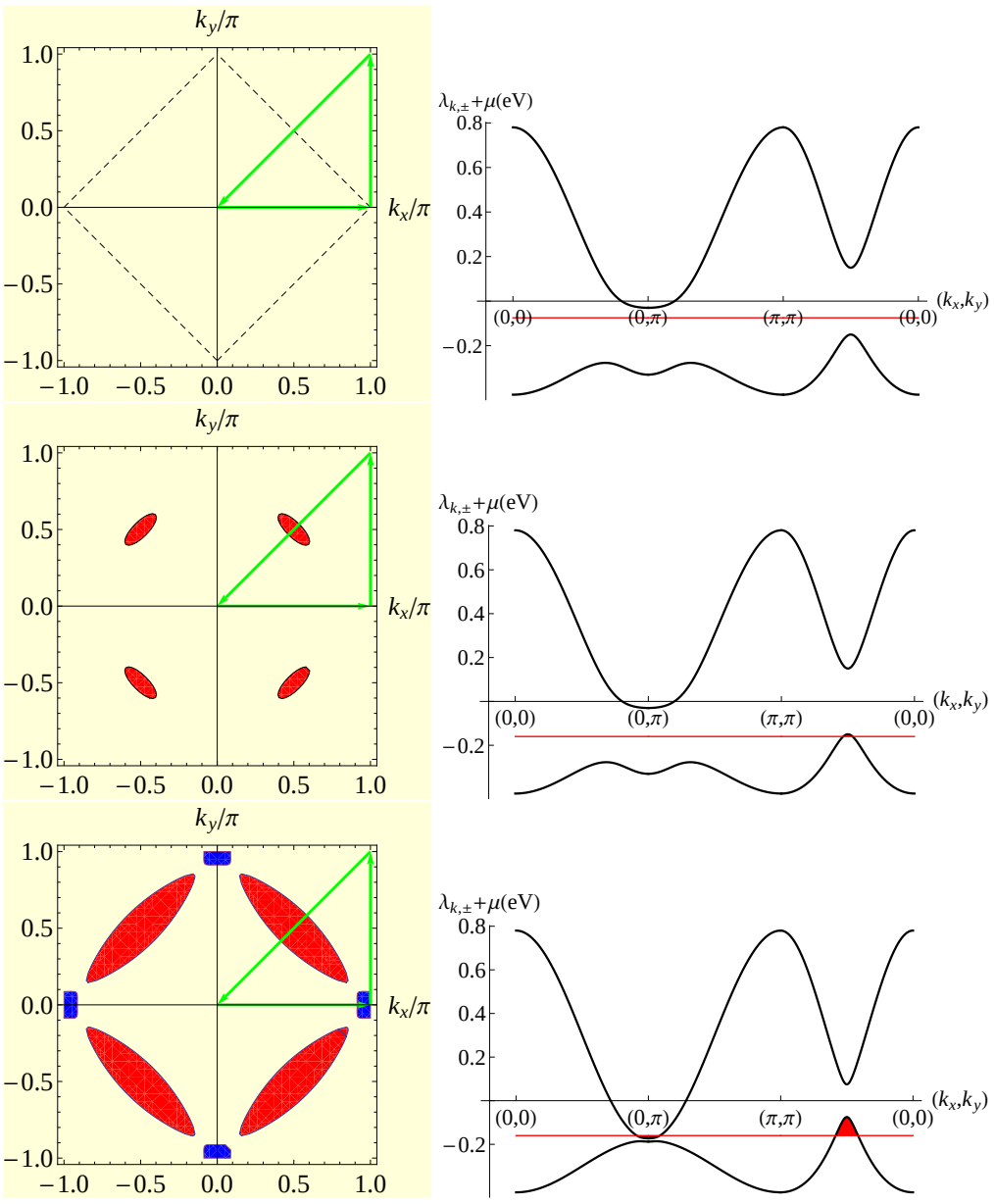

Figure 3.6: Region plots (left) of the first Brillouin zone and energy spectrum (right) along the triangular route indicated by the green arrows. Here, for illustration, we have chosen $t = 0.15$ eV and $t' = 0.3t$. Top: as $W_0 = t$ and $\Delta_0 = -t$, and $\mu = -0.075$ eV, the spectrum is fully gapped. Middle: when μ is lowered to -0.16 eV, the hole pockets open up at $(\pi/2, \pi/2)$ and symmetry-related points. Bottom: $W_0 = 0.05t$ and $\Delta_0 = -0.5t$ decrease, leading to the opening of two electron pockets at $(\pi, 0)$ and symmetry-related points with enlarged hole pockets.

3.4 Experimental detection

While there are many speculations about the nature of the pseudogap, they largely fall into two categories: 1) it is a crossover between a Mott insulator and a Fermi liquid, without any sharp, coherent excitations, and 2) it reflects a broken symmetry, with quasiparticles due to a reconstructed Fermi surface that, despite strong correlations in the system, can behave in many ways as weakly interacting particles. The resolution of this dichotomy will ultimately be settled by experiments, which, to date, have shown some support for both. In the absence of a definitive evidence one way or the other, we have adopted the second perspective (to some extent motivated by recent quantum oscillation experiments [61, 22]) to see what consequences there may be of having a broken symmetry phase with sufficiently hidden order, in particular one that has striking similarities to topological insulators.

A prime characteristic of a broken symmetry is that deep in the broken symmetry phase, an effective mean-field, or a Hartree-Fock Hamiltonian, suffices in discussing the properties of matter, and the symmetries alone determine the excitation spectra and the collective modes. It is only in the proximity of quantum critical points that such a description breaks down, but that is not the subject of discussion here. Moreover, those properties that are determined by symmetries alone should be robust and can be understood in the weak-coupling limit, simplifying our task of exploring correlated electron systems.

The mixed st-DDW order parameters considered here are even more hidden than the corresponding sDDW. Not only do they not modulate charge or spin, but as long as spin-orbit coupling is absent, they are also *invisible to elastic neutron scattering* because there is no associated staggered magnetic field, as in an sDDW.

Inelastic neutron scattering can detect its signature in terms of a spin gap at low energies in the longitudinal susceptibility and signatures in the transverse susceptibility of quasi-Goldstone modes, and even onset of a finite frequency resonance mode. Recall that at any finite temperatures SU(2) symmetry cannot be spontaneously broken in two dimensions; interlayer coupling is necessary to stabilize it. Thus the scale of symmetry breaking must be considerably smaller than

$t \sim J$, and the signature must be sought at higher energies. It could be a challenge to disentangle the signal from inelastic spin-density-wave excitations. On the other hand since the quasiparticle excitations are essentially identical to the sDDW, the quantum oscillation properties will be similar [12, 61, 22, 28, 27], except perhaps those in a tilted field [28, 82]. The essence of this order parameters is modulation of spin current and kinetic energy. So, it will require probes that can detect higher-order correlation functions, such as the two-magnon Raman scattering. In the presence of modest spin-orbit coupling, it may be possible to find small shifts of nuclear quadrupolar frequency (NQR). The modulation of the kinetic energy arising from the d_{xy} component, in particular staggered modulation of t', may lead to anomalies in the propagation of ultrasound [7] at a temperature where such an order is formed, presumably at the pseudogap temperature T^*. The detection of the unique features of the proposed order parameter, the spin Hall effect and edge currents, would be even more challenging.

The effects of nonmagnetic impurities on the mixed st-DDW state studied here are rather subtle. We expect such disorder to couple only weakly to spin currents. Generically, disorder will couple differently to the $i\sigma d_{x^2-y^2}$ and d_{xy} components since each breaks a different symmetry. However, by breaking both the point group and lattice translation symmetries, disorder can enable mixing with (generally incommensurate) density wave states in other angular momentum channels. For example, at the level of Landau theory, we expect terms in the free energy proportional to the product of quadratic powers of the component order parameters, which would be proportional to the impurity concentration, thus inducing spin- or charge-density waves. As long as spin rotational symmetry is preserved in the normal state, the phase transition into the $i\sigma d_{x^2-y^2}$ state can remain sharp.

From the standpoint of topological order at zero temperature, the effects of weak disorder are somewhat simpler. Since the density wave phase considered here is a gapped phase with topological order that is protected by time reversal symmetry, it remains robust against weak nonmagnetic disorder [35, 79]. Thus, the phase can still be described in terms of its topology at zero temperature, a feature which it shares with topological band insulators.

Lastly, we remark that in the presence of magnetic impurities, the phase is not sharply defined,

either as a broken symmetry or in terms of its underlying topology.

In terms of microscopic models beyond the phenomenology discussed here, it is almost certain that correlated hopping processes will play a key role [72]. Finally, since $d_{x^2-y^2}$ and d_{xy} are two distinct irreducible representations on a square lattice, generically they will each have their own transition temperatures, as dictated by Landau theory. The development of the d_{xy} order parameter would be at a higher temperature compared to the triplet component, which breaks SU(2) and therefore requires interlayer coupling. Thus it follows that when applied to cuprates there must be two transitions in the pseudogap regime. Since the topological phase studied here arises from spontaneous symmetry breaking, it can support charged skyrmion textures in analogy with Ref. [31]. The properties of such textures will be the topic of Chapters 4 and 5.

CHAPTER 4

Charge-$2e$ skyrmion condensate in a hidden-order state

4.1 Introduction

It has become very much in vogue to argue that topological aspects of condensed matter bear no relation to broken symmetries [79, 35]. In a strict sense this need not be so [80, 95, 108]. One can construct examples where a broken-symmetry state has interesting topological properties and can even be protected by the broken symmetry itself. An interesting example of a mixed singlet-triplet d-density wave (st-DDW) and its possible relevance to one of the many competing phases in the high-temperature cuprate phase diagram was demonstrated in Chapter 3, where it was found that the system exhibits the quantized spin Hall effect even without any explicit spin-orbit coupling.

In particular, we considered a density wave of nonzero angular momentum ($\ell = 2$) of a mixed singlet and triplet varieties such that in the half-filled limit, it is a gapped insulator. Unlike the semimetallic singlet d-density wave (sDDW) [13], the spin Hall effect is quantized for a range of chemical potential. The state is a topological Mott insulator [80, 95, 108] because it originates from electron-electron interaction that leads to a broken symmetry. The addition of charge carriers, doping, results in Lifshitz transitions destroying the quantization but not the very existence of the spin Hall effect [41]. It is remarkable that such an unconventional broken symmetry, possibly relevant to high-temperature superconductors, has an intimate similarity to topological insulators, which have been explored recently [35, 79].

In this chapter we illustrate another remarkable aspect of the mixed st-DDW order: we show that the system exhibits charge-$2e$ skyrmions, which can condense into a remarkable superconducting state. As we shall discuss, such a mixed st-DDW system, and the resulting superconductivity is

potentially relevant to the hidden-order (HO) state in the heavy-fermion compound $\mathrm{URu_2Si_2}$ [69].

An early attempt at such a non-BCS mechanism of superconductivity was made by Wiegmann [104], as an extension of Fröhlich mechanism to higher dimensions. More recently, several interesting papers have led to discussions of superconductivity in single- and bilayer graphenes. Grover and Senthil [31] have provided a mechanism in which electrons hopping on a honeycomb lattice can lead to a charge-$2e$ skyrmionic condensate, possibly relevant to single layer graphene. To a certain degree we follow their formalism; see also the earlier work in Ref. [94] of charge-e skyrmions in a quantum Hall ferromagnet. As to bilayer graphene, a charge-$4e$ skyrmionic condensate has been suggested by Lu and Herbut [64] and Moon [67].

The difference between our present work and the more recent papers on graphene is an unusual *spontaneously broken symmetry* leading to superconductivity and not the noninteracting band structure of a material. We also point out possible implications for the mysterious HO state in $\mathrm{URu_2Si_2}$, in particular for its superconductivity. In terms of theoretical work, we have provided explicit calculations of the angular momentum of the condensate, an intriguing quantized charge pumping, a derivation of the nonlinear σ model on which the existence of skyrmions rests, and a full analysis of the spin-orbit coupling, correcting mistakes in a seminal work [73]. In addition, we have gone beyond the adiabatic approximation, as in Ref. [31], thus fully confirming our final results.

It is appropriate to comment on what we mean by "hidden order." An order parameter can often be inferred from its macroscopic consequences in terms of certain generalized rigidities. Sometimes its direct microscopic signature is difficult to detect: a direct determination of superconducting order requires a subtle Josephson effect [46], and even antiferromagnetic order requires microscopic neutron scattering probes. Density wave states of higher angular momentum, such as the mixed st-DDW, are even harder to detect. They do not lead to a net charge density wave or spin density wave to be detected by common s-wave probes. It is further undetectable because it does not even break time-reversal invariance. A discussion of possible experimental detections of particle-hole condensates of higher angular momentum was given in Ref. [71]. Thus, it is fair to conclude that the state we consider here is a good candidate for a hidden order.

It is also necessary to remark on the realization of particle-hole condensates of higher angular momentum. An effective low energy theory of a strongly correlated system is bound to have a multitude of coupling constants, perhaps hierarchically arranged. In such cases, we can generally expect a phase diagram with a multitude of broken-symmetry states. It is a profound mystery as to why nontrivial examples are so few and far between. A partial reason could be, as stated above, that these states are unresponsive to common s-wave probes employed in condensed matter physics and therefore appear to be hidden [13].

The next question is whether these low-energy effective Hamiltonians are contrived. If so, it would be of little value to pursue them. However, simple Hartree-Fock analyses have shown that they certainly are not: an onsite repulsion U, a nearest neighbor interaction V, and an exchange interaction J are sufficient in a single-band model [71, 73, 42]; see also more recent papers by Laughlin [58, 59].

The structure of this chapter is as follows: in Sec. 4.2, we construct the low-energy effective action of the mixed st-DDW system. In Sec. 4.3, we compute the charge and the spin of a skyrmion and verify that the skyrmions in this system are bosons, which can lead to a superconducting phase transition. In Sec. 4.4, we compute the angular momentum of a skyrmion. In Sec. 4.5, we study the charge pumping due to a time-dependent inhomogeneous spin texture that is interesting in its own right. In Sec. 4.6 we discuss mainly the problem of $\mathrm{URu_2Si_2}$. In Appendix A, the derivation of the nonlinear σ model and the details of computing the Chern-Simons coefficients and charge pumping are provided.

4.2 Effective action

In momentum space the mixed st-DDW order parameter is [c and $c^\dagger$ are fermonic annihilation and creation operators, respectively, $Q = (\pi, \pi)$, and the lattice constant is set to unity]

$$\langle c^\dagger_{k+Q,\alpha} c_{k,\beta} \rangle \propto i(\vec{\sigma} \cdot \hat{N})_{\alpha\beta} W_k + \delta_{\alpha\beta} \Delta_k, \tag{4.1}$$

where $\hat{N}$ is a unit vector, $\vec{\sigma}$ are the Pauli matrices acting on spin indices, and the form factors

$$W_k \equiv \frac{W_0}{2}(\cos k_x - \cos k_y), \tag{4.2}$$

$$\Delta_k \equiv \Delta_0 \sin k_x \sin k_y, \tag{4.3}$$

correspond to the $d_{x^2-y^2}$ and d_{xy} density wave, respectively [71]. It is not necessary that d_{xy} and $d_{x^2-y^2}$ transitions be close to each other, nor are they required to be close in energy [41].

If we choose the spin quantization axis to be $\hat{z}$, the up spins represent circulating spin currents corresponding to the order parameter $(id_{x^2-y^2} + d_{xy})$ and the down spins to $(-id_{x^2-y^2} + d_{xy})$. So, there are net circulating spin currents alternating from one plaquette to the next but no circulating charge currents. By the choice of the quantization axis we have explicitly broken SU(2) symmetry, but not U(1), and the coset space of the order parameter $S^2 \equiv SU(2)/U(1)$. Such a state can admit skyrmions in two dimensions, ignoring the possibility of hedgehog configurations in $(2+1)$ dimensions. See the derivation of the nonlinear σ model in Appendix A.1.

The mean-field Hamiltonian is

$$\mathcal{H} = \sum_{k,\alpha,\beta} \psi^\dagger_{k,\alpha} \left[\delta_{\alpha\beta}(\tau^z \epsilon_k + \tau^x \Delta_k) - (\vec{\sigma} \cdot \hat{N})_{\alpha\beta} \tau^y W_k \right] \psi_{k\beta}, \tag{4.4}$$

where the summation is over the reduced Brillouin zone (RBZ) bounded by $k_y \pm k_x = \pm\pi$, the spinor is $\psi^\dagger_{k,\alpha} \equiv (c^\dagger_{k,\alpha}, c^\dagger_{k+Q,\alpha})$, and $\epsilon_k \equiv -2t(\cos k_x + \cos k_y)$; addition of longer ranged hopping will not change our conclusions [41]. Here τ^i $(i = x, y, z)$ are Pauli matrices acting on the two-component spinor. It is not necessary but convenient to construct a low-energy effective field theory. For this we expand around the points $K_1 \equiv (\frac{\pi}{2}, \frac{\pi}{2})$ and $K_2 \equiv (-\frac{\pi}{2}, \frac{\pi}{2})$, which would have been the two distinct nodal points in the absence of the d_{xy} term, and $K_3 \equiv (0, \pi)$, which would have been the nodal point in the absence of the $d_{x^2-y^2}$ term. This allows us to develop an effective low-energy theory by separating the fast modes from the slow modes. After that we make a sequence of transformations for simplicity: (1) transform the Hamiltonian to the real space, which allows us to formulate the skyrmion problem; (2) perform a $\pi/2$ rotation along the τ^y-direction, which allows us to match to the notation of Ref. [73] for the convenience of the reader; (3) label $\psi_{K_i+q,\alpha}$ by $\psi_{i\alpha}$, since K_i is now a redundant notation; (4) construct the imaginary-time effective

action, with the definition $\bar{\psi} \equiv -i\psi^\dagger \tau^z$. Finally, after suppressing the spin indices, and with the definitions $\gamma^0 \equiv \tau^z$, $\gamma^x \equiv \tau^y$, and $\gamma^y \equiv -\tau^x$, we obtain the effective action in a more compact notation:

$$\begin{aligned} S &= \sum_{j=1,2} \int d^3x\, \bar{\psi}_j \left[-i\gamma^0 \partial_\tau - 2it\gamma^x(\eta_j \partial_x + \partial_y) + i\frac{W_0}{2}(\vec{\sigma}\cdot\hat{N})\gamma^y(-\eta_j\partial_x + \partial_y) + i\eta_j \Delta_0 \right] \psi_j \\ &\quad + \int d^3x \bar{\psi}_3 \left[-i\gamma^0\partial_\tau - W_0(\vec{\sigma}\cdot\hat{N})\gamma^y \right] \psi_3, \end{aligned} \tag{4.5}$$

where $\eta_1 = 1$ and $\eta_2 = -1$. There is no spatial derivative in the ψ_3 terms since the expansion of the $d_{x^2-y^2}$ gap around the nodal point $K_3 = (0, \pi)$ is

$$W_{K_3+q} = \frac{W_0}{2}(2 - \frac{q_x^2}{2} - \frac{q_y^2}{2} + \cdots), \tag{4.6}$$

where the second- (and higher-) order derivative terms are dropped when linearizing the action. In other words, the $d_{x^2-y^2}$ term behaves as a mass term at the K_3 point.

4.3 The charge and spin of a skyrmion

First we will compute the charge of the skyrmions in the system by following Grover and Senthil's adiabatic argument [31]. Consider the action around $K_1 = (\frac{\pi}{2}, \frac{\pi}{2})$ when the order parameter is uniform (say, $\hat{N} = \hat{z}$). The results for $K_2 = (-\frac{\pi}{2}, \frac{\pi}{2})$ and $K_3 = (0, \pi)$ follow identically. In Chapter 3 we showed that the nontrivial topology leads to a quantized spin Hall conductance in the st-DDW state as long as the system is fully gapped [41]. The spin quantum Hall effect implies that the external gauge fields A^c and A^s couple to charge and spin currents, respectively. In the presence of these external gauge fields, we add minimal coupling in the action by

$$\frac{1}{i}\partial_\mu = p_\mu \to p_\mu + A^c_\mu + \frac{\sigma^z}{2} A^s_\mu. \tag{4.7}$$

Then the action is

$$\begin{aligned} S_1[A^c, A^s] &= \int d^3x\, \bar{\psi}_1 \left[-i\gamma^0\partial_\tau + \gamma^0 \left(A^c_\tau + \frac{\sigma^z}{2} A^s_\tau \right) - 2it\gamma^x(\partial_x + \partial_y) \right. \\ &\quad + 2t\gamma^x \left(A^c_x + \frac{\sigma^z}{2} A^s_x + A^c_y + \frac{\sigma^z}{2} A^s_y \right) + i\frac{W_0}{2}\sigma^z\gamma^y(-\partial_x + \partial_y) \\ &\quad \left. - \frac{W_0}{2}\sigma^z\gamma^y(-A^c_x - \frac{\sigma^z}{2}A^s_x + A^c_y + \frac{\sigma^z}{2}A^s_y) + i\Delta_0 \right] \psi_1, \end{aligned} \tag{4.8}$$

where we set $e = \hbar = 1$. The nonvanishing transverse spin conductance implies that the low-energy effective action for the gauge fields is given by

$$S_{\text{eff}} = \frac{i}{2\pi} \int d^3x \epsilon^{\mu\nu\lambda} A^c_\mu \partial_\nu A^s_\lambda, \tag{4.9}$$

and the charge current is induced by the spin gauge field

$$j^c_\mu = \frac{1}{2\pi} \epsilon^{\mu\nu\lambda} \partial_\nu A^s_\lambda. \tag{4.10}$$

Consider now a static configuration of the $\hat{N}$ field with unit Pontryagin index in the polar coordinate (r, θ):

$$\hat{N}(r, \theta) = [\sin\alpha(r)\cos\theta, \sin\alpha(r)\sin\theta, \cos\alpha(r)] \tag{4.11}$$

with the boundary conditions $\alpha(r = 0) = 0$ and $\alpha(r \to \infty) = \pi$. Performing a unitary transformation at all points in space such that $U^\dagger(\vec{\sigma} \cdot \hat{N})U = \sigma^z$, and defining $\psi = U\psi'$, and $\bar{\psi} = \bar{\psi}' U^\dagger$, we obtain

$$\begin{aligned} S_1 &= \int d^3x\ \bar{\psi}'_1 \left[-i\gamma^0 \partial_\tau - 2it\gamma^x(\partial_x + \partial_y) + i\frac{W_0}{2}\sigma^z\gamma^y(-\partial_x + \partial_y) + i\Delta_0 \right] \psi'_1 \\ &\quad + \int d^3x\ \bar{\psi}'_1 \left[-i\gamma^0 (U^\dagger \partial_\tau U) - 2it\gamma^x (U^\dagger \partial_x U + U^\dagger \partial_y U) \right. \\ &\qquad \left. + i\frac{W_0}{2}\sigma^z\gamma^y(-U^\dagger \partial_x U + U^\dagger \partial_y U) \right] \psi'_1 \end{aligned} \tag{4.12}$$

To proceed, we write down the explicit form for $U(r, \theta)$, which is

$$U(r, \theta) = \begin{pmatrix} \cos\frac{\alpha(r)}{2} & -\sin\frac{\alpha(r)}{2} e^{-i\theta} \\ \sin\frac{\alpha(r)}{2} e^{i\theta} & \cos\frac{\alpha(r)}{2} \end{pmatrix}. \tag{4.13}$$

In the far-field limit, $U^\dagger \partial_x U = (\frac{-i\sin\theta}{r})\sigma^z$, and $U^\dagger \partial_y U = (\frac{i\cos\theta}{r})\sigma^z$; substituting into Eq. (4.12) and introducing $f_\mu = -iU^\dagger \partial_\mu U$, we get

$$\begin{aligned} S_1 &= \int d^3x\ \bar{\psi}'_1 \left[-i\gamma^0 \partial_\tau - 2it\gamma^x(\partial_x + \partial_y) + i\frac{W_0}{2}\sigma^z\gamma^y(-\partial_x + \partial_y) + i\Delta_0 \right] \psi'_1 \\ &\quad + \int d^3x\ \bar{\psi}'_1 \left[2t\gamma^x(f_x + f_y) + \frac{W_0}{2}\sigma^z\gamma^y(f_x - f_y) \right] \psi'_1 \end{aligned} \tag{4.14}$$

Equating the above equation and Eq. (4.8), we obtain, in the far-field limit,

$$A^c_x = A^c_y = 0;\ A^s_x = -\frac{2\sin\theta}{r};\ A^s_y = \frac{2\cos\theta}{r}. \tag{4.15}$$

In other words, the process of tuning the order parameter from σ^z to $\left(\hat{\sigma}\cdot\hat{N}(r,\theta)\right)$ is equivalent to adding an external spin gauge field

$$\vec{A}^s = -\frac{2\sin\theta}{r}\hat{x} + \frac{2\cos\theta}{r}\hat{y} = \frac{2}{r}\hat{\theta}. \tag{4.16}$$

The total flux of this gauge field is clearly 4π. Suppose we adiabatically construct the skyrmion configuration $\hat{N}(r,\theta)$ from the ground state $\hat{z}$ in a very long time period $\tau_p \to \infty$. During the process, we effectively thread a spin gauge flux of 4π. The transverse spin Hall conductance implies that a radial current j_r^c will be induced by the 4π spin gauge flux of $\vec{A}^s(t)$, which is now time dependent: $\vec{A}^s(t=0)=0$ and $\vec{A}^s(t=\tau_p)=\vec{A}^s$, that is,

$$j_r^c(t) = -\frac{1}{2\pi}\partial_t A_\theta^s(t). \tag{4.17}$$

As a result, charge will be transferred from the center to the boundary, and the total charge transferred is

$$Q^c = \int_0^{\tau_p} dt \int_0^{2\pi} r d\theta j_r^c(t) = -2. \tag{4.18}$$

Therefore, after restoring the unit of charge to e, we obtain a skyrmion with charge $2e$; its spin is 0.

It is important to verify the adiabatic result by a different method. This can be done by a computation of the Chern number [106]. The charge and spin of the skyrmions are associated with the coefficients of the Chern-Simons terms by the following relations: $Q_{\text{skyrmion}} = C_2 e$ and $S_{\text{skyrmion}} = C_1\frac{\hbar}{2}$, where C_1 and C_2 are

$$C_1 = \frac{\epsilon_{\mu\nu\lambda}}{24\pi^2}\text{Tr}\left[\int d^3k G\frac{\partial G^{-1}}{\partial k_\mu}G\frac{\partial G^{-1}}{\partial k_\nu}G\frac{\partial G^{-1}}{\partial k_\lambda}\right], \tag{4.19}$$

$$C_2 = \frac{\epsilon_{\mu\nu\lambda}}{24\pi^2}\text{Tr}\left[\int d^3k (\vec{\sigma}\cdot\hat{z}) G\frac{\partial G^{-1}}{\partial k_\mu}G\frac{\partial G^{-1}}{\partial k_\nu}G\frac{\partial G^{-1}}{\partial k_\lambda}\right], \tag{4.20}$$

where G is the Green's function matrix and the trace Tr is taken over the spin index and other discrete indices.

If the Green's function matrix is diagonal in the spin index, then the Chern-Simons coefficients for up and down spins can be computed separately:

$$\mathcal{N}(G_\sigma) = \frac{\epsilon_{\mu\nu\lambda}}{24\pi^2}\text{Tr}\left[\int d^3k G_\sigma\frac{\partial G_\sigma^{-1}}{\partial k_\mu}G_\sigma\frac{\partial G_\sigma^{-1}}{\partial k_\nu}G_\sigma\frac{\partial G_\sigma^{-1}}{\partial k_\lambda}\right], \tag{4.21}$$

and $C_1 = \mathcal{N}(G_\uparrow) + \mathcal{N}(G_\downarrow)$, $C_2 = \mathcal{N}(G_\uparrow) - \mathcal{N}(G_\downarrow)$. Furthermore, it can be shown (see Appendix A.2) that for

$$G_\sigma^{-1} = i\omega\hat{I} - \hat{\tau}\cdot\vec{h}_\sigma \tag{4.22}$$

with $\vec{h}_\sigma$ being the Anderson's pseudospin vector [4] of the Hamiltonian, the Chern-Simons coefficient for spin σ can be written as

$$\mathcal{N}(G_\sigma) = -\int \frac{d^2k}{4\pi}\ \hat{h}_\sigma \cdot \frac{\partial \hat{h}_\sigma}{\partial k_x} \times \frac{\partial \hat{h}_\sigma}{\partial k_y}, \tag{4.23}$$

where $\hat{h}_\sigma \equiv \vec{h}_\sigma/|\vec{h}_\sigma|$ is the unit vector of $\vec{h}_\sigma$. Here C_1 and C_2 are the total Chern number and the spin Chern number $\mathcal{N}_{\text{spin}}$ defined in Chapter 3, respectively [41]. For the st-DDW system, we have $\vec{h}_\sigma \equiv (\Delta_k, -\sigma W_k, \epsilon_k)$. Explicitly, $C_1 = -1+1 = 0$ and $C_2 = -1-1 = -2$; thus the results are the same as above.

Because a skyrmion in the system carries integer spin, it obeys bosonic statistics and may undergo Bose-Einstein condensate. As a result, the charge-$2e$ skyrmion condensate will lead to a superconducting phase transition. But what about its orbital angular momentum? In the following section, we will prove that it is zero resulting in an s-wave singlet state. This is a bit surprising given the original d-wave form factor.

4.4 The angular momentum of a skyrmion

To compute the angular momentum carried by a skyrmion in the system, we consider the angular momentum density due to the electromagnetic field. For a static spin texture it is clearly zero, because $\vec{E} = 0$. For a time-dependent texture it is little harder to prove. Consider the spin texture $\hat{N}(r,\theta,t)$ with

$$N_x(r,\theta,t) = \sin\alpha(r,t)\cos\beta(\theta,t), \tag{4.24}$$

$$N_y(r,\theta,t) = \sin\alpha(r,t)\sin\beta(\theta,t), \tag{4.25}$$

$$N_z(r,t) = \cos\alpha(r,t), \tag{4.26}$$

where $\alpha(r,t)$ and $\beta(\theta,t)$ are smooth functions, and $\alpha(r,t)$ satisfies the boundary conditions $\alpha(r=0,t)=0$ and $\alpha(r\to\infty,t)=\pi$ for any t, and $\frac{\partial\alpha(r,t)}{\partial r}|_{r\to\infty}=\frac{\partial\alpha(r,t)}{\partial t}|_{r\to\infty}=0$ in the far-field limit. The unitary matrix is now time dependent. After a little algebra, we obtain the time-dependent gauge fields in the far-field limit to be

$$A^s_x(r,\theta,t) = \frac{-2\sin\theta}{r}\frac{\partial\beta(\theta,t)}{\partial\theta}, \tag{4.27}$$

$$A^s_y(r,\theta,t) = \frac{2\cos\theta}{r}\frac{\partial\beta(\theta,t)}{\partial\theta}. \tag{4.28}$$

So, $\Phi(\theta,t)=A^s_t(\theta,t)=2\frac{\partial\beta(\theta,t)}{\partial t}$ and $\vec{A}^s(r,\theta,t)=A^s_x(r,\theta,t)\hat{x}+A^s_y(r,\theta,t)\hat{y}=A^s_\theta(r,\theta,t)\hat{\theta}$, where

$$A^s_\theta(r,\theta,t)=\frac{2}{r}\frac{\partial\beta(\theta,t)}{\partial\theta}. \tag{4.29}$$

Therefore, the electric field will have a nonzero $\hat{\theta}$ component, $\vec{E}=E_\theta\hat{\theta}$, and the magnetic field will have a nonzero $\hat{z}$ component, $\vec{B}=B_z\hat{z}$, where

$$E_\theta = -\frac{1}{r}\frac{\partial A^s_t(\theta,t)}{\partial\theta}-\frac{\partial A^s_\theta(r,t)}{\partial t}=-\frac{4}{r}\frac{\partial^2\beta(\theta,t)}{\partial\theta\partial t} \tag{4.30}$$

$$B_z = \frac{\partial A^s_\theta(r,t)}{\partial r}=-\frac{2}{r^2}\frac{\partial\beta(\theta,t)}{\partial\theta}. \tag{4.31}$$

As a result, the angular momentum density still vanishes,

$$\vec{L}_{\text{field}}=\frac{1}{4\pi c}\vec{r}\times(E_\theta\hat{\theta}\times B_z\hat{z})=0. \tag{4.32}$$

It is possible that superconductivity with nonzero angular momentum may be realized when the interaction between particles is included, which will be the topic of Chapter 5. It would be interesting to explore what other kinds of quantum numbers are carried by the topological textures in the model we have studied.

4.5 Quantized charge pumping

In Sec.4.3, we considered a static spin texture and obtained charge-$2e$ skyrmions in the system. If we consider a time-dependent spin texture, which has a smooth variation in one spatial direction, say, $\hat{y}$, and is uniform in the other, $\hat{x}$, charge will be pumped from one side of the system to the

other along $\hat{x}$ [109]. This charge pumping effect can be understood from the effective gauge action, which is

$$S_{\text{eff}}[A^c_\mu, A^s_\mu] = \frac{C_2}{4\pi}\int d^3x \epsilon^{\mu\nu\lambda} A^c_\mu \partial_\nu A^s_\lambda, \tag{4.33}$$

where the integral is over the real time, t, instead of the imaginary time, τ. Therefore, the charge current induced by the spin gauge field will be

$$j^c_\mu = \frac{\delta S_{\text{eff}}[A^c_\mu, A^s_\mu]}{\delta A^c_\mu} = \frac{C_2}{4\pi}\epsilon^{\mu\nu\lambda}\partial_\nu A^s_\lambda = \frac{C_2}{8\pi}\epsilon^{\mu\nu\lambda}F^s_{\nu\lambda}, \tag{4.34}$$

where we define the spin gauge flux $F^s_{\mu\nu} \equiv \partial_\mu A^s_\nu - \partial_\nu A^s_\mu$. After some straightforward algebra (see Appendix A.3), the spin gauge flux can be written in terms of the $\hat{N}$ vector,

$$F^s_{\mu\nu} = \hat{N}\cdot[(\partial_\mu \hat{N})\times(\partial_\nu \hat{N})]. \tag{4.35}$$

As a result, even in the absence of an external electromagnetic field, a charge current may be induced by a time-dependent inhomogeneous spin texture because

$$j^c_\mu = \frac{C_2}{8\pi}\epsilon^{\mu\nu\lambda}\hat{N}\cdot[(\partial_\nu \hat{N})\times(\partial_\lambda \hat{N})]. \tag{4.36}$$

To demonstrate the charge response induced by the spin texture, we consider the following configuration with unit Pontryagin index,

$$\hat{N}(y,t) = [\sin\theta(t)\cos\phi(y), \sin\theta(t)\sin\phi(y), \cos\theta(t)]\,, \tag{4.37}$$

where $\theta(t)$ and $\phi(y)$ are smooth functions of t and y, respectively, with boundary conditions $\theta(t=0)=0$, $\theta(t=\tau_p)=\pi$, and $\phi(y\to\pm\infty)=\pm\pi$. Therefore, we have an induced charge current along the $\hat{x}$ direction,

$$\begin{aligned} j^c_x &= \frac{C_2}{8\pi}\epsilon^{x\nu\lambda}\hat{N}\cdot[(\partial_\nu \hat{N})\times(\partial_\lambda \hat{N})] \\ &= \frac{C_2}{4\pi}\hat{N}\cdot[(\partial_y \hat{N})\times(\partial_t \hat{N})]. \end{aligned} \tag{4.38}$$

Interestingly, we can show that the pumped charge is quantized,

$$Q_{\text{pumped}} = \int_0^{\tau_p} dt \int_{-\infty}^{\infty} dy\; j^c_x$$

$$
\begin{aligned}
&= \frac{C_2}{4\pi}\int_0^{\tau_p} dt \int_{-\infty}^{\infty} dy\ \hat{N}\cdot[(\partial_y\hat{N})\times(\partial_t\hat{N})] \\
&= \frac{C_2}{4\pi}\int_0^{\pi} d\theta \int_{-\pi}^{\pi} d\phi\ \hat{N}\cdot[(\partial_\theta\hat{N})\times(\partial_\phi\hat{N})] \\
&= C_2, \qquad (4.39)
\end{aligned}
$$

where we have used that, for the spin texture with unit Pontryagin index,

$$
\int_0^{\pi} d\theta \int_{-\pi}^{\pi} d\phi\ \hat{N}\cdot[(\partial_\theta\hat{N})\times(\partial_\phi\hat{N})] = 4\pi. \qquad (4.40)
$$

After restoring the unit of charge, we have $Q_{\text{pumped}} = C_2\, e$. So far we have considered the spin texture with unit Pontryagin index. If the spin texture is generalized to a general Pontryagin index, N_P, then the pumped charge will be $Q_{\text{pumped}} = C_2 N_P\, e$.

How could we observe this charge pumping experimentally? We need to control the direction of the $\hat{N}$ vector so that it can be the time-dependent inhomogeneous spin texture discussed above. In topological chiral magnets [109], the $\hat{N}$ vector is the net ferromagnetic moment, which aligns along the external magnetic field, so one can apply a time-dependent magnetic field $\vec{H}(t) = H(t)\hat{x}$ coupling to the $\hat{N}$ vector and control the magnitude of $\hat{x}$ component of $\hat{N}$.

In the mixed st-DDW, however, the situation is more complicated. In the presence of an external magnetic field, there will be a spin-flop transition and the $\hat{N}$ vector will lie in the plane perpendicular to the external field [73]. In other words, we cannot fully control the direction of $\hat{N}$ with a time-dependent magnetic field. Therefore, it would be a challenge to measure the pumped charges in the system.

Nevertheless, the charge pumping effect provides, at least, a different conceptual approach to probe the topological properties of the system in addition to the quantized spin Hall conductance. For the quantum spin Hall effect, a spin current is induced by the external electric field [41], whereas for the charge pumping effect, a charge current will be induced by the spin texture. It would, of course, be interesting if one can manipulate the $\hat{N}$ vector experimentally because a charge current is easier to detect than a spin current.

4.6 Discussion and application to the HO state in $\mathrm{URu_2Si_2}$

There are two points that we have glossed over. The first is rather simple: in the ordered phase at $T = 0$, there are also Goldstone modes that can be easily seen by integrating out the fermions resulting in a nonlinear σ model involving $\hat{N}$, the form of which is entirely determined by symmetry. These do not lead to any interesting physics, such as charge-$2e$ skyrmions that condense into a superconducting state. At finite temperatures they could lead to a renormalized classical behavior [11]. The second point is more subtle: we have assumed that the hedgehog configurations are absent. This would require, as pointed out by Grover and Senthil [31], that the energy of the skyrmion (especially in the limit $\Delta_0 \to 0$) is smaller than individual pairs of electrons, a question that is likely to be model dependent. If this assumption is correct, however, the transition from the mixed st-DDW state to the superconducting state will correspond to a deconfined quantum critical point, which otherwise would have been a first-order transition, as in Landau theory [92, 91, 55].

We suggest that the superconducting phase driven by the skyrmion condensate may be realized in the $\mathrm{URu_2Si_2}$, which hosts an exotic HO phase, with broken translational symmetry below $T_{\mathrm{HO}} \approx 17.5$ K and a superconducting phase below $T_c \approx 1.5$ K [69]. Recently, Fujimoto [26] proposed a triplet d density wave with the order parameter $\langle c^\dagger_{k,1,\alpha} c_{k+Q_0,2,\beta} \rangle = \vec{d}(k) \cdot \vec{\sigma}_{\alpha\beta}$ with $\vec{d}(k) = i(\Delta_1 \sin \frac{(k_x - k_y)}{\sqrt{2}} \sin k_z, 0, 0)$ to describe this state [26]; here 1 and 2 refer to two different bands and $Q_0 = (0, 0, 1)$ is the nesting vector; even the earlier work in Ref. [42] involving circulating spin current is not entirely unrelated. The order parameter considered in Ref. [26] is different but a close cousin of the order parameter considered in our work; the circulating staggered spin currents in Ref. [26] lie on the diagonal planes instead and the crucial d_{xy} part is missing there. As mentioned in Sec. 4.2, the mixed st-DDW gives rise to net circulating spin currents alternating from one plaquette to the next in the square lattice. Notice that the coefficient of the d_{xy} component is real, so in the tight-binding model the presence of the d_{xy} term affects the kinetic energy, but does not produce any charge current or spin current. As a result, the addition of the singlet d_{xy} component in the present work modulates only the next-nearest-neighbor hopping, and the spin current patterns remain unaffected. As mentioned above the spin currents lie on the diagonal

planes in the three-dimensional lattice. For the purpose of illustration, in Fig. 4.1 we plot the spin current pattern due to the order parameter in Ref. [26]. On each diagonal plane, there are two copies of the staggered circulating spin current patterns. Each of them is the same as the one in the mixed st-DDW system because, as explained above, the d_{xy} component has no effect on the spin current pattern.

That the currents are in the diagonal planes instead of being square planar is conceptually not important, but is necessary to explain the nematicity observed in the experiments [75]. We now discuss the role of spin-orbit coupling before making our final comments.

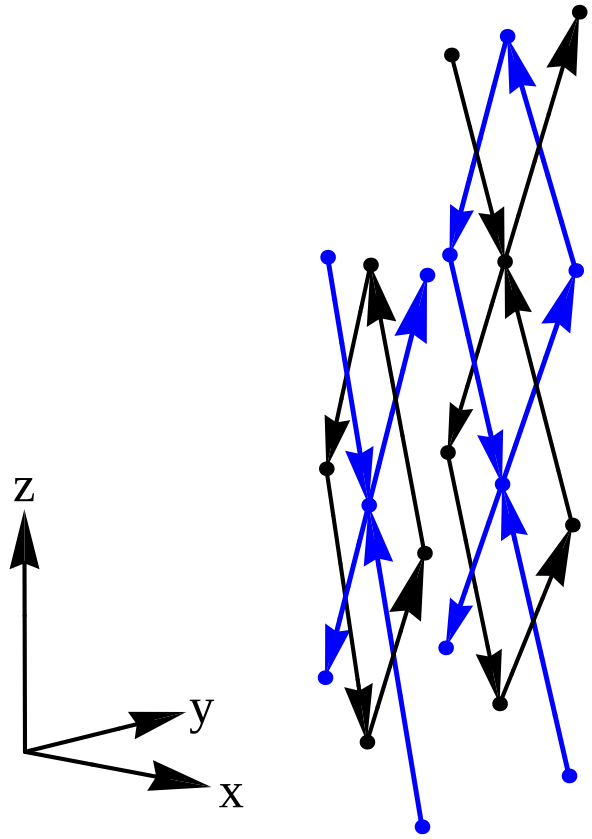

Figure 4.1: The spin current pattern due to the order parameter in Ref. [26]. The U atoms are marked by the dots. The directions of the spin currents are marked by the arrows. Black and blue colors indicate two independent sets of staggered circulating spin current patterns. The Ru and Si atoms are not shown for clarity.

4.6.1 Spin-orbit coupling

It will be shown below that the order of magnitude of the spin-orbit energy is

$$E_{\text{SO}} \approx \left[(\hat{N}\cdot\hat{z})^2 - 1\right]\left(\frac{\Lambda_0^2}{W}\right)\left(\frac{W_0}{W}\right)^2\left[1 + O\left(\frac{W_0}{W}\right)^2\right], \tag{4.41}$$

correcting a mistake in Ref. [73]. Here Λ_0 is the strength of the spin-orbit coupling, given by

$$\mathcal{H}_{\text{SO}} = \sum_k c^\dagger_{k\alpha}\vec{\Lambda}(k)\cdot\vec{\sigma}_{\alpha\beta}c_{k\beta}, \tag{4.42}$$

where $\vec{\Lambda}(k) = \frac{\Lambda_0}{\sqrt{2}}[\hat{x}\sin k_y - \hat{y}\sin k_x]$. In the presence of spin-orbit coupling, the Hamiltonian is

$$\begin{aligned}
& \mathcal{H}_{\text{total}} \\
= \;& \mathcal{H} + \mathcal{H}_{\text{SO}} \\
= \;& \sum_k \Psi_k^\dagger \begin{pmatrix} \epsilon_k & \Delta_k + iN_zW_k & \Lambda_x(k) - i\Lambda_y(k) & iW_k(N_x - iN_y) \\ \Delta_k - iN_zW_k & -\epsilon_k & -iW_k(N_x - iN_y) & -\Lambda_x(k) + i\Lambda_y(k) \\ \Lambda_x(k) + i\Lambda_y(k) & iW_k(N_x + iN_y) & \epsilon_k & \Delta_k - iN_zW_k \\ -iW_k(N_x + iN_y) & -\Lambda_x(k) - i\Lambda_y(k) & \Delta_k + iN_zW_k & -\epsilon_k \end{pmatrix}\Psi_k,
\end{aligned} \tag{4.43}$$

where $\Psi_k^\dagger$ is the four-component spinor $(c^\dagger_{k,\uparrow}, c^\dagger_{k+Q,\uparrow}, c^\dagger_{k,\downarrow}, c^\dagger_{k+Q,\downarrow})$. In the absence of spin-orbit coupling, the eigenvalues are $\pm E_{0k}$ with $E_{0k} = \sqrt{\epsilon_k^2 + W_k^2 + \Delta_k^2}$. On the other hand, when spin-orbit coupling is present, the eigenvalues of the upper and lower bands now become $\lambda_{\text{up},\pm} = E_{k,\pm}$, $\lambda_{\text{low},\pm} = -E_{k,\pm}$, respectively, where

$$E_{k,\pm} = \sqrt{\epsilon_k^2 + W_k^2 + \Delta_k^2 + \Lambda_k^2 \pm 2\left[(\epsilon_k^2 + W_k^2)\Lambda_k^2 - W_k^2(\hat{N}\cdot\vec{\Lambda}_k)^2\right]^{\frac{1}{2}}} \tag{4.44}$$

with $\Lambda_k^2 \equiv |\vec{\Lambda}_k|^2 = \Lambda_x^2(k) + \Lambda_y^2(k)$. When the d_{xy} component is absent, $\Delta_k = 0$, and the results of Ref. [73] are recovered. Consider the following two cases separately.

4.6.1.1 $\hat{N} \parallel \hat{z}$

Since the chemical potential is at the midgap, we can focus on the lower bands. When $\hat{N} = \hat{z}$, we have $\hat{N}\cdot\vec{\Lambda}_k = 0$ and

$$\lambda^z_{\text{low},\pm} \;=\; -\sqrt{E_{0k}^2 + \Lambda_k^2 \pm 2\left[E_{0k}^2\Lambda_k^2\right]^{\frac{1}{2}}}$$

$$= \quad -E_{0k} \mp |\vec{\Lambda}_k| \tag{4.45}$$

Assuming that $\Lambda_0 \ll W_0, \Delta_0 \ll W$ with the electronic bandwidth $W = 8t$, the change in the ground-state energy will be

$$\begin{aligned} E_{\text{SO}} &= \sum_k \left[(\lambda^z_{\text{low},+} + \lambda^z_{\text{low},-}) - 2(-E_{0k}) \right] \\ &= \sum_k \left[(-E_{0k} - |\vec{\Lambda}_k| - E_{0k} + |\vec{\Lambda}_k|) + 2E_{0k} \right] = 0 \end{aligned} \tag{4.46}$$

4.6.1.2 $\hat{N} \perp \hat{z}$

When $\hat{N}$ lies in xy-plane, we have $\hat{N} \cdot \vec{\Lambda}_k = |\vec{\Lambda}_k| \cos\phi_k$, where ϕ_k is the angle between $\hat{N}$ and $\vec{\Lambda}_k$, and

$$\cos\phi_k = \frac{\hat{N} \cdot \vec{\Lambda}_k}{|\vec{\Lambda}_k|} = \frac{N_x \Lambda_x(k) + N_y \Lambda_y(k)}{\sqrt{\Lambda_x^2(k) + \Lambda_y^2(k)}}. \tag{4.47}$$

The eigenvalues of the lower bands are now

$$\begin{aligned} \lambda^{xy}_{\text{low},\pm} &= -\sqrt{E_{0k}^2 + \Lambda_k^2 \pm 2\left[E_{0k}^2 \Lambda_k^2 - W_k^2 \Lambda_k^2 \cos^2\phi_k\right]^{\frac{1}{2}}} \\ &\approx -E_{0k} \mp (1 - \frac{1}{2}\frac{W_k^2}{E_{0k}^2})|\vec{\Lambda}_k| - \frac{1}{2}\frac{W_k^2}{E_{0k}}\frac{\Lambda_k^2}{E_{0k}^2}\left[1 + O(\frac{W_k^2}{E_{0k}^2})\right], \end{aligned} \tag{4.48}$$

where we have used $\cos^2\phi_k \approx O(1)$. Notice that the signs of the second-order terms for $\lambda^{xy}_{\text{low},+}$ and $\lambda^{xy}_{\text{low},-}$ are both negative, leading to the net change in the ground state energy, which is opposite to the $\hat{N} = \hat{z}$ case. Assuming that $\Lambda_0 \ll W_0, \Delta_0 \ll W$, the change in the ground-state energy per lattice site will be

$$\begin{aligned} E_{\text{SO}} &= \sum_k \left[(\lambda^{xy}_{\text{low},+} + \lambda^{xy}_{\text{low},-}) - 2(-E_{0k}) \right] \\ &\approx -\sum_k \frac{\Lambda_k^2 W_k^2}{E_{0k}^3}\left[1 + O\left(\frac{W_k^2}{E_{0k}^2}\right)\right] \\ &= -\frac{\Lambda_0^2}{W}\left(\frac{W_0}{W}\right)^2\left[1 + O\left(\frac{W_0}{W}\right)^2\right] < 0, \end{aligned} \tag{4.49}$$

Therefore, $\hat{N}$ vector should lie in the xy plane in the presence of spin-orbit interaction and the result stated above follows.

As large as the spin-orbit coupling may be for U atoms, E_{SO} is still a small energy scale. However, if other anisotropies are absent, the order parameter would be in the XY plane, resulting in vortices; exchange anisotropy can also result in an easy-axis anisotropy, in which case spin textures could be Ising domain walls that can trap electrons. Although skyrmions are finite-energy solutions, vortices cost infinite energy unless they are bound in pairs. We speculate that charge $2e$-skyrmionic condensation is a more likely scenario, but the crossover in the texture is an interesting topic for further research.

The following remarks about URu_2Si_2 are relevant: in both magnetic field-temperature (H-T) and pressure-temperature (P-T) phase diagrams, the superconducting phase is enclosed within the HO phase [69]. This implies that the superconducting phase is closely related to the HO phase, and is probably induced by it. Throughout our calculation, ignoring of course skyrmions, we have assumed that the system is half-filled. The lower band is filled and the upper band is empty, and the topological invariant is quantized. If this is not the case, then there will be no quantized spin Hall conductance, but an induced superconducting phase from charge $2e$-skyrmionic condensation; doping will result in conducting midgap states, as in polyacetylene [38]. Of course, such a topological superconducting phase is very sensitive to disorder. Indeed, this may be supported by the destruction of the HO and superconducting phases with 4% Rh substitution on the Ru site [69]. To summarize, we can find a rationale for a HO phase enclosing a superconducting phase at lower temperatures.

CHAPTER 5

Chiral d-wave superconductivity in URu_2Si_2

5.1 Introduction

The identity of the order parameter in $\mathrm{URu_2Si_2}$ (URS) [69], a heavy-fermion material, below the so called hidden-order (HO) transition at $T_{\mathrm{HO}} = 17.5$ K is unknown despite its discovery more than a quarter century ago [87, 51, 37, 56, 18, 34, 42, 66, 26, 19, 24, 14, 100, 15, 84, 23, 43, 78, 85, 112]. Buried deep inside this phase lies a much less explored unconventional superconducting (SC) state at a temperature $T_c \sim 1.5$ K [76, 65, 88, 20, 69]. It is natural that there must be an intimate relation between the two. It is our central interest to explore this connection and to provide a mechanism for the unconventional SC state. We posit that an intriguing density wave state, termed mixed singlet-triplet d-density wave (st-DDW) [41, 40], is responsible for the HO. This state has no net charge or spin modulations and does not break time reversal symmetry (TRS). Thus, it is naturally impervious to common experimental probes. However, it does have topological order with a quantized spin Hall conductance [41]. We then construct a global phase diagram in which there is a deconfined quantum critical point (QCP) [92, 91], which is ultimately responsible for the basic mechanism of superconductivity. The skyrmionic spin texture in this density wave state fractionalizes into fermonic merons and antimerons [92], which results in two copies of unconventional chiral d-wave BCS superconductors [50, 110]. The deconfinement takes place only at the QCP. On one side of it merons and antimerons are paired to form skyrmions, but on the other side merons pairs with merons, and similarly for antimerons. The resulting SC state breaks TRS, which can be directly detected by polar Kerr effect (PKE) measurements [49]; in contrast, the HO state which does not break TRS should not exhibit PKE except perhaps for impurity effects. Determination of the density wave state posited here is also possible through two-magnon Raman scattering, nuclear

quadrupolar resonance, or the skyrmions themselves. In a more general context, our work reflects the rich possibilities of emergent behavior in condensed matter systems.

Density wave states of higher angular momenta are intriguing objects [71]. They are particle-hole condensates in contrast to particle-particle condensates in a superconductor. Because there are no exchange requirements between a particle and a hole, the orbital wave function cannot constrain the spin wave function. Of particular interest is the angular momentum $\ell = 2$: its singlet counterpart has been suggested to be the cause of the pseudogap in high-temperature superconductors [13]. Physically, it reflects staggered circulating charge currents in a two-dimensional square lattice. The triplet counterpart consists of circulating staggered spin current but not charge current. An attempt was made to relate it to the HO phase of URS to explain the observed anisotropic magnetic susceptibility [26, 75, 93]. While this is an interesting idea, so far it has not been able to provide a mechanism for superconductivity, which must be related to the HO state.

In contrast, we consider a mixed st-DDW, which mixes the triplet and the singlet density waves in the $\ell = 2$ channel; see Refs. [41, 40] for details. In Chapter 4, skyrmions are introduced as spin textures in the st-DDW state. They are shown to have zero angular momentum, charge $2e$ bosons, and therefore one could only predict an s-wave BEC condensate. However, available experiments [50, 110] show that the superconductivity is not s-wave, but chiral d-wave, breaking TRS. In this chapter we propose a totally new unconventional pairing mechanism arising from the fractionalization of skyrmions into merons and antimerons. The mechanism resolves the paradox that skyrmions may have zero angular momentum, but the superconductivity can be a chiral d-wave condensate. We also predict PKE at the onset of the superconductivity, but not in the HO state, which does not break TRS.

5.2 Nontrivial topology and charge $2e$ skyrmions

URS has a body-centered-tetragonal structure, and the order parameter and the band structure must be consistent with it; see Fig. 5.1. We consider the tight-binding model with the URS crystal structure [84] and the st-DDW order on the diagonal planes, which leads to the observed anisotropic

magnetic susceptibility. This model is merely a low-energy effective Hamiltonian, which is sufficient to illustrate our mechanism of superconductivity, but clearly cannot capture all aspects of URS:

$$\begin{aligned}\mathcal{H}_0 &= \sum_{k,\sigma}\left(\epsilon_k^{(1)} c_{1\sigma,k}^\dagger c_{1\sigma,k} + \epsilon_k^{(2)} c_{2\sigma,k}^\dagger c_{2\sigma,k}\right) + \sum_k \left(C_k c_{1+,k}^\dagger c_{2+,k} + C_k^* c_{1-,k}^\dagger c_{2-,k} + \text{H.c.}\right) \\ &\quad + \sum_k \left(D_k c_{1+,k}^\dagger c_{2-,k} - D_k^* c_{1-,k}^\dagger c_{2+,k} + \text{H.c.}\right), \end{aligned} \tag{5.1}$$

where $c_{\alpha\sigma,k}^\dagger$ is the creation operator of $5f$ electron with band index $\alpha = 1, 2$ and spin index $\sigma = \pm$, and the band structure is

$$\begin{aligned}\epsilon_k^{(\alpha)} &\equiv 8t\cos\left(\frac{k_x a}{2}\right)\cos\left(\frac{k_y a}{2}\right)\cos\left(\frac{k_z c}{2}\right) + 2t'_\alpha\left[\cos(k_x a) + \cos(k_y a)\right] \\ &\quad + 4t''_\alpha \cos(k_x a)\cos(k_y a) - \mu + \text{sgn}(\alpha)\frac{\Delta_{12}}{2}, \end{aligned} \tag{5.2}$$

where $\text{sgn}(\alpha) = \pm 1$ for $\alpha = 1, 2$, respectively. Here a and c are the lattice constants. t, t'_α, and t''_α are the hopping amplitudes along the body diagonals, in-plane axes, and in-plane diagonals, respectively. Δ_{12} is the crystal-field splitting and μ is the chemical potential. Notice that t, t'_α, and t''_α describe the hopping terms of the $5f$ electrons between the U atoms, and our conclusion holds as long as t is nonzero (See below and Appendix B). As in Ref. [84], we will take $C_k = 0$. D_k is related to the hybridization due to the Ru atoms, and has the form

$$D_k \equiv 4t_{12}\left[\sin\left(\frac{k_x a + k_y a}{2}\right) - i\sin\left(\frac{k_x a - k_y a}{2}\right)\right]\sin\left(\frac{k_z c}{2}\right) \tag{5.3}$$

Then the st-DDW order parameter is defined to be

$$\langle c_{\alpha\sigma,k+Q}^\dagger c_{\alpha\sigma',k}\rangle = \delta_{\sigma\sigma'}\Delta_k + i(\vec{\sigma}\cdot\hat{N})_{\sigma\sigma'}W_k, \tag{5.4}$$

where σ and σ' are spin indices and the nesting vector is $\vec{Q} = \frac{2\pi}{c}\hat{z}$, consistent with the fact that quantum oscillation frequencies are hardly changed between HO and the large-moment antiferromagnetic phase (LMAF) [70, 36]; W_k and Δ_k are the form factors for the triplet and the singlet components of the density wave order,

$$W_k = W_0 \sin\left(\frac{k_x a - k_y a}{2}\right)\sin\left(\frac{k_z c}{2}\right), \tag{5.5}$$

and

$$\Delta_k = \frac{\Delta_0}{2}\left[\cos\left(k_x a - k_y a\right) - \cos\left(k_z c\right)\right]. \tag{5.6}$$

We have checked that the inclusion of the hybridization, t_{12}, barely alters the ground-state energy. To be explicit, we found the change in the ground-state energy per lattice site is

$$\Delta E_{\text{hyb}} \approx -\frac{|t_{12}|^2}{W}\left(\frac{W_0}{W}\right)^2, \tag{5.7}$$

where $W = 8t$ is the bandwidth. ΔE_{hyb} is much smaller than W_0 and Δ_0 because $\left(\frac{W_0}{W}\right)^2 \approx 0.01$. Therefore, the inclusion of the hybridization will not affect our conclusion. Furthermore, it has also been pointed out that the Fermi surface does not depend strongly on t_{12} [84], so t_{12} will be neglected in the following discussion. In addition, the inclusion of the explicit spin-orbit coupling in the two-dimensional st-DDW model has been analyzed in Ref. [40], and it has been shown that the change in the ground-state energy per lattice site is

$$\Delta E_{\text{SO}} \approx \left[(\hat{N}\cdot\hat{z})^2 - 1\right]\frac{\Lambda_0^2}{W}\left(\frac{W_0}{W}\right)^2\left[1 + O\left(\frac{W_0}{W}\right)^2\right]. \tag{5.8}$$

Here Λ_0 is the strength of the spin-orbit coupling, given by

$$\mathcal{H}_{\text{SO}} = \sum_k c^\dagger_{k\alpha}\vec{\Lambda}(k)\cdot\vec{\sigma}_{\alpha\beta}c_{k\beta}, \tag{5.9}$$

where $\vec{\Lambda}(k) = \frac{\Lambda_0}{\sqrt{2}}[\hat{x}\sin k_y - \hat{y}\sin k_x]$. Although $\Lambda_0 \approx W$ for U atoms, ΔE_{SO} is still a small energy scale because of the small factor $\left(\frac{W_0}{W}\right)^2$. Therefore, the charge-$2e$ skyrmionic texture that we invoke below is unlikely to be affected by the explicit spin-orbit coupling, which will be neglected in the discussion. Notice that the order parameter itself cannot be factorized into spin and orbital parts, so it requires spin-orbit interaction to be realized. In other words, the spin-orbit interaction is present in the model even though we do not include it in the Hamiltonian explicitly.

At the mean-field level, we can choose the $\hat{N}$ vector to be uniform and perpendicular to the diagonal planes ($x + y =$ constant). The real space picture of the order parameter form factors are shown in Fig. 5.1. Note that this is different from Ref. [26], where there are two copies of spin current patterns on the diagonal planes and the singlet component is missing [40]. The spin currents are unaffected by the singlet component, as that only produces modulations of the bare

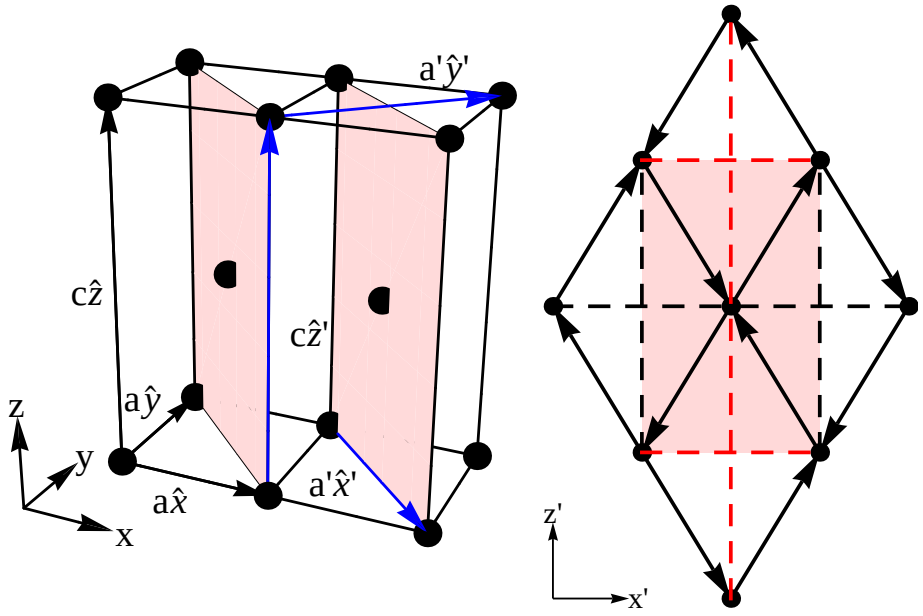

Figure 5.1: Left: the crystal structure of the URS material. The modulated hopping and spin current patterns are on the diagonal planes ($x + y =$ constant), which is highlighted with the pink color. The black points indicate the positions of the U atoms. The black arrows indicate three primitive vectors, $a\hat{x}$, $a\hat{y}$ and $c\hat{z}$. The blue arrows indicate three vectors for the rotated coordinate: $a'\hat{x}'$, $a'\hat{y}'$ and $c\hat{z}'$. Here $\hat{x}' = \frac{(\hat{x}-\hat{y})}{\sqrt{2}}$, $\hat{y}' = \frac{(\hat{x}+\hat{y})}{\sqrt{2}}$, $\hat{z}' = \hat{z}$, and $a' = \sqrt{2}a$. Right: the spin current patterns and hopping modulations on the diagonal planes. The arrows indicate the directions of the circulating spin currents due to the triplet component of the mixed st-DDW order. The red and black dashed lines indicate different signs of the modulated hopping terms due to the singlet component of the mixed st-DDW order. The Ru and Si atoms are not shown for clarity.

kinetic energy. Thus, we obtain similar anisotropic susceptibilities, as in Ref. [26]. However, Δ_0 has an important consequence on the basic nature of the HO state. One of the experimental signatures of the HO state is a jump in the specific heat $\frac{\Delta C}{T} \approx 270$ mJ/mol-K^2 at $T_{\rm HO}$, followed by an exponential drop below $T_{\rm HO}$, which can be fitted with a gap of ≈ 11 meV [76]. The specific heat for the mixed st-DDW state also exhibits a similar exponential behavior when we consider the fully gapped $k_{y'}a' = \pi$ plane; see Fig. 5.1 for the rotation of the coordinate axes. This implies that the specific heat reflects primarily the quasi-two-dimensional part of the spectrum, which justifies that it is a good approximation to consider the system as a collection of quasi-two-dimensional diagonal planes, with low carrier concentration. With the gap parameters of $W_0 = 14$ meV and $\Delta_0 = 13$ meV, we obtained the exponential drop $C(T) \propto e^{-\frac{\Delta}{T}}$, which is consistent with experiments, except for lower temperature linear behavior due to the fact that the three-dimensional Fermi surface is only partially gapped. Importantly, our basic mechanism of superconductivity depends on the quantized spin Hall effect on the diagonal planes, which is absent if $\Delta_0 = 0$ (cf. below).

A useful way to proceed is to sketch a proposed phase diagram in which we introduce a quantum parameter λ in addition to the physical parameters pressure P and temperature T as shown in Fig. 5.2. λ controls the skyrmion gap $W_0(\lambda)$ such that $W_0(\lambda < \lambda_c) = 0$ and $W_0(\lambda > \lambda_c) \neq 0$. A skyrmion, which is a distinct spin texture in the st-DDW, is shown in Fig. 5.3. We must emphasize that the hedgehog configurations are assumed to be suppressed because the particle-hole excitations are of much higher energy [31]. Therefore the skyrmion number is conserved in the two-dimensional diagonal planes. The state at $T = 0, P = 0$ is connected, as is the entire SC state, by continuity from the second order phase transition between the SC and the quantum spin Hall insulator (QSHI); λ_c is a deconfined quantum critical point [31]. This critical point is described by the field theory of merons and antimerons, fractional particles that emerge at λ_c, but are not present in either side of it. λ can be computed from a suitable microscopic Hamiltonian; for instance, λ may be a function of the on-site Coulomb interaction, U, the nearest neighbor direct interaction, V, and the exchange interaction, J, in the extended Hubbard model [42].

The eigenvalues and the eigenvectors of the mean-field Hamiltonian can be used to compute

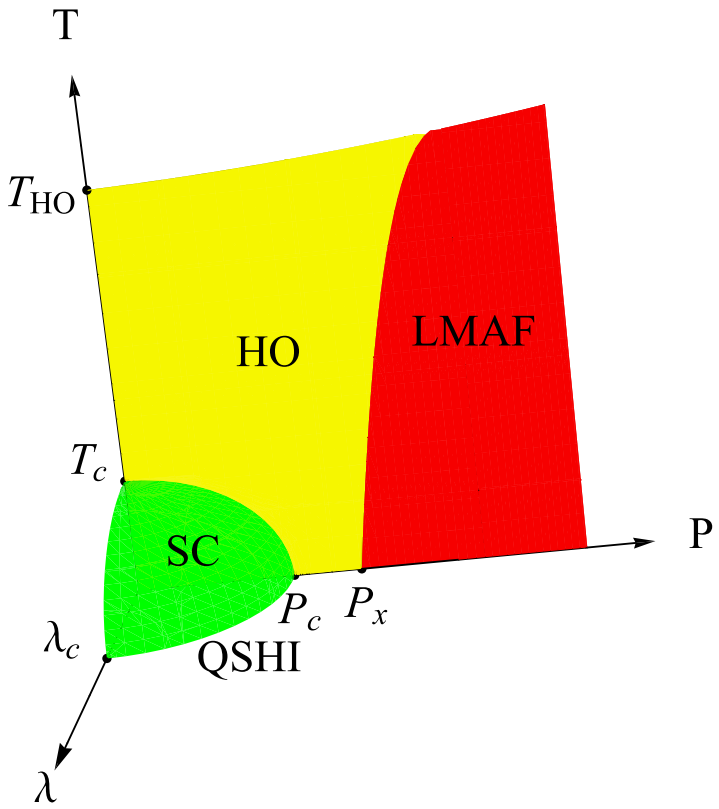

Figure 5.2: The proposed phase diagram with the quantum parameter (λ), pressure (P), and temperature (T) axes. Here λ is a tuning parameter such that the skyrmion gap $W_0(\lambda < \lambda_c) = 0$ and $W_0(\lambda > \lambda_c) \neq 0$. λ_c is a deconfined quantum critical point between the QSHI and SC as $T = P = 0$. T_{HO} and T_c are the HO and SC transition temperatures as $P = \lambda = 0$, respectively. Along the P axis, P_c indicates the phase transition between the HO and SC states, while P_x indicates the phase transition between the HO and LMAF states. In some literatures P_c coincides with P_x, which does not affect our main conclusion. In addition, there should be phase boundaries in the λ-P and λ-T planes, which are not relevant to this work.

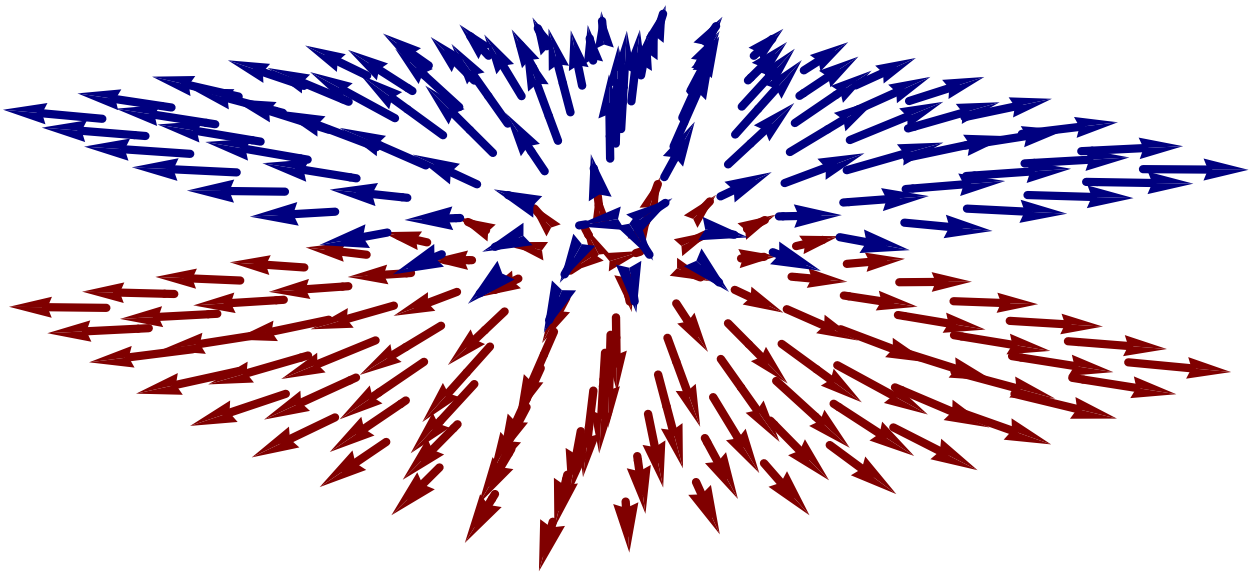

Figure 5.3: The merons $\psi^{\dagger}_{+,\sigma}(\vec{r})$ and $\psi^{\dagger}_{-,\sigma}(\vec{r})$. $\psi^{\dagger}_{+,\sigma}(\vec{r})$ creates a meron with $\hat{N}(r \to 0) = \hat{y}'$ and $\hat{N}(r \to \infty) = \frac{(x',0,z')}{r}$; $\psi^{\dagger}_{-,\sigma}(\vec{r})$ creates a meron with $\hat{N}(r \to 0) = -\hat{y}'$ and $\hat{N}(r \to \infty) = \frac{(x',0,z')}{r}$. Each meron above is half a skyrmion. A composite of a meron $\psi^{\dagger}_{+,\sigma}(\vec{r})$ and an antimeron $\psi_{-,\sigma'}(\vec{r})$ makes one skyrmion [92].

the Berry curvature, $\vec{\Omega}_{\sigma,\pm}$, for the upper and the lower bands ($\pm$),

$$\vec{\Omega}_{\sigma,\pm} \equiv \vec{\bigtriangledown}_k \times \langle \Phi_{\sigma,\pm}(k) | i \vec{\bigtriangledown}_k | \Phi_{\sigma,\pm}(k) \rangle, \tag{5.10}$$

where $|\Phi_{\sigma,\pm}(k)\rangle$ are the corresponding eigenstates. The Berry curvature is necessary for the computation of the physical charge and flux carried by the skyrmions. Notice that although a two-band tight-binding model is considered here, the Berry curvature for these two bands are identical because the t', t'' and Δ_{12} terms commute with the Hamiltonian and do not enter the eigenvectors. Therefore, the band index α and the crystal-field splitting Δ_{12} can be dropped. Since the mixed st-DDW order is on the diagonal planes, one finds that the nonzero contribution to the Berry phase arises from the component of the Berry curvature perpendicular to the diagonal planes. The result does not depend on the details of the band parameters as long as t, W_0, and Δ_0 are all nonzero (See Appendix B). In other words, we need a mixing of the triplet and the singlet density wave orders in order to have nontrivial topology. As in the two-dimensional model discussed in Chapters 3 and 4, the total Chern number is zero, but the spin Chern number is nonzero. Therefore, the topology of the system is nontrivial, and there will be a quantized spin Hall conductance on the $x'z'$ planes, $\sigma^{\text{spin}}_{x'z'} = \frac{e}{2\pi}$. Because of this the charge current corresponds to a physical charge (See Appendix B). Then, the skyrmionic spin texture can be constructed on the $x'z'$ plane, and one can find that the skyrmions in the system carry physical flux 4π, as in Refs. [31, 40]. As a skyrmion is adiabatically threaded through the system, a net charge of $-2e$ is displaced to the boundary at infinity; by charge neutrality of the total system, the skyrmion should have physical charge $2e$ and flux 4π.

5.3 chiral d-wave pairing

A skyrmion is a composite of a meron with a flux of 2π and charge e, and an antimeron with a flux of -2π and charge $-e$, as shown in Fig. 5.3. In the HO phase, the fractional particles are confined in skyrmions while in the SC phase they are bound into Cooper pairs (See Fig. 5.4). Let $\psi^\dagger_{s,\sigma}(\vec{r})$ be the creation operator of a meron at $\vec{r}$, where $s = \pm$ labels the flux of $\pm 2\pi$ and the spin index $\sigma = \uparrow$ and $\downarrow$ for up and down spin, respectively. Pairing of $\langle \psi^\dagger_{s,\sigma}(\vec{r}) \psi^\dagger_{s',\sigma'}(\vec{r}') \rangle$ thus results in a charge $2e$ superconductivity for $s = s'$. Motivated by experiments [50], we will be interested in

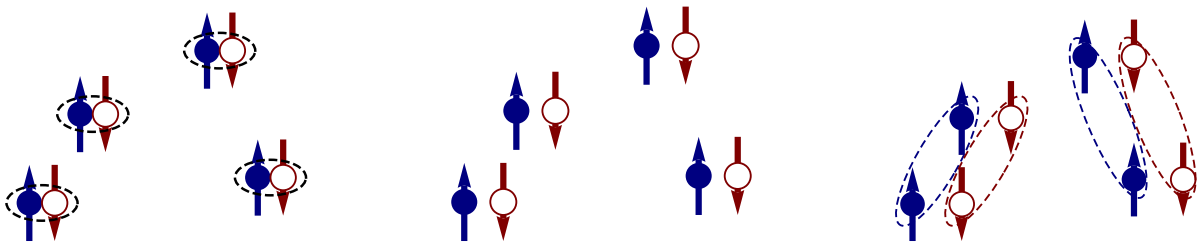

Figure 5.4: Deconfinement and pairing of the merons and antimerons. The up (down) arrows indicate a flux of $2\pi(-2\pi)$. The solid (open) circles indicate merons (antimerons). The dashed lines indicate the confinement and pairing. The colors are associated with the meron texture in Fig. 5.3. The spins of the merons are not shown for simplicity. Left: in the HO phase, merons and antimerons are confined in skyrmions. Middle: at the critical point, the merons and antimerons are deconfined. Right: in the SC phase, the merons and antimerons are separately confined again into Cooper pairs.

the spin-singlet pairing, so we will set $\sigma = -\sigma'$. Here we assume that the length scale of a meron is much smaller than the distance between the merons, so we can treat them as point particles.

The interaction Hamiltonian can be described by the coupling between the charge current $\vec{j}(\vec{r})$ and the gauge field $\vec{A}(\vec{r})$, which is associated with the flux of the merons and antimerons, $\mathcal{H}_{\text{int}} = \int d^2r \vec{j}(\vec{r}) \cdot \vec{A}(\vec{r})$. Notice that we will set $\hbar = c = 1$ for simplicity. With the continuity equation for the charge and current densities of the merons and antimerons, and assuming that the kinetic energy of the particles is $\epsilon_k = \frac{k^2}{2m}$ with the effective mass m, we may write the interaction in terms of the $\psi_{s,\sigma}(\vec{r})$ operators. This immediately leads to the spin-singlet pairing Hamiltonian in the momentum space

$$\mathcal{H}_{\text{int}} = \sum_{\vec{k},\vec{k}'} \sum_{s} V_{k'k} \psi^{\dagger}_{k',s,\uparrow} \psi^{\dagger}_{-k',s,\downarrow} \psi_{-k,s,\downarrow} \psi_{k,s,\uparrow}, \tag{5.11}$$

where $V_{k'k} \equiv \frac{4\pi i}{m} \frac{(\vec{k}\times\vec{k}')_{y'}}{|\vec{k}-\vec{k}'|^2}$. $\mathcal{H}_{\text{int}}$ clearly breaks TRS, so we expect the SC state to break TRS as well.

The interaction is similar to the one discussed in the half-filled Landau level problem [30] as well as the one proposed in the context of the hole-doped cuprates [68], though there are significant

differences as well. In Ref. [30], the flux attached to a particle is $\pi\epsilon$ instead of 2π so that fractional statistics could be studied by varying ϵ. The particles considered there were spinless fermions, so an odd-parity pairing state was obtained. Furthermore, the interaction (5.11) is different from the one in Ref. [68] because we express $\rho(\vec{r}) = \sum_{s,\sigma}(se)\psi^\dagger_{s,\sigma}(\vec{r})\psi_{s,\sigma}(\vec{r})$ and $\left(\vec{\nabla}\times\vec{A}(\vec{r})\right)_{y'} = \frac{2\pi}{e}\sum_{s,\sigma} s\psi^\dagger_{s,\sigma}(\vec{r})\psi_{s,\sigma}(\vec{r})$ differently. In Ref. [68], the resulting interaction depends on the sign of s, so the $s = \pm$ part leads to a $(d_{x^2-y^2} \mp id_{xy})$ superconductivity, respectively. As a result, the addition of these two components gives a $d_{x^2-y^2}$ superconductivity in cuprates, but *not* a chiral state.

In Eq. (5.11) we can see that the $s = +$ and $s = -$ parts in our case are two independent copies. With the kinetic energy term, the total Hamiltonian is

$$\mathcal{H}_{\text{total}} = \sum_{\vec{k},s,\sigma} \xi_k \psi^\dagger_{k,s,\sigma}\psi_{k,s,\sigma} + \mathcal{H}_{\text{int}} \tag{5.12}$$

where $\xi_k = \epsilon_k - \epsilon_F$ with the Fermi energy ϵ_F. Defining the gap $\Delta^{sc}_k \equiv -\sum_{k'} V_{kk'}\langle\psi_{-k',\downarrow}\psi_{k',\uparrow}\rangle$, the gap equation can be obtained within the mean-field approximation. At zero temperature, it gives

$$\Delta^{sc}_k = -\sum_{k'} V_{kk'}\frac{\Delta^{sc}_{k'}}{2\sqrt{\xi^2_{k'} + |\Delta^{sc}_{k'}|^2}}. \tag{5.13}$$

As mentioned above, a similar gap equation has been analyzed in Refs. [30, 68]. For ℓ wave pairing, the solution will be $\Delta^{sc}_k = |\Delta^{sc}_k|e^{-i\ell\phi_k}$, where ϕ_k denotes the direction of the wave vector, and we will choose it to be the angle between $\vec{k}$ and $\vec{k}'$. The magnitude of the gap can be written as

$$|\Delta^{sc}_k| \;=\; \begin{cases} \Delta^{sc}_F\left(\frac{k}{k_F}\right)^l, & \text{for } k \le k_F \\ \Delta^{sc}_F\left(\frac{k_F}{k}\right)^l, & \text{for } k \ge k_F \end{cases} \tag{5.14}$$

with the Fermi wave vector k_F and $\Delta^{sc}_F = |\Delta^{sc}_{k_F}|$. The gap equation can be solved numerically. For $\ell = 1, 2, 3, 4\cdots$, $\Delta^{sc}_F/\epsilon_F = 0.9160, 0.4058, 0.2644, 0.1968\cdots$. Since we have spin singlet pairing, the dominant channel will be $\ell = 2$. Hence the SC gap in the continuum limit will be $\Delta^{sc}_k \propto \left[(k^2_{x'} - k^2_{z'}) - 2ik_{x'}k_{z'}\right]$. In the lattice, the gap can be written as

$$\Delta^{sc}_k \propto \left\{\left[\cos\left(k_x a - k_y a\right) - \cos\left(k_z c\right)\right] + 4i\sin\left(\frac{k_x a - k_y a}{2}\right)\sin\left(\frac{k_z c}{2}\right)\right\} \tag{5.15}$$

with the original coordinate. Notice that in order to compare the lattice to the continuum case, one needs to rescale the anisotropic lattice constants a' and c in the diagonal planes; i.e. to rescale the pink rectangles in Fig. 5.1 into squares. Within a numerical prefactor the gap is proportional to the Fermi energy ϵ_F of merons because there are no other available scales. Thus, the knowledge of the $T = 0$ gap from experiments determines ϵ_F, a microscopic calculation of which would be exceedingly difficult.

5.4 Discussion

Notice that the meron-antimeron pair which constitutes a skyrmion is not the same as the meron-meron Cooper pair as shown in Fig. 5.4. This is the reason why a skyrmion has zero angular momentum [40] while a Cooper pair formed by the merons may have nonzero angular momentum. Our theory is consistent with quantum oscillation measurements, carried out at milliKelvin temperature and high enough field to destroy the SC state, once the three-dimensional character of the structure is taken into account. Of course our simple band structure cannot correctly obtain all the observed frequencies [24]. In three dimensions, we predict point nodes, in agreement with the specific heat measurements [110], but not line nodes, as inferred from the thermal conductivity measurements [50]. Clearly there is room for many future improvements, but the prediction of polar Kerr rotation [49] should establish the nature of the SC state, a chiral d-wave superconductor, a condensate made out of fractionalized particles. This is now confirmed in the latest measurements of Kapitulnik and his collaborators in the SC state, but not in the HO state except for impurity effects (A. Kapitulnik, private communication). A less direct measurement of broken TRS was recently presented in Ref. [63].

APPENDIX A

The derivations of equations in Chapter 4

A.1 Derivation of the nonlinear σ model

To derive the nonlinear σ model, we compute the effective action by integrating out fermions. We start with the action $S = \sum_{j=1}^{3} S_j$, where

$$S_j \equiv \int d^3x \bar{\psi}_j \left[G_j^{-1}\right] \psi_j, \tag{A.1}$$

with $G_j^{-1} \equiv G_{0,j}^{-1} + \Sigma_j$.

For $j = 1, 2$, we have

$$G_{0,j}^{-1} \equiv -i\sigma^0\tau^z\partial_\tau - 2it\sigma^0\tau^y(\eta_j\partial_x + \partial_y), \tag{A.2}$$

$$\Sigma_j \equiv i\eta_j\Delta_0\sigma^0\tau^0 - i\frac{W_0}{2}(\vec{\sigma}\cdot\hat{N})\tau^x(-\eta_j\partial_x + \partial_y), \tag{A.3}$$

and for $j = 3$, we have

$$G_{0,3}^{-1} \equiv -i\sigma^0\tau^z\partial_\tau, \tag{A.4}$$

$$\Sigma_3 \equiv W_0(\vec{\sigma}\cdot\hat{N})\tau^x. \tag{A.5}$$

The effective action will be $S_{\text{eff}} = \sum_{j=1}^{3} S_{\text{eff},j}$ with

$$S_{\text{eff},j} = -\ln\left[\int D\bar{\psi}_j D\psi_j e^{-S_j}\right] = -\ln\left[\det|G_j^{-1}|\right], \tag{A.6}$$

where the fermion operators can be integrated out easily since the Hamiltonian has only bilinear fermion operator terms. Using the mathematical identity $\ln\det|A| = \text{tr}\ln A$ with tr being the

trace, we have

$$\begin{aligned} S_{\text{eff},j} &= -\text{tr}\ln G_{0,j}^{-1}\left[1+G_{0,j}\Sigma_j\right] \\ &= -\text{tr}\ln G_{0,j}^{-1} - \text{tr}\left[G_{0,j}\Sigma_j\right] + \frac{1}{2}\text{tr}\left[G_{0,j}\Sigma_j G_{0,j}\Sigma_j\right] + \cdots, \end{aligned} \tag{A.7}$$

where we have used $\ln(1+x) = x - \frac{x^2}{2} + \cdots$.

The zeroth-order term is the effective action for free particles and the first-order term vanishes, so our goal is to compute the second-order terms:

$$\begin{aligned} S^{(2)}_{\text{eff},j} &\equiv \frac{1}{2}\text{tr}\left[G_{0,j}\Sigma_j G_{0,j}\Sigma_j\right] \\ &= \frac{1}{2}\int d\tau \int d\tau' \int d^2x \int d^2x' \text{Tr}\left[G_{0,j}(x,\tau;x',\tau')\Sigma_j(x',\tau')G_{0,j}(x',\tau';x,\tau)\Sigma_j(x,\tau)\right] \\ &= \frac{1}{2}\sum_{\tilde{k},\tilde{q}} \text{Tr}\left[G_{0,j}(\tilde{k})\Sigma_j(\tilde{q})G_{0,j}(\tilde{k}+\tilde{q})\Sigma_j(-\tilde{q})\right], \end{aligned} \tag{A.8}$$

where $\tilde{k} \equiv (k_0, k_x, k_y)$, $\tilde{q} \equiv (q_0, q_x, q_y)$, and $G_{0,j}(\tilde{k})$ can be obtained by inverting Eqs.(A.2) and (A.4). Here Tr is the trace over discrete indices.

Putting all together, taking long-wavelength limit ($\tilde{q} \to 0$) and keeping only terms up to the second-order derivative, we have, for $j = 1, 2$,

$$S^{(2)}_{\text{eff},j} \approx \left[-\Delta_0^2 + (\frac{W_0}{2})^2(-\eta_j q_x + q_y)^2(\hat{N}_{\tilde{q}}\cdot\hat{N}_{-\tilde{q}})\right], \tag{A.9}$$

where terms which are odd in $\tilde{k}$ and $\tilde{q}$ are dropped.

Using the relation $\sum_{\tilde{q}} f_{\tilde{q}} f_{-\tilde{q}} = \int d\tau d^2x |f(\vec{x},\tau)|^2$, we obtain

$$S^{(2)}_{\text{eff},1} + S^{(2)}_{\text{eff},2} \approx \frac{1}{g_1}\int d\tau d^2x \left[\left|\partial_X \hat{N}\right|^2 + \left|\partial_Y \hat{N}\right|^2\right], \tag{A.10}$$

where the constant terms are dropped, (X, Y) is the coordinate after a $\pi/4$ rotation, and

$$\frac{1}{g_1} \equiv \sum_{\tilde{k}} \frac{-W_0^2}{2(k_0^2 + 4t^2(k_x+k_y)^2)} \tag{A.11}$$

Similarly, for $j = 3$, we obtain

$$\begin{aligned} S^{(2)}_{\text{eff},j} &\approx -2\sum_{\tilde{k},\tilde{q}} \frac{W_0^2}{k_0^2}(\frac{q_0}{k_0})^2(\hat{N}_{\tilde{q}}\cdot\hat{N}_{-\tilde{q}}) \\ &= \frac{1}{g_3}\int d\tau d^2x \left|\partial_\tau \hat{N}\right|^2, \end{aligned} \tag{A.12}$$

where

$$\frac{1}{g_3} \equiv \sum_{\tilde{k}} \frac{2W_0^2}{k_0^4}. \tag{A.13}$$

Therefore, we obtain the nonlinear σ model,

$$S_{\text{eff}} \approx \frac{1}{g}\int d\tau d^2x \left|\partial_\mu \hat{N}\right|^2, \tag{A.14}$$

where the constant terms and higher-order terms are dropped, and it is rescaled in order to obtain a familiar form.

A.2 Chern-Simons coefficients

In this appendix we are going to prove that

$$\begin{aligned}\mathcal{N}(G_\sigma) &= \frac{\epsilon_{\mu\nu\lambda}}{24\pi^2}\text{Tr}\left[\int d^3k G_\sigma \frac{\partial G_\sigma^{-1}}{\partial k_\mu} G_\sigma \frac{\partial G_\sigma^{-1}}{\partial k_\nu} G_\sigma \frac{\partial G_\sigma^{-1}}{\partial k_\lambda}\right] \\ &= -\int \frac{d^2k}{4\pi}\hat{h}_\sigma \cdot \frac{\partial \hat{h}_\sigma}{\partial k_x} \times \frac{\partial \hat{h}_\sigma}{\partial k_y}.\end{aligned} \tag{A.15}$$

We start by taking (μ, ν, λ) to be $(0, x, y)$, and obtain

$$\begin{aligned} G_\sigma \frac{\partial G_\sigma^{-1}}{\partial \omega} &= \frac{1}{(i\omega)^2 - |\vec{h}_\sigma|^2}\left[(i\omega\hat{I} + \hat{\tau}\cdot\vec{h}_\sigma)\cdot(i\hat{I})\right] \\ &= \frac{1}{(i\omega)^2 - |\vec{h}_\sigma|^2}(-\omega\hat{I} + i\hat{\tau}\cdot\vec{h}_\sigma),\end{aligned} \tag{A.16}$$

and

$$\begin{aligned} G_\sigma \frac{\partial G_\sigma^{-1}}{\partial k_x} &= \frac{1}{(i\omega)^2 - |\vec{h}_\sigma|^2}\left[i\omega\hat{I} + \hat{\tau}\cdot\vec{h}_\sigma\right]\left(-\hat{\tau}\cdot\frac{\partial\vec{h}_\sigma}{\partial k_x}\right) \\ &= \frac{-1}{(i\omega)^2 - |\vec{h}_\sigma|^2}\left[\left(\vec{h}_\sigma\cdot\frac{\partial\vec{h}_\sigma}{\partial k_x}\right)\hat{I} + i\hat{\tau}\cdot\left(\omega\frac{\partial\vec{h}_\sigma}{\partial k_x} + \vec{h}_\sigma\times\frac{\partial\vec{h}_\sigma}{\partial k_x}\right)\right],\end{aligned} \tag{A.17}$$

where we have used the matrix identity $(\hat{\tau}\cdot\vec{a})(\hat{\tau}\cdot\vec{b}) = (\vec{a}\cdot\vec{b})\hat{I} + i\hat{\tau}\cdot(\vec{a}\times\vec{b})$. Similarly,

$$G_\sigma \frac{\partial G_\sigma^{-1}}{\partial k_y} = \frac{-1}{(i\omega)^2 - |\vec{h}_\sigma|^2}\left[\left(\vec{h}_\sigma\cdot\frac{\partial\vec{h}_\sigma}{\partial k_y}\right)\hat{I} + i\hat{\tau}\cdot\left(\omega\frac{\partial\vec{h}_\sigma}{\partial k_y} + \vec{h}_\sigma\times\frac{\partial\vec{h}_\sigma}{\partial k_y}\right)\right]. \tag{A.18}$$

Therefore,

$$
\begin{aligned}
& G_\sigma \frac{\partial G_\sigma^{-1}}{\partial k_x} G_\sigma \frac{\partial G_\sigma^{-1}}{\partial k_y} \\
= \; & \frac{1}{((i\omega)^2 - |\vec{h}_\sigma|^2)^2} \Bigg\{ \left(\vec{h}_\sigma \cdot \frac{\partial \vec{h}_\sigma}{\partial k_x}\right)\left(\vec{h}_\sigma \cdot \frac{\partial \vec{h}_\sigma}{\partial k_y}\right) \hat{I} \\
& + i\hat{\tau} \cdot \Bigg[\left(\vec{h}_\sigma \cdot \frac{\partial \vec{h}_\sigma}{\partial k_x}\right)\left(\omega \frac{\partial \vec{h}_\sigma}{\partial k_y} + \vec{h}_\sigma \times \frac{\partial \vec{h}_\sigma}{\partial k_y}\right) \\
& + \left(\vec{h}_\sigma \cdot \frac{\partial \vec{h}_\sigma}{\partial k_y}\right)\left(\omega \frac{\partial \vec{h}_\sigma}{\partial k_x} + \vec{h}_\sigma \times \frac{\partial \vec{h}_\sigma}{\partial k_x}\right) \Bigg] \\
& - \left[\hat{\tau} \cdot \left(\omega \frac{\partial \vec{h}_\sigma}{\partial k_x} + \vec{h}_\sigma \times \frac{\partial \vec{h}_\sigma}{\partial k_x}\right)\right]\left[\hat{\tau} \cdot \left(\omega \frac{\partial \vec{h}_\sigma}{\partial k_y} + \vec{h}_\sigma \times \frac{\partial \vec{h}_\sigma}{\partial k_y}\right)\right] \Bigg\} \qquad \text{(A.19)}
\end{aligned}
$$

Since we are going to multiply it with the antisymmetric tensor $\epsilon_{\mu\nu\lambda}$, the terms which are symmetric under $(x \leftrightarrow y)$ will vanish. Therefore, only the last term in the braces contributes,

$$
\begin{aligned}
& \left[\hat{\tau} \cdot \left(\omega \frac{\partial \vec{h}_\sigma}{\partial k_x} + \vec{h}_\sigma \times \frac{\partial \vec{h}_\sigma}{\partial k_x}\right)\right]\left[\hat{\tau} \cdot \left(\omega \frac{\partial \vec{h}_\sigma}{\partial k_y} + \vec{h}_\sigma \times \frac{\partial \vec{h}_\sigma}{\partial k_y}\right)\right] \\
= \; & i\hat{\tau} \cdot \Bigg[\omega^2 \left(\frac{\partial \vec{h}_\sigma}{\partial k_x} \times \frac{\partial \vec{h}_\sigma}{\partial k_y}\right) + \omega \vec{h}_\sigma \left(\frac{\partial \vec{h}_\sigma}{\partial k_x} \cdot \frac{\partial \vec{h}_\sigma}{\partial k_y}\right) - \omega \frac{\partial \vec{h}_\sigma}{\partial k_y}\left(\vec{h}_\sigma \cdot \frac{\partial \vec{h}_\sigma}{\partial k_x}\right) \\
& - \omega \vec{h}_\sigma \left(\frac{\partial \vec{h}_\sigma}{\partial k_x} \cdot \frac{\partial \vec{h}_\sigma}{\partial k_y}\right) + \omega \frac{\partial \vec{h}_\sigma}{\partial k_x}\left(\vec{h}_\sigma \cdot \frac{\partial \vec{h}_\sigma}{\partial k_y}\right) + \left(\vec{h}_\sigma \cdot \frac{\partial \vec{h}_\sigma}{\partial k_x} \times \frac{\partial \vec{h}_\sigma}{\partial k_y}\right)\vec{h}_\sigma \Bigg], \qquad \text{(A.20)}
\end{aligned}
$$

where we used the following mathematical identities:

$$
\vec{a} \times (\vec{b} \times \vec{c}) = \vec{b}(\vec{a} \cdot \vec{c}) - \vec{c}(\vec{a} \cdot \vec{b}), \;\; (\vec{a} \times \vec{b}) \times (\vec{a} \times \vec{c}) = [\vec{a} \cdot (\vec{b} \times \vec{c})]\vec{a}.
$$

Therefore, after combining with ϵ_{0xy} and taking the trace, we have

$$
\begin{aligned}
& \epsilon_{0xy} \mathrm{Tr}\left[G_\sigma \frac{\partial G_\sigma^{-1}}{\partial \omega} G_\sigma \frac{\partial G_\sigma^{-1}}{\partial k_x} G_\sigma \frac{\partial G_\sigma^{-1}}{\partial k_y}\right] \\
= \; & \frac{-1}{[(i\omega)^2 - |\vec{h}_\sigma|^2]^3} \mathrm{Tr}\Bigg(-i\omega\hat{\tau} \cdot \left[\omega^2 \left(\frac{\partial \vec{h}_\sigma}{\partial k_x} \times \frac{\partial \vec{h}_\sigma}{\partial k_y}\right) + \left(\vec{h}_\sigma \cdot \frac{\partial \vec{h}_\sigma}{\partial k_x} \times \frac{\partial \vec{h}_\sigma}{\partial k_y}\right)\vec{h}_\sigma\right] \\
& - (\hat{\tau} \cdot \vec{h}_\sigma)\left\{\hat{\tau} \cdot \left[\omega^2 \left(\frac{\partial \vec{h}_\sigma}{\partial k_x} \times \frac{\partial \vec{h}_\sigma}{\partial k_y}\right) + \left(\vec{h}_\sigma \cdot \frac{\partial \vec{h}_\sigma}{\partial k_x} \times \frac{\partial \vec{h}_\sigma}{\partial k_y}\right)\vec{h}_\sigma\right]\right\}\Bigg) \\
= \; & \frac{2}{[(i\omega)^2 - |\vec{h}_\sigma|^2]^3} \left\{\vec{h}_\sigma \cdot \left[\omega^2 \left(\frac{\partial \vec{h}_\sigma}{\partial k_x} \times \frac{\partial \vec{h}_\sigma}{\partial k_y}\right) + \left(\vec{h}_\sigma \cdot \frac{\partial \vec{h}_\sigma}{\partial k_x} \times \frac{\partial \vec{h}_\sigma}{\partial k_y}\right)\vec{h}_\sigma\right]\right\}
\end{aligned}
$$

$$= \frac{-2}{[(i\omega)^2 - |\vec{h}_\sigma|^2]^2}\left(\vec{h}_\sigma \cdot \frac{\partial \vec{h}_\sigma}{\partial k_x} \times \frac{\partial \vec{h}_\sigma}{\partial k_y}\right), \tag{A.21}$$

where we have used the fact that Pauli matrices are traceless, so the only contribution will be the term proportional to $\hat{I}$.

We have six nonzero terms because of the $\epsilon_{\mu\nu\lambda}$ tensor, so

$$\begin{aligned}
\mathcal{N}(G_\sigma) &= -\frac{2\times 6}{24\pi^2}\int d^3k \frac{1}{[(i\omega)^2 - |\vec{h}_\sigma|^2]^2}\left(\vec{h}_\sigma \cdot \frac{\partial \vec{h}_\sigma}{\partial k_x} \times \frac{\partial \vec{h}_\sigma}{\partial k_y}\right) \\
&= -\int \frac{d^2k}{4\pi}\frac{1}{|\vec{h}_\sigma|^3}\left(\vec{h}_\sigma \cdot \frac{\partial \vec{h}_\sigma}{\partial k_x} \times \frac{\partial \vec{h}_\sigma}{\partial k_y}\right) \\
&= -\int \frac{d^2k}{4\pi}\ \hat{h}_\sigma \cdot \frac{\partial \hat{h}_\sigma}{\partial k_x} \times \frac{\partial \hat{h}_\sigma}{\partial k_y},
\end{aligned} \tag{A.22}$$

where the energy integral was done by computing the residue of the second-order pole.

A.3 Spin gauge flux $F^s_{\mu\nu}$ in terms of $\hat{N}$

In the main text, we obtain the spin gauge field to be

$$f_\mu = \frac{\sigma^z}{2}A^s_\mu, \tag{A.23}$$

where $f_\mu = -iU^\dagger \partial_\mu U$. Therefore, we can write the spin gauge field in terms of the unitary matrix,

$$A^s_\mu = \mathrm{Tr}\left[\sigma^z \cdot \frac{\sigma^z}{2}A^s_\mu\right] = \mathrm{Tr}\left[\sigma^z f_\mu\right] = -i\mathrm{Tr}\left[\sigma^z U^\dagger \partial_\mu U\right], \tag{A.24}$$

and we have

$$F^s_{\mu\nu} = \partial_\mu A^s_\nu - \partial_\nu A^s_\mu = -i\mathrm{Tr}\left[\sigma^z(\partial_\mu U^\dagger)(\partial_\nu U) - \sigma^z(\partial_\nu U^\dagger)(\partial_\mu U)\right]. \tag{A.25}$$

Assume that the spin texture has a general form

$$\hat{N}(\vec{x},t) = [\sin\theta(\vec{x},t)\cos\phi(\vec{x},t), \sin\theta(\vec{x},t)\sin\phi(\vec{x},t), \cos\theta(\vec{x},t)], \tag{A.26}$$

where $\theta(\vec{x},t)$ and $\phi(\vec{x},t)$ can be any smooth function of position and time. Then, we have the unitary matrix

$$U(\vec{x},t) = \begin{pmatrix} \cos\frac{\theta(\vec{x},t)}{2} & -\sin\frac{\theta(\vec{x},t)}{2}e^{-i\phi(\vec{x},t)} \\ \sin\frac{\theta(\vec{x},t)}{2}e^{i\phi(\vec{x},t)} & \cos\frac{\theta(\vec{x},t)}{2} \end{pmatrix}, \tag{A.27}$$

$$\partial_\mu U^\dagger(\vec{x},t) = \begin{pmatrix} -\frac{1}{2}\sin\frac{\theta}{2}\partial_\mu\theta & e^{-i\phi}(\frac{1}{2}\cos\frac{\theta}{2}\partial_\mu\theta - i\sin\frac{\theta}{2}\partial_\mu\phi) \\ e^{i\phi}(-\frac{1}{2}\cos\frac{\theta}{2}\partial_\mu\theta - i\sin\frac{\theta}{2}\partial_\mu\phi) & -\frac{1}{2}\sin\frac{\theta}{2}\partial_\mu\theta \end{pmatrix}, \tag{A.28}$$

and

$$\partial_\nu U(\vec{x},t) = \begin{pmatrix} -\frac{1}{2}\sin\frac{\theta}{2}\partial_\nu\theta & e^{-i\phi}(-\frac{1}{2}\cos\frac{\theta}{2}\partial_\nu\theta + i\sin\frac{\theta}{2}\partial_\nu\phi) \\ e^{i\phi}(\frac{1}{2}\cos\frac{\theta}{2}\partial_\nu\theta + i\sin\frac{\theta}{2}\partial_\nu\phi) & -\frac{1}{2}\sin\frac{\theta}{2}\partial_\nu\theta \end{pmatrix}, \tag{A.29}$$

where we have suppressed the arguments of $\theta(\vec{x},t)$ and $\phi(\vec{x},t)$.

Therefore, we can calculate the product of the last two matrices, and express the spin gauge flux as

$$F^s_{\mu\nu} = -i\left[\frac{i}{2}\sin\theta(\partial_\mu\theta\partial_\nu\phi - \partial_\nu\theta\partial_\mu\phi)\right] \times 2 = \sin\theta\left(\partial_\mu\theta\partial_\nu\phi - \partial_\nu\theta\partial_\mu\phi\right). \tag{A.30}$$

In addition, we can also write $\hat{N}\cdot(\partial_\mu\hat{N}\times\partial_\nu\hat{N})$ in terms of $\theta(\vec{x},t)$ and $\phi(\vec{x},t)$,

$$\begin{aligned} & \hat{N}\cdot(\partial_\mu\hat{N}\times\partial_\nu\hat{N}) \\ = & \begin{vmatrix} \sin\theta(\vec{x},t)\cos\phi(\vec{x},t) & \sin\theta(\vec{x},t)\sin\phi(\vec{x},t) & \cos\theta(\vec{x},t) \\ [\cos\theta(\vec{x},t)\cos\phi(\vec{x},t)\partial_\mu\theta(\vec{x},t) & [\cos\theta(\vec{x},t)\sin\phi(\vec{x},t)\partial_\mu\theta(\vec{x},t) & -\sin\theta(\vec{x},t)\partial_\mu\theta(\vec{x},t) \\ -\sin\theta(\vec{x},t)\sin\phi(\vec{x},t)\partial_\mu\phi(\vec{x},t)] & +\sin\theta(\vec{x},t)\cos\phi(\vec{x},t)\partial_\mu\phi(\vec{x},t)] & \\ [\cos\theta(\vec{x},t)\cos\phi(\vec{x},t)\partial_\nu\theta(\vec{x},t) & [\cos\theta(\vec{x},t)\sin\phi(\vec{x},t)\partial_\nu\theta(\vec{x},t) & -\sin\theta(\vec{x},t)\partial_\nu\theta(\vec{x},t) \\ -\sin\theta(\vec{x},t)\sin\phi(\vec{x},t)\partial_\nu\phi(\vec{x},t)] & +\sin\theta(\vec{x},t)\cos\phi(\vec{x},t)\partial_\nu\phi(\vec{x},t)] & \end{vmatrix}, \\ = & \sin\theta\left(\partial_\mu\theta\partial_\nu\phi - \partial_\nu\theta\partial_\mu\phi\right), \end{aligned} \tag{A.31}$$

where, again, we suppressed the arguments of $\theta(\vec{x},t)$ and $\phi(\vec{x},t)$. Finally, we obtain

$$F^s_{\mu\nu} = \hat{N}\cdot(\partial_\mu\hat{N}\times\partial_\nu\hat{N}). \tag{A.32}$$

APPENDIX B

Some details of Chapter 5

B.1 Mean-field Hamiltonian

The mean-field Hamiltonian with the mixed st-DDW order is

$$\mathcal{H} = \sum_k \Psi_k^\dagger A_k \Psi_k, \tag{B.1}$$

where the summation is over the reduced Brillouin zone (RBZ). The spinor, $\Psi_k^\dagger$, is defined in terms of the fermion operators $(c_{k,\uparrow}^\dagger, c_{k+Q,\uparrow}^\dagger, c_{k,\downarrow}^\dagger, c_{k+Q,\downarrow}^\dagger)$ and the matrix A_k is

$$A_k = \begin{pmatrix} \epsilon_k - \mu & \Delta_k + iW_k & 0 & 0 \\ \Delta_k - iW_k & \epsilon_{k+Q} - \mu & 0 & 0 \\ 0 & 0 & \epsilon_k - \mu & \Delta_k - iW_k \\ 0 & 0 & \Delta_k + iW_k & \epsilon_{k+Q} - \mu \end{pmatrix}, \tag{B.2}$$

where μ is the chemical potential and the nesting vector is $\vec{Q} = \frac{2\pi}{c}\hat{z}$. Here the form factors W_k, Δ_k, and the band structure ϵ_k are

$$\begin{aligned} \epsilon_k &\equiv 8t\cos\left(\frac{k_x a}{2}\right)\cos\left(\frac{k_y a}{2}\right)\cos\left(\frac{k_z c}{2}\right) 2t'\left[\cos(k_x a) + \cos(k_y a)\right] \\ &\quad +4t''\cos(k_x a)\cos(k_y a), \end{aligned} \tag{B.3}$$

$$W_k \equiv W_0 \sin\left(\frac{k_x a - k_y a}{2}\right)\sin\left(\frac{k_z c}{2}\right), \tag{B.4}$$

$$\Delta_k \equiv \frac{\Delta_0}{2}\left[\cos\left(k_x a - k_y a\right) - \cos\left(k_z c\right)\right], \tag{B.5}$$

where t, t', and t'' are the hopping amplitudes along the body diagonals, in-plane axes, and in-plane diagonals, respectively. Notice that although a two-band tight-binding model is considered

in Ref. [84], the Berry curvature for these two bands are the same because the t', t'' and Δ_{12} terms commute with the Hamiltonian. Therefore, for simplicity the band index α and the crystal-field splitting Δ_{12} have been dropped.

The eigenvalues of the Hamiltonian are

$$\lambda_{k,\pm} = \epsilon_{2k} - \mu \pm E_k, \tag{B.6}$$

where $E_k = \sqrt{\epsilon_{1k}^2 + W_k^2 + \Delta_k^2}$, the $+(-)$ sign indicates the upper (lower) band, and

$$\epsilon_{1k} \equiv \frac{\epsilon_k - \epsilon_{k+Q}}{2} = 8t \cos\left(\frac{k_x a}{2}\right) \cos\left(\frac{k_y a}{2}\right) \cos\left(\frac{k_z c}{2}\right), \tag{B.7}$$

$$\epsilon_{2k} \equiv \frac{\epsilon_k + \epsilon_{k+Q}}{2} = 2t' \left[\cos(k_x a) + \cos(k_y a)\right] + 4t'' \cos(k_x a) \cos(k_y a) \tag{B.8}$$

B.2 Topological invariant

The topology of the system can be studied by computing the Berry phase of the eigenstates, and we define the Berry curvature, $\vec{\Omega}_{\sigma,\pm}$, as

$$\vec{\Omega}_{\sigma,\pm} \equiv \vec{\bigtriangledown}_k \times \langle \Phi_{\sigma,\pm}(k) | i \vec{\bigtriangledown}_k | \Phi_{\sigma,\pm}(k) \rangle, \tag{B.9}$$

where $|\Phi_{\sigma,\pm}(k)\rangle$ are the corresponding eigenstates. The Berry phase will be the integral of the Berry curvature over the reduced Brillouin zone (RBZ).

Since the mixed st-DDW order is on the diagonal planes, one may expect that the nonzero contribution to Berry phase arises from the component of the Berry curvature perpendicular to the diagonal planes. This is indeed the case, and in order to simplify the calculation, we first rotate the coordinate along z axis by 45°, i.e. $x' = \frac{(x-y)}{\sqrt{2}}$, $\frac{y'=(x+y)}{\sqrt{2}}$, and $z' = z$.

$$\epsilon_{1k} = 4t \left[\cos\left(\frac{k_{x'} a'}{2}\right) + \cos\left(\frac{k_{y'} a'}{2}\right)\right] \cos\left(\frac{k_{z'} c}{2}\right), \tag{B.10}$$

$$\epsilon_{2k} = 4t' \cos\left(\frac{k_{x'} a'}{2}\right) \cos\left(\frac{k_{y'} a'}{2}\right) + 2t'' \left[\cos\left(k_{x'} a'\right) + \cos\left(k_{y'} a'\right)\right], \tag{B.11}$$

$$W_k = W_0 \sin\left(\frac{k_{x'} a'}{2}\right) \sin\left(\frac{k_{z'} c}{2}\right), \tag{B.12}$$

$$\Delta_k = \frac{\Delta_0}{2} \left[\cos\left(k_{x'} a'\right) - \cos\left(k_{z'} c\right)\right], \tag{B.13}$$

where $a' = \sqrt{2}a$. The crystal structure is shown in Fig. 5.1 in Chapter 5, where we can find the primitive vectors in the rotated coordinate are $\frac{a'}{2}(\hat{x}' + \hat{y}')$, $\frac{a'}{2}(-\hat{x}' + \hat{y}')$ and $c\hat{z}'$. Therefore, the RBZ is bounded by $|k_{x'}a' \pm k_{y'}a'| = 2\pi$ and $|k_{z'}c| = \pi$. The spin-current patterns are now in the $x'z'$ planes (y' = constant). We choose the spin quantization axis to be y' axis, so $\sigma = \pm 1$ means the spin is along $\pm\hat{y}'$ direction.We will see below the nonzero contribution to the Berry phase is only from the y' component.

The Hamiltonian can be written as

$$\mathcal{H} = \sum_{k,\sigma} (c^{\dagger}_{k,\sigma}, c^{\dagger}_{k+Q,\sigma}) \left(\epsilon_{2k}\tau^0 + \vec{h}_\sigma \cdot \vec{\tau} \right) \begin{pmatrix} c_{k,\sigma} \\ \\ c_{k+Q,\sigma} \end{pmatrix}, \tag{B.14}$$

where τ^0 is 2×2 identity matrix and $\vec{\tau}$ are the Pauli matrices acting on the two-component spinor. Here the pseudospin vector is defined as $\vec{h}_\sigma \equiv (\Delta_k, -\sigma W_k, \epsilon_{1k})$. We have shown that the Berry curvature can be written in terms of the pseudospin vector $\vec{h}_\sigma$ [41]. The x', y' and z' components of the Berry curvature have the following forms,

$$(\Omega_{\sigma,\pm})_{x'} = \mp \frac{1}{2E_k^3} \vec{h}_\sigma \cdot \left(\frac{\partial \vec{h}_\sigma}{\partial k_{y'}} \times \frac{\partial \vec{h}_\sigma}{\partial k_{z'}} \right), \tag{B.15}$$

$$(\Omega_{\sigma,\pm})_{y'} = \mp \frac{1}{2E_k^3} \vec{h}_\sigma \cdot \left(\frac{\partial \vec{h}_\sigma}{\partial k_{z'}} \times \frac{\partial \vec{h}_\sigma}{\partial k_{x'}} \right), \tag{B.16}$$

$$(\Omega_{\sigma,\pm})_{z'} = \mp \frac{1}{2E_k^3} \vec{h}_\sigma \cdot \left(\frac{\partial \vec{h}_\sigma}{\partial k_{x'}} \times \frac{\partial \vec{h}_\sigma}{\partial k_{y'}} \right). \tag{B.17}$$

Notice that the Berry curvature does not depend on the t', t'' terms. To be explicit, we have

$$\begin{aligned} (\Omega_{\sigma,\pm})_{x'} &= \mp \frac{(-\sigma)}{2E_k^3} \begin{vmatrix} \Delta_k & W_k & \epsilon_{1k} \\ \frac{\partial \Delta_k}{\partial k_{y'}} & \frac{\partial W_k}{\partial k_{y'}} & \frac{\partial \epsilon_{1k}}{\partial k_{y'}} \\ \frac{\partial \Delta_k}{\partial k_{z'}} & \frac{\partial W_k}{\partial k_{z'}} & \frac{\partial \epsilon_{1k}}{\partial k_{z'}} \end{vmatrix} \\ &= \pm\sigma \frac{tW_0\Delta_0 a'c}{4E_k^3} \sin\left(\frac{k_{x'}a'}{2}\right) \sin\left(\frac{k_{y'}a'}{2}\right) \cos^2\left(\frac{k_{z'}c}{2}\right) \\ &\quad \times [-2 + \cos(k_{x'}a') + \cos(k_{z'}c)] \end{aligned} \tag{B.18}$$

For the y' component, we have

$$\begin{aligned}(\Omega_{\sigma,\pm})_{y'} &= \mp\frac{(-\sigma)}{2E_k^3}\begin{vmatrix} \Delta_k & W_k & \epsilon_{1k} \\ \frac{\partial\Delta_k}{\partial k_{z'}} & \frac{\partial W_k}{\partial k_{z'}} & \frac{\partial\epsilon_{1k}}{\partial k_{z'}} \\ \frac{\partial\Delta_k}{\partial k_{x'}} & \frac{\partial W_k}{\partial k_{x'}} & \frac{\partial\epsilon_{1k}}{\partial k_{x'}} \end{vmatrix} \\ &= \pm\sigma\frac{tW_0\Delta_0 a'c}{8E_k^3}\left[2-\cos\left(k_{x'}a'\right)-\cos\left(k_{z'}c\right)\right] \\ &\quad\times\left\{2+\cos\left(k_{x'}a'\right)+\cos\left(k_{z'}c\right)+\cos\left(\frac{k_{x'}a'}{2}\right)\cos\left(\frac{k_{y'}a'}{2}\right)\left[3+\cos\left(k_{z'}c\right)\right]\right\}\end{aligned} \tag{B.19}$$

For the z' component, we have

$$\begin{aligned}(\Omega_{\sigma,\pm})_{z'} &= \mp\frac{(-\sigma)}{2E_k^3}\begin{vmatrix} \Delta_k & W_k & \epsilon_{1k} \\ \frac{\partial\Delta_k}{\partial k_{x'}} & \frac{\partial W_k}{\partial k_{x'}} & \frac{\partial\epsilon_{1k}}{\partial k_{x'}} \\ \frac{\partial\Delta_k}{\partial k_{y'}} & \frac{\partial W_k}{\partial k_{y'}} & \frac{\partial\epsilon_{1k}}{\partial k_{y'}} \end{vmatrix} \\ &= \pm\sigma\frac{tW_0\Delta_0 a'^2}{8E_k^3}\cos\left(\frac{k_{x'}a'}{2}\right)\sin\left(\frac{k_{y'}a'}{2}\right)\sin\left(k_{z'}c\right)\left[-2+\cos\left(k_{x'}a'\right)+\cos\left(k_{z'}c\right)\right]\end{aligned} \tag{B.20}$$

Although $(\Omega_{\sigma,\pm})_{x'}$ and $(\Omega_{\sigma,\pm})_{z'}$ are nonzero, their integrals over the RBZ are zero. In other words, because of the planar structure of the order parameter, the Berry curvature and the topology will be similar to the two-dimensional model [41]. Under time reversal, the $k_{y'}a' = \pi$ plane maps onto the $k_{y'}a' = -\pi$ plane, which is equivalent to the $k_{y'}a' = \pi$ plane because there is a reflection symmetry under $k_{y'} \leftrightarrow -k_{y'}$. Therefore, the $k_{y'}a' = \pi$ plane maps onto itself under time reversal, so there is a topological invariant associated with the $k_{y'}a' = \pi$ plane [86]. On the other hand, the $k_{y'}a' = 0$ plane, which also maps onto itself under time reversal, is not fully gapped, so topological invariant is not well defined on this plane. In addition, for $k_{y'}a' = \pi$, the spectrum is fully gapped, which leads to an exponential behavior of the specific heat consistent with experiments and therefore implies that the relevant physics is on the $k_{y'}a' = \pi$ plane.

For the y' component, we thus project the Berry curvature to the $k_{y'}a' = \pi$ plane and perform the integral. The Chern number for each band will be

$$N_{\sigma,\pm} = \frac{1}{2\pi}\int_{-\frac{\pi}{a'}}^{\frac{\pi}{a'}} dk_{x'}\int_{-\frac{\pi}{c}}^{\frac{\pi}{c}} dk_{z'}(\Omega_{\sigma,\pm})_{y'} = \pm\sigma, \tag{B.21}$$

where the last integral was performed using Mathematica and the result does not depend on the details of the band parameters as long as t, W_0, and Δ_0 are all nonzero. Therefore, the topology of the system is nontrivial, and there will be a quantized spin Hall conductance on the $x'z'$ planes, $\sigma^{\text{spin}}_{x'z'} = \frac{e}{2\pi}$. Then, the skyrmionic spin texture can be constructed on the $x'z'$ plane, and one can find that the skyrmions in the system carry charge $2e$ as in Refs. [31, 40].

B.3 Skyrmions in the system

B.3.1 Low-energy action

As mentioned above, because of the planar structure of the order parameter, the interesting physics, such as the spin current patterns and the quantized spin Hall conductance, will be on the diagonal $x'z'$ planes ($y' =$ constant). So we may project the system onto the $x'z'$ planes to construct the linearized low-energy action. Again, the spin quantization axis is along y' axis, which is perpendicular to the $x'z'$ planes.

Defining the spinor $\psi^\dagger_{k,\alpha} \equiv (c^\dagger_{k,\alpha}, c^\dagger_{k+Q,\alpha})$ (not to be confused with the meron operator in Chapter 5), the Hamiltonian can be written as

$$\mathcal{H} = \sum_{\alpha,\beta}\sum_{k}\psi^\dagger_{k,\alpha}\left[\delta_{\alpha\beta}\tau^z\epsilon_{1k} + \delta_{\alpha\beta}\tau^x\Delta_k - (\vec{\sigma}\cdot\hat{N})_{\alpha\beta}\tau^y W_k\right]\psi_{k,\beta}, \tag{B.22}$$

where τ^i $(i = x, y, z)$ are Pauli matrices acting on the two-component spinor. For simplicity we have set $t' = t'' = \mu = 0$ and $k_{y'}a' = \pi$, so

$$\epsilon_{1k} = 4t\cos\left(\frac{k_{x'}a'}{2}\right)\cos\left(\frac{k_{z'}c}{2}\right), \tag{B.23}$$

$$W_k = W_0\sin\left(\frac{k_{x'}a'}{2}\right)\sin\left(\frac{k_{z'}c}{2}\right), \tag{B.24}$$

$$\Delta_k = \frac{\Delta_0}{2}\left[\cos\left(k_{x'}a'\right) - \cos\left(k_{z'}c\right)\right] \tag{B.25}$$

We can construct the low-energy effective model by linearizing the action around the following points,

$$\vec{K}_1 \equiv \frac{\pi}{c}\hat{z}', \tag{B.26}$$

$$\vec{K}_2 \equiv \frac{\pi}{a'}\hat{x}', \tag{B.27}$$

$$\vec{K}_3 \equiv \frac{\pi}{a'}\hat{x}' + \frac{\pi}{c}\hat{z}', \tag{B.28}$$

where $\vec{K}_1$ and $\vec{K}_2$ are the nodal points in the absence of the singlet component ($\Delta_0 = 0$), and $\vec{K}_3$ is the nodal point in the absence of triplet component ($W_0 = 0$).

Therefore, the linearized low-energy action will be

$$\begin{aligned} S = \int d^3x \Big\{ & \psi_1^\dagger \left[-\partial_\tau + 2t\tau^z c(\frac{1}{i}\partial_{z'}) - \tau^x\Delta_0 + (\vec{\sigma}\cdot\hat{N})\tau^y \frac{W_0}{2} a'(\frac{1}{i}\partial_{x'}) \right] \psi_1 \\ & + \psi_2^\dagger \left[-\partial_\tau + 2t\tau^z a'(\frac{1}{i}\partial_{x'}) + \tau^x\Delta_0 + (\vec{\sigma}\cdot\hat{N})\tau^y \frac{W_0}{2} c(\frac{1}{i}\partial_{z'}) \right] \psi_2 \\ & + \psi_3^\dagger \left[-\partial_\tau + (\vec{\sigma}\cdot\hat{N})\tau^y W_0 \right] \psi_3 \Big\}, \end{aligned} \tag{B.29}$$

where we have introduced the imaginary time $i\partial_t = -\partial_\tau$.

Notice that there is no spatial derivative in the ψ_3 term since the expansion of the form factor W_k around the nodal point K_3 is

$$W_{K_3+q} = W_0(1 - \frac{q_{x'}^2 a'^2}{8} - \frac{q_{z'}^2 c^2}{8} + \cdots), \tag{B.30}$$

where the second- (and higher-) order derivative terms are dropped when linearizing the action. In other words, the W_k term behaves as a mass term at the K_3 point.

B.3.2 The charges of the skyrmions: an adiabatic argument

We will compute the charge of skyrmions in the system by the adiabatic argument [31]. Consider the action around $\vec{K}_1$ when the order parameter is uniform (say, $\hat{N} = \hat{y}'$). The results for $\vec{K}_2$ and $\vec{K}_3$ follow identically.

$$S_1 = \int d^3x \psi_1^\dagger \left[-\partial_\tau + 2t\tau^z c(\frac{1}{i}\partial_{z'}) - \tau^x\Delta_0 + \sigma^{y'}\tau^y \frac{W_0}{2} a'(\frac{1}{i}\partial_{x'}) \right] \psi_1 \tag{B.31}$$

As mentioned above, the spin quantization axis is now along y' axis, so $\sigma = \pm 1$ means the spin is along $\pm\hat{y}'$ direction, and the Pauli spin matrices are

$$\sigma^{x'} = \begin{pmatrix} 0 & -i \\ i & 0 \end{pmatrix}; \quad \sigma^{y'} = \begin{pmatrix} 1 & 0 \\ 0 & -1 \end{pmatrix}; \quad \sigma^{z'} = \begin{pmatrix} 0 & 1 \\ 1 & 0 \end{pmatrix} \tag{B.32}$$

In the previous section we have shown that the nontrivial topology leads to a quantized spin Hall conductance on the $x'z'$ planes. The quantized spin Hall conductance implies that the external gauge fields A^c_μ and A^s_μ couple to spin and charge currents, respectively. In the presence of these external gauge fields, we add minimal coupling in the action by taking

$$\frac{1}{i}\partial_\mu \to \frac{1}{i}\partial_\mu + A^c_\mu + \frac{\sigma^{y'}}{2}A^s_\mu, \tag{B.33}$$

and the action can be written as

$$\begin{aligned} S_1[A^c, A^s] \;=\; & \int d^3x \psi_1^\dagger \left[-i\left(\frac{1}{i}\partial_\tau + A^c_\tau + \frac{\sigma^{y'}}{2}A^s_\tau\right) + 2t\tau^z c\left(\frac{1}{i}\partial_{z'} + A^c_{z'} + \frac{\sigma^{y'}}{2}A^s_{z'}\right)\right. \\ & \left. -\tau^x\Delta_0 + \sigma^{y'}\tau^y\frac{W_0}{2}a'\left(\frac{1}{i}\partial_{x'} + A^c_{x'} + \frac{\sigma^{y'}}{2}A^s_{x'}\right)\right]\psi_1, \end{aligned} \tag{B.34}$$

where we set $e = \hbar = c = 1$. The nonvanishing transverse spin conductance implies that the low energy effective action for the gauge fields is given by

$$S_{1,\text{eff}} = \frac{i}{2\pi}\int d^3x\, \epsilon^{\mu\nu\lambda}A^c_\mu\partial_\nu A^s_\lambda, \tag{B.35}$$

and the charge current is induced by the spin gauge field

$$j^c_\mu = \frac{1}{2\pi}\epsilon^{\mu\nu\lambda}\partial_\nu A^s_\lambda. \tag{B.36}$$

Notice that the prefactor comes from the quantized spin Hall conductance $\sigma^{\text{spin}}_{x'z'} = \frac{e}{2\pi}$, so this is a physical charge current.

Consider a static configuration of the $\hat{N}$ field with Pontryagin index one,

$$\hat{N}(r,\theta) = \left[\sin\alpha(r)\sin\theta, \cos\alpha(r), \sin\alpha(r)\cos\theta\right], \tag{B.37}$$

where (r,θ) is the polar coordinate defined on the $x'z'$ planes and $\alpha(r)$ satisfies the boundary conditions $\alpha(r=0) = 0$ and $\alpha(r\to\infty) = \pi$. This field configuration corresponds to a skyrmion,

and now the action is

$$S_1 = \int d^3x\psi_1^\dagger \left[-\partial_\tau + 2t\tau^z c(\frac{1}{i}\partial_{z'}) - \tau^x\Delta_0 + (\vec{\sigma}\cdot\hat{N})\tau^y\frac{W_0}{2}a'(\frac{1}{i}\partial_{x'})\right]\psi_1 \quad \text{(B.38)}$$

We can perform a unitary transformation at all points in space such that

$$U^\dagger(\vec{\sigma}\cdot\hat{N})U = \sigma^{y'} \quad \text{(B.39)}$$

Defining $\psi = U\psi'$, and plugging into Eq.(B.38), we obtain

$$\begin{aligned} S_1 &= \int d^3x\psi_1'^\dagger U^\dagger \left[-\partial_\tau + 2t\tau^z c(\frac{1}{i}\partial_{z'}) - \tau^x\Delta_0 + (\vec{\sigma}\cdot\hat{N})\tau^y\frac{W_0}{2}a'(\frac{1}{i}\partial_{x'})\right] U\psi_1' \\ &= \int d^3x\psi_1'^\dagger \left[-\partial_\tau + 2t\tau^z c(\frac{1}{i}\partial_{z'}) - \tau^x\Delta_0 + \sigma^{y'}\tau^y\frac{W_0}{2}a'(\frac{1}{i}\partial_{x'})\right]\psi_1' \\ &\quad + \int d^3x\psi_1'^\dagger \left[-\left(U^\dagger\partial_\tau U\right) + 2t\tau^z c\left(\frac{1}{i}U^\dagger\partial_{z'}U\right) + \sigma^{y'}\tau^y\frac{W_0}{2}a'\left(\frac{1}{i}U^\dagger\partial_{x'}U\right)\right]\psi_1' \end{aligned} \quad \text{(B.40)}$$

Equating Eq.(B.40) and Eq.(B.34), we have, as $r\to\infty$,

$$\frac{1}{i}U^\dagger\partial_{x'}U = \frac{\sigma^{y'}}{2}A^s_{x'}, \quad \text{(B.41)}$$

$$\frac{1}{i}U^\dagger\partial_{z'}U = \frac{\sigma^{y'}}{2}A^s_{z'}, \quad \text{(B.42)}$$

and $A^c_\tau = A^s_\tau = A^c_{x'} = A^c_{z'} = 0$.

In the far-field limit, the unitary matrix is

$$U(r\to\infty,\theta) = \begin{pmatrix} 0 & -e^{-i\theta} \\ e^{i\theta} & 0 \end{pmatrix}, \quad \text{(B.43)}$$

so the spin gauge field will be

$$\vec{A}^s = -\frac{2\sin\theta}{r}\hat{z}' + \frac{2\cos\theta}{r}\hat{x}' = \frac{2}{r}\hat{\theta}, \quad \text{(B.44)}$$

which is in the $x'z'$ planes.

In other words, threading a skyrmion into the system is equivalent to adding an external spin gauge field $\vec{A}^s$ with a flux of 4π in the y' direction. Suppose we adiabatically construct the

skyrmionic configuration $\hat{N}(r,\theta)$ from the ground state $\hat{y}'$ in a very large time period $\tau_p \to \infty$. During the process, we effectively thread a spin gauge flux of 4π adiabatically into the $x'z'$ planes. The quantized spin Hall conductance implies that a radial current will be induced by the 4π spin gauge flux of $\vec{A}^s(t)$, which is now time-dependent: $\vec{A}^s(t=0)=0$ and $\vec{A}^s(t=\tau_p)=\vec{A}^s$. That is,

$$j_r^c(t) = -\frac{1}{2\pi}\partial_t A_\theta^s(t). \tag{B.45}$$

As a result, charge will be transferred from the center to the boundary, and the total charge transferred during the process can be computed by performing the integral

$$Q^c = \int_0^{\tau_p} dt \int_0^{2\pi} r d\theta \; j_r^c(t) = -2. \tag{B.46}$$

Therefore, we obtain a skyrmion with charge $2e$ and flux 4π, as in the two-dimensional model [40].

REFERENCES

[1] A. J. Achkar, R. Sutarto, X. Mao, F. He, A. Frano, S. Blanco-Canosa, M. Le Tacon, G. Ghiringhelli, L. Braicovich, M. Minola, M. Moretti Sala, C. Mazzoli, Ruixing Liang, D. A. Bonn, W. N. Hardy, B. Keimer, G. A. Sawatzky, and D. G. Hawthorn, *Distinct charge orders in the planes and chains of ortho-III-ordered $YBa_2Cu_3O_{6+\delta}$ superconductors identified by resonant elastic X-ray scattering*, Phys. Rev. Lett. **109** (2012), 167001.

[2] G. Aeppli, T. E. Mason, S. M. Hayden, H. A. Mook, and J. Kulda, *Nearly singular magnetic fluctuations in the normal state of a high-T_c cuprate superconductor*, Science **278** (1997), 1432.

[3] O. K. Andersen, A. I. Liechtenstein, O. Jepsen, and F. Paulsen, *LDA energy bands, low-energy Hamiltonians, t', t'', $t_\perp(\boldsymbol{k})$, and $J_\perp$*, J. Phys. Chem. Solids **56** (1995), 1573.

[4] P. W. Anderson, *Coherent excited states in the theory of superconductivity: Gauge invariance and the Meissner effect*, Phys. Rev. **110** (1958), 827.

[5] P. W. Anderson, *Basic Notions of Condensed Matter Physics*, Westview Press, Boulder, CO, 1997.

[6] B. Andrei Bernevig and Shou-Cheng Zhang, *Quantum spin Hall effect*, Phys. Rev. Lett. **96** (2006), 106802.

[7] S. Bhattacharya, M. J. Higgins, D. C. Johnston, A. J. Jacobson, J. P. Stokes, D. P. Goshorn, and J. T. Lewandowski, *Elastic anomalies and phase transitions in high-T_c superconductors*, Phys. Rev. Lett. **60** (1988), 1181–1184.

[8] E. Blackburn, J. Chang, M. Hücker, A. T. Holmes, N. B. Christensen, Ruixing Liang, D. A. Bonn, W. N. Hardy, U. Rütt, O. Gutowski, M. v. Zimmermann, E. M. Forgan, and S. M. Hayden, *X-ray diffraction observations of a charge-density-wave order in superconducting ortho-II $YBa_2Cu_3O_{6.54}$ single crystals in zero magnetic field*, Phys. Rev. Lett. **110** (2013), 137004.

[9] Henrik Bruus and Karsten Flensberg, *Many-Body Quantum Theory in Condensed Matter Physics - An Introduction*, Oxford University Press, 2004.

[10] Sudip Chakravarty, *Quantum oscillations and key theoretical issues in high temperature superconductors from the perspective of density waves*, Rep. Prog. Phys. **74** (2011), 022501.

[11] Sudip Chakravarty, Bertrand I. Halperin, and David R. Nelson, *Two-dimensional quantum Heisenberg antiferromagnet at low temperatures*, Phys. Rev. B **39** (1989), 2344–2371.

[12] Sudip Chakravarty and Hae-Young Kee, *Fermi pockets and quantum oscillations of the Hall coefficient in high-temperature superconductors*, Proc. Natl. Acad. Sci. U.S.A. **105** (2008), 8835–8839.

[13] Sudip Chakravarty, R. B. Laughlin, Dirk K. Morr, and Chetan Nayak, *Hidden order in the cuprates*, Phys. Rev. B **63** (2001), 094503.

[14] P. Chandra, P. Coleman, J. A. Mydosh, and V. Tripathi, *Hidden orbital order in the heavy fermion metal URu_2Si_2*, Nature **417** (2002), 831–834.

[15] Premala Chandra, Piers Coleman, and Rebecca Flint, *Hastatic order in the heavy-fermion compound URu_2Si_2*, Nature **493** (2013), 621–626.

[16] J. Chang, E. Blackburn, A. T. Holmes, N. B. Christensen, J. Larsen, J. Mesot, Ruixing Liang, D. A. Bonn, W. N. Hardy, A. Watenphul, M. v. Zimmermann, E. M. Forgan, and S. M. Hayden, *Direct observation of competition between superconductivity and charge density wave order in $YBa_2Cu_3O_{6.67}$*, Nat. Phys. **8** (2012), 871.

[17] Andrey V. Chubukov and David M. Frenkel, *Renormalized perturbation theory of magnetic instabilities in the two-dimensional Hubbard model at small doping*, Phys. Rev. B **46** (1992), 11884–11901.

[18] Francesco Cricchio, Fredrik Bultmark, Oscar Grånäs, and Lars Nordström, *Itinerant magnetic multipole moments of rank five as the hidden order in URu_2Si_2*, Phys. Rev. Lett. **103** (2009), 107202.

[19] Tanmoy Das, *Spin-orbit density wave induced hidden topological order in URu_2Si_2*, Sci. Rep. **2** (2012), 596.

[20] A. de Visser, F. E. Kayzel, A. A. Menovsky, J. J. M. Franse, J. van den Berg, and G. J. Nieuwenhuys, *Thermal expansion and specific heat of monocrystalline URu_2Si_2*, Phys. Rev. B **34** (1986), 8168–8171.

[21] Nicolas Doiron-Leyraud, *The Fermi surface of cuprate superconductors*, Physics in Canada **62** (2011), 89.

[22] Nicolas Doiron-Leyraud, Cyril Proust, David LeBoeuf, Julien Levallois, Jean-Baptiste Bonnemaison, Ruixing Liang, D. A. Bonn, W. N. Hardy, and Louis Taillefer, *Quantum oscillations and the Fermi surface in an underdoped high-T_c superconductor*, Nature **447** (2007), 565–568.

[23] Yonatan Dubi and Alexander V. Balatsky, *Hybridization wave as the "hidden order" in URu_2Si_2*, Phys. Rev. Lett. **106** (2011), 086401.

[24] S. Elgazzar, J. Rusz, M. Amft, P. M. Oppeneer, and J. A. Mydosh, *Hidden order in URu_2Si_2 originates from Fermi surface gapping induced by dynamic symmetry breaking*, Nature Mater. **8** (2009), 337–341.

[25] I. Eremin and D. Manske, *Fermi-liquid-based theory for the in-plane magnetic anisotropy in untwinned high-T_c superconductors*, Phys. Rev. Lett. **94** (2005), 067006.

[26] Satoshi Fujimoto, *Spin nematic state as a candidate of the hidden order phase of URu_2Si_2*, Phys. Rev. Lett. **106** (2011), 196407.

[27] David Garcia-Aldea and Sudip Chakravarty, *Multiple quantum oscillation frequencies in $YBa_2Cu_3O_{6+\delta}$ and bilayer splitting*, New J. Phys. **12** (2010), 105005.

[28] David Garcia-Aldea and Sudip Chakravarty, *Singlet versus triplet particle-hole condensates in quantum oscillations in cuprates*, Phys. Rev. B **82** (2010), 184526.

[29] G. Ghiringhelli, M. Le Tacon, M. Minola, S. Blanco-Canosa, C. Mazzoli, N. B. Brookes, G. M. De Luca, A. Frano, D. G. Hawthorn, F. He, T. Loew, M. Moretti Sala, D. C. Peets, M. Salluzzo, E. Schierle, R. Sutarto, G. A. Sawatzky, E. Weschke, B. Keimer, and L. Braicovich, *Long-range incommensurate charge fluctuations in (Y,Nd)$Ba_2Cu_3O_{6+x}$*, Science **337** (2012), 821–825.

[30] Martin Greiter, X.G. Wen, and Frank Wilczek, *Paired Hall states*, Nucl. Phys. B **374** (1992), 567–614.

[31] Tarun Grover and T. Senthil, *Topological spin Hall states, charged skyrmions, and superconductivity in two dimensions*, Phys. Rev. Lett. **100** (2008), 156804.

[32] Christoph J. Halboth and Walter Metzner, *d-wave superconductivity and Pomeranchuk instability in the two-dimensional Hubbard model*, Phys. Rev. Lett. **85** (2000), 5162–5165.

[33] F. D. M. Haldane, *Model for a quantum Hall effect without Landau levels: Condensed-matter realization of the "parity anomaly"*, Phys. Rev. Lett. **61** (1988), 2015–2018.

[34] Hisatomo Harima, Kazumasa Miyake, and Jacques Flouquet, *Why the hidden order in URu_2Si_2 is still hidden—one simple answer*, J. Phys. Soc. Jpn. **79** (2010), 033705.

[35] M. Z. Hasan and C. L. Kane, *Colloquium : Topological insulators*, Rev. Mod. Phys. **82** (2010), 3045–3067.

[36] E. Hassinger, G. Knebel, T. D. Matsuda, D. Aoki, V. Taufour, and J. Flouquet, *Similarity of the Fermi surface in the hidden order state and in the antiferromagnetic state of URu_2Si_2*, Phys. Rev. Lett. **105** (2010), 216409.

[37] K. Haule and G. Kotliar, *Arrested Kondo effect and hidden order in URu_2Si_2*, Nature Phys. **5** (2009), 796–799.

[38] A. J. Heeger, S. Kivelson, J. R. Schrieffer, and W. P. Su, *Solitons in conducting polymers*, Rev. Mod. Phys. **60** (1988), 781–850.

[39] V. Hinkov, P. Bourges, S. Pailhes, Y. Sidis, A. Ivanov, C. D. Frost, T. G. Perring, C. T. Lin, D. P. Chen, and B. Keimer, *Spin dynamics in the pseudogap state of a high-temperature superconductor*, Nat. Phys. **3** (2007), 780.

[40] Chen-Hsuan Hsu and Sudip Chakravarty, *Charge-$2e$ skyrmion condensate in a hidden-order state*, Phys. Rev. B **87** (2013), 085114.

[41] Chen-Hsuan Hsu, S. Raghu, and Sudip Chakravarty, *Topological density wave states of nonzero angular momentum*, Phys. Rev. B **84** (2011), 155111.

[42] Hiroaki Ikeda and Yoji Ohashi, *Theory of unconventional spin density wave: A possible mechanism of the micromagnetism in U-based heavy fermion compounds*, Phys. Rev. Lett. **81** (1998), 3723–3726.

[43] Hiroaki Ikeda, Michi Suzuki, Ryotaro Arita, Tetsuya Takimoto, Takasada Shibauchi, and Yuji Matsuda, *Emergent rank-5 nematic order in URu_2Si_2*, Nature Phys. **8** (2012), 528.

[44] J.-P. Ismer, I. Eremin, and Dirk K. Morr, *Dynamical spin susceptibility and the resonance peak in the pseudogap region of the underdoped cuprate superconductors*, Phys. Rev. B **73** (2006), 104519.

[45] Hong-Min Jiang, Jian Zhou, and Jian-Xin Li, *Spin dynamics in the pseudogap state: phase fluctuation versus d-density wave*, New J. Phys. **13** (2011), 113016.

[46] B. D. Josephson, *The discovery of tunnelling supercurrents*, Rev. Mod. Phys. **46** (1974), 251.

[47] C. L. Kane and E. J. Mele, *Quantum spin Hall effect in graphene*, Phys. Rev. Lett. **95** (2005), 226801.

[48] C. L. Kane and E. J. Mele, *Z_2 Topological order and the quantum spin Hall effect*, Phys. Rev. Lett. **95** (2005), 146802.

[49] Aharon Kapitulnik, Jing Xia, Elizabeth Schemm, and Alexander Palevski, *Polar Kerr effect as probe for time-reversal symmetry breaking in unconventional superconductors*, New J. Phys. **11** (2009), 055060.

[50] Y. Kasahara, T. Iwasawa, H. Shishido, T. Shibauchi, K. Behnia, Y. Haga, T. D. Matsuda, Y. Onuki, M. Sigrist, and Y. Matsuda, *Exotic superconducting properties in the electron-hole-compensated heavy-fermion "semimetal" URu_2Si_2*, Phys. Rev. Lett. **99** (2007), 116402.

[51] Annamaria Kiss and Patrik Fazekas, *Group theory and octupolar order in URu_2Si_2*, Phys. Rev. B **71** (2005), 054415.

[52] S. A. Kivelson, E. Fradkin, and V. J. Emery, *Electronic liquid-crystal phases of a doped Mott insulator*, Nature **393** (1998), 550–553.

[53] P. Kotetes and G. Varelogiannis, *Meissner effect without superconductivity from a chiral d-density wave*, Phys. Rev. B **78** (2008), 220509.

[54] P. Kotetes and G. Varelogiannis, *Chirality induced tilted-hill giant Nernst signal*, Phys. Rev. Lett. **104** (2010), 106404.

[55] A.B. Kuklov, N.V. Prokof'ev, B.V. Svistunov, and M. Troyer, *Deconfined criticality, runaway flow in the two-component scalar electrodynamics and weak first-order superfluid-solid transitions*, Annals of Physics **321** (2006), 1602 – 1621.

[56] Hiroaki Kusunose and Hisatomo Harima, *On the hidden order in URu_2Si_2 — antiferro hexadecapole order and its consequences*, J. Phys. Soc. Jpn. **80** (2011), 084702.

[57] L. D. Landau and E. M. Lifshitz, *Statistical Physics*, Pergamon Press, Oxford, 1980.

[58] R. B. Laughlin, *Fermi-liquid computation of the phase diagram of high-T_c cuprate superconductors with an orbital antiferromagnetic pseudogap*, Phys. Rev. Lett. **112** (2014), 017004.

[59] R. B. Laughlin, *Hartree-Fock computation of the high-T_c cuprate phase diagram*, Phys. Rev. B **89** (2014), 035134.

[60] M. Le Tacon, G. Ghiringhelli, J. Chaloupka, M. Moretti Sala, V. Hinkov, M. W. Haverkort, M. Minola, M. Bakr, K. J. Zhou, S. Blanco-Canosa, C. Monney, G. L. Song, Y. T.and Sun, C. T. Lin, G. M. De Luca, M. Salluzzo, G. Khaliullin, T. Schmitt, L. Braicovich, and B. Keimer, *Intense paramagnon excitations in a large family of high-temperature superconductors*, Nat. Phys. **7** (2011), 725.

[61] David LeBoeuf, Nicolas Doiron-Leyraud, Julien Levallois, R. Daou, J.-B. Bonnemaison, N. E. Hussey, L. Balicas, B. J. Ramshaw, Ruixing Liang, D. A. Bonn, W. N. Hardy, S. Adachi, Cyril Proust, and Louis Taillefer, *Electron pockets in the Fermi surface of hole-doped high-T_c superconductors*, Nature **450** (2007), 533.

[62] David LeBoeuf, Nicolas Doiron-Leyraud, B. Vignolle, Mike Sutherland, B. J. Ramshaw, J. Levallois, R. Daou, Francis Laliberté, Olivier Cyr-Choinière, Johan Chang, Y. J. Jo, L. Balicas, Ruixing Liang, D. A. Bonn, W. N. Hardy, Cyril Proust, and Louis Taillefer, *Lifshitz critical point in the cuprate superconductor $YBa_2Cu_3O_y$ from high-field Hall effect measurements*, Phys. Rev. B **83** (2011), 054506.

[63] G. Li, Q. Zhang, D. Rhodes, B. Zeng, P. Goswami, R. E. Baumbach, P. H. Tobash, F. Ronning, J. D. Thompson, E. D. Bauer, and L. Balicas, *Bulk evidence for a time-reversal symmetry broken superconducting state in URu_2Si_2*, Phys. Rev. B **88** (2013), 134517.

[64] Chi-Ken Lu and Igor F. Herbut, *Zero modes and charged skyrmions in graphene bilayer*, Phys. Rev. Lett. **108** (2012), 266402.

[65] M. B. Maple, J. W. Chen, Y. Dalichaouch, T. Kohara, C. Rossel, M. S. Torikachvili, M. W. McElfresh, and J. D. Thompson, *Partially gapped fermi surface in the heavy-electron superconductor URu_2Si_2*, Phys. Rev. Lett. **56** (1986), 185–188.

[66] V. P. Mineev and M. E. Zhitomirsky, *Interplay between spin-density wave and induced local moments in URu_2Si_2*, Phys. Rev. B **72** (2005), 014432.

[67] Eun-Gook Moon, *Skyrmions with quadratic band touching fermions: A way to achieve charge $4e$ superconductivity*, Phys. Rev. B **85** (2012), 245123.

[68] T. Morinari, *Mechanism of $d_{x^2-y^2}$-wave superconductivity based on hole-doping-induced spin texture in high T_c cuprates*, Phys. Rev. B **73** (2006), 064504.

[69] J. A. Mydosh and P. M. Oppeneer, *Colloquium : Hidden order, superconductivity, and magnetism: The unsolved case of URu_2Si_2*, Rev. Mod. Phys. **83** (2011), 1301–1322.

[70] M. Nakashima, H. Ohkuni, Y. Inada, R. Settai, Y. Haga, E. Yamamoto, and Y. Onuki, *The de Haas-van Alphen effect in URu_2Si_2 under pressure*, J. Phys.: Condens. Matter **15** (2003), S2011.

[71] Chetan Nayak, *Density-wave states of nonzero angular momentum*, Phys. Rev. B **62** (2000), 4880–4889.

[72] Chetan Nayak and Eugene Pivovarov, *$d_{x^2-y^2}$ density-wave order and its role in the phase diagram of extended Hubbard models*, Phys. Rev. B **66** (2002), 064508.

[73] A A Nersesyan, G I Japaridze, and I G Kimeridze, *Low-temperature magnetic properties of a two-dimensional spin nematic state*, J. Phys.: Condens. Matter **3** (1991), 3353.

[74] M. R. Norman, D. Pines, and C. Kallin, *The pseudogap: friend or foe of high T_c ?*, Adv. Phys. **54** (2005), 715–733.

[75] R. Okazaki, T. Shibauchi, H. J. Shi, Y. Haga, T. D. Matsuda, E. Yamamoto, Y. Onuki, H. Ikeda, and Y. Matsuda, *Rotational symmetry breaking in the hidden-order phase of URu_2Si_2*, Science **331** (2011), 439–442.

[76] T. T. M. Palstra, A. A. Menovsky, J. van den Berg, A. J. Dirkmaat, P. H. Kes, G. J. Nieuwenhuys, and J. A. Mydosh, *Superconducting and magnetic transitions in the heavy-fermion system URu_2Si_2*, Phys. Rev. Lett. **55** (1985), 2727–2730.

[77] E. Pavarini, I. Dasgupta, T. Saha-Dasgupta, O. Jepsen, and O. K. Andersen, *Band-structure trend in hole-doped cuprates and correlation with T_c*, Phys. Rev. Lett. **87** (2001), 047003.

[78] C. Pépin, M. R. Norman, S. Burdin, and A. Ferraz, *Modulated spin liquid: A new paradigm for URu_2Si_2*, Phys. Rev. Lett. **106** (2011), 106601.

[79] Xiao-Liang Qi and Shou-Cheng Zhang, *Topological insulators and superconductors*, Rev. Mod. Phys. **83** (2011), 1057–1110.

[80] S. Raghu, Xiao-Liang Qi, C. Honerkamp, and Shou-Cheng Zhang, *Topological Mott insulators*, Phys. Rev. Lett. **100** (2008), 156401.

[81] R. Rajaraman, *Solitons and Instantons - An Introduction to Solitons and Instantons in Quantum Field Theory*, North-Holland Personal Library, 1983.

[82] B. J. Ramshaw, Baptiste Vignolle, James Day, Ruixing Liang, W. N. Hardy, Cyril Proust, and D. A. Bonn, *Angle dependence of quantum oscillations in $YBa_2Cu_3O_{6.59}$ shows free-spin behaviour of quasiparticles*, Nat. Phys. **7** (2011), 234–238.

[83] Y. Ran, A. Vishwanath, and D. Lee, *A direct transition between a Neel ordered Mott insulator and a $d_{x^2-y^2}$ superconductor on the square lattice*, e-print (2008), arXiv:0806.2321v2.

[84] Jeffrey G. Rau and Hae-Young Kee, *Hidden and antiferromagnetic order as a rank-5 superspin in URu_2Si_2*, Phys. Rev. B **85** (2012), 245112.

[85] Peter S. Riseborough, B. Coqblin, and S. G. Magalhães, *Phase transition arising from the underscreened Anderson lattice model: A candidate concept for explaining hidden order in URu_2Si_2*, Phys. Rev. B **85** (2012), 165116.

[86] Rahul Roy, *Characterization of three-dimensional topological insulators by two-dimensional invariants*, New J. Phys. **12** (2010), 065009.

[87] P. Santini and G. Amoretti, *Crystal field model of the magnetic properties of URu_2Si_2*, Phys. Rev. Lett. **73** (1994), 1027–1030.

[88] W. Schlabitz, J. Baumann, B. Pollit, U. Rauchschwalbe, H.M. Mayer, U. Ahlheim, and C.D. Bredl, *Superconductivity and magnetic order in a strongly interacting fermi-system: URu_2Si_2*, Z. Phys. B **62** (1986), 171–177.

[89] Andreas P. Schnyder, Dirk Manske, Christopher Mudry, and Manfred Sigrist, *Theory for inelastic neutron scattering in orthorhombic high-T_c superconductors*, Phys. Rev. B **73** (2006), 224523.

[90] J. R. Schrieffer, X. G. Wen, and S. C. Zhang, *Dynamic spin fluctuations and the bag mechanism of high-T_c superconductivity*, Phys. Rev. B **39** (1989), 11663.

[91] T. Senthil, Leon Balents, Subir Sachdev, Ashvin Vishwanath, and Matthew P. A. Fisher, *Quantum criticality beyond the Landau-Ginzburg-Wilson paradigm*, Phys. Rev. B **70** (2004), 144407.

[92] T. Senthil, Ashvin Vishwanath, Leon Balents, Subir Sachdev, and Matthew P. A. Fisher, *Deconfined quantum critical points*, Science **303** (2004), 1490–1494.

[93] T. Shibauchi and Y. Matsuda, *Thermodynamic evidence for broken fourfold rotational symmetry in the hidden-order phase of URu_2Si_2*, Physica C **481** (2012), 229–234.

[94] S. L. Sondhi, A. Karlhede, S. A. Kivelson, and E. H. Rezayi, *Skyrmions and the crossover from the integer to fractional quantum Hall effect at small Zeeman energies*, Phys. Rev. B **47** (1993), 16419–16426.

[95] Kai Sun, Hong Yao, Eduardo Fradkin, and Steven A. Kivelson, *Topological insulators and nematic phases from spontaneous symmetry breaking in 2d Fermi systems with a quadratic band crossing*, Phys. Rev. Lett. **103** (2009), 046811.

[96] Sumanta Tewari, Chuanwei Zhang, Victor M. Yakovenko, and S. Das Sarma, *Time-reversal symmetry breaking by a $(d+id)$ density-wave state in underdoped cuprate superconductors*, Phys. Rev. Lett. **100** (2008), 217004.

[97] D. J. Thouless, M. Kohmoto, M. P. Nightingale, and M. den Nijs, *Quantized Hall conductance in a two-dimensional periodic potential*, Phys. Rev. Lett. **49** (1982), 405–408.

[98] Tom Timusk and Bryan Statt, *The pseudogap in high-temperature superconductors: an experimental survey*, Rep. Prog. Phys. **62** (1999), 61.

[99] K. v. Klitzing, G. Dorda, and M. Pepper, *New method for high-accuracy determination of the fine-structure constant based on quantized Hall resistance*, Phys. Rev. Lett. **45** (1980), 494–497.

[100] C. M. Varma and Lijun Zhu, *Helicity order: Hidden order parameter in URu_2Si_2*, Phys. Rev. Lett. **96** (2006), 036405.

[101] G. E. Volovik, *The universe in a Helium droplet*, Oxford University Press, New York, 2003, and references therein.

[102] Klaus von Klitzing, *The quantized Hall effect*, Rev. Mod. Phys. **58** (1986), 519–531.

[103] Xiao-Gang Wen, *Topological orders and edge excitations in fractional quantum Hall states*, Adv. Phys. **44** (1995), 405–473.

[104] P. B. Wiegmann, *Topological electronic liquids: Electronic physics of one dimension beyond the one spatial dimension*, Phys. Rev. B **59** (1999), 15705–15728.

[105] Jing Xia, Elizabeth Schemm, G. Deutscher, S. A. Kivelson, D. A. Bonn, W. N. Hardy, R. Liang, W. Siemons, G. Koster, M. M. Fejer, and A. Kapitulnik, *Polar Kerr-effect measurements of the high-temperature $YBa_2Cu_3O_{6+x}$ superconductor: Evidence for broken symmetry near the pseudogap temperature*, Phys. Rev. Lett. **100** (2008), 127002.

[106] V. M. Yakovenko, *Spin, statistics and charge of solitons in (2+1)-dimensional theories*, Fizika **21S3** (1989), 231, arXiv:cond-mat/9703195.

[107] Hiroyuki Yamase and Walter Metzner, *Magnetic excitations and their anisotropy in $YBa_2Cu_3O_{6+\delta}$: Slave-boson mean-field analysis of the bilayer t-J model*, Phys. Rev. B **73** (2006), 214517.

[108] Bohm-Jung Yang and Hae-Young Kee, *Searching for topological density-wave insulators in multiorbital square-lattice systems*, Phys. Rev. B **82** (2010), 195126.

[109] Bohm-Jung Yang and Naoto Nagaosa, *Skyrmion quantum numbers and quantized pumping in two-dimensional topological chiral magnets*, Phys. Rev. B **84** (2011), 245123.

[110] K. Yano, T. Sakakibara, T. Tayama, M. Yokoyama, H. Amitsuka, Y. Homma, P. Miranovic, M. Ichioka, Y. Tsutsumi, and K. Machida, *Field-angle-dependent specific heat measurements and gap determination of a heavy fermion superconductor URu_2Si_2*, Phys. Rev. Lett. **100** (2008), 017004.

[111] Hong Yao, Dung-Hai Lee, and Steven Kivelson, *Fermi-surface reconstruction in a smectic phase of a high-temperature superconductor*, Phys. Rev. B **84** (2011), 012507.

[112] Ting Yuan, Jeremy Figgins, and Dirk K. Morr, *Hidden order transition in URu_2Si_2: Evidence for the emergence of a coherent Anderson lattice from scanning tunneling spectroscopy*, Phys. Rev. B **86** (2012), 035129.

[113] Chuanwei Zhang, Sumanta Tewari, and S. Das Sarma, *Berry-phase-mediated topological thermoelectric transport in gapped single and bilayer graphene*, Phys. Rev. B **79** (2009), 245424.